TÉCNICO LISBOA

Minicircle production and delivery to human mesenchymal stem/stromal cells for angiogenesis stimulation

Liliana Isabel Casimiro Brito

Thesis to obtain the Master of Science Degree in

Biotechnology

Supervisors: Professor Gabriel António Amaro Monteiro

Doctor Teresa Catarina Páscoa Madeira

Examination Committee

Chairperson: Professor Arsénio do Carmo Sales Mendes Fialho

Supervisor: Doctor Teresa Catarina Páscoa Madeira

Member of the Committee: Professor Duarte Miguel de França Teixeira dos Prazeres

December 2014

Acknowledgments

The world and the human being are not perfect but in community, some hard tasks can be definitely solved. People do not easily acknowledge others for their support, so this section is one of the most important of my thesis. Therefore, I would like to dedicate all my work and results to the kind people who have contributed in their own way to the production of this dissertation.

First of all, I would like to thank my supervisors, Professor Gabriel Monteiro and Doctor Catarina Madeira for their orientation, recommendations and especially their motivation words to keep me focused, and also to Professor Cláudia Lobato da Silva and Professor Joaquim Sampaio Cabral, who opened this master thesis opportunity especially for me and which represents a really interesting and forefront field of clinical biotechnology.

Special thanks to researchers who directly produced science with me: Michaela Simcikova, Ana Marisa Salgueiro, Joana Boura and Cláudia Alves. Without their knowledge transfer, support, advices, troubleshooting and brainstorming, the development process had been more difficult. Also, I would like to thank to all my laboratory colleagues for the pleasant experience that we shared together.

Moreover, I would like to acknowledge to a special person who is no longer present, my grandmother, because she contributed greatly to whom I am today and educated me that the hard work is the key to success. I do not keen on fail, however I realize that every time I make a mistake, I learn much more than if I had a correct result, because it obligates me to rethink in all my strategy and leads to the improvement of my planning capacity, organization and adaptation skills.

Finally, I would like to express gratitude to my family and friends that believe every time in my potential and capacity and are a constant source of love, concern, support and strength during all these years. An acknowledgement is not enough to demonstrate how lucky I am to their presence in my life and I promise that I will do everything to make them be proud of me.

"I know what I want, I have a goal, an opinion,

I have a religion and love. Let me be myself and then I am satisfied.

I know that I'm a woman, a woman with inward strength and plenty of courage."

Anne Frank

Abstract

The potential of mesenchymal stem cells (MSC) has attracted much attention in regenerative medicine owing to their apparent usefulness as replacement cells due to their properties (multilineage differentiation potential, hypoimmunogenicity and immunomodulatory properties and migration ability). MSC transplantation associated to angiogenic gene therapy is a promising strategy of treatment for cardiovascular diseases (CVD). Although MSC intrinsically produce vascular endothelial growth factor (VEGF), which is a protein involved in the angiogenesis stimulation, its overexpression can enhance their therapeutic properties in cardiac regeneration.

Regarding gene delivery methods, non-viral systems are a priority in gene therapy field. As an alternative to conventional plasmid DNA, this master thesis explored the minicircle technology. VEGF-GFP encoding minicircles were produced by *Escherichia coli* BW2P *in vivo* recombination induced in the mid-late exponential phase which led to recombination efficiencies over 90%. Regarding the purification, minicircle population represents roughly 15% of the sample and its recovery from anion exchange (AEC) and hydrophobic interaction (HIC) chromatography was 50-67% and 40-46%, respectively, and must be improved.

MSC transfected with minicircles attained a maximum of 31±8% of GFP-expressing cells, considering the CMV and mCMV+hEF1α CpGfree promoters and no significant difference was observed in comparison with pVAX-VEGF-GFP. However, higher survival of MC MSC transfected cells and ELISA results showed an at least 1.3-fold higher VEGF concentration than pVAX-VEGF-GFP after 7 days of transfection. The hEf1α and hEf1α CpGfree promoters showed low levels of expression.

This work showed that minicircles hold potential to enhance MSC therapy efficacy for the treatment of CVD through angiogenesis.

Keywords: Mesenchymal stem cells, angiogenesis, cardiovascular diseases, non-viral gene therapy, minicircle

Resumo

O potencial das células estaminais mesenquimais (MSC) tem atraído muita atenção na medicina regenerativa devido à sua utilidade aparente como células de substituição, devido às suas propriedades (diferenciação em múltiplas linhagens celulares, baixa imunogenicidade, propriedades imunomodulatórias e capacidade de migração). O transplante de MSC associado à terapia angiogénica é uma estratégia promissora para o tratamento de doenças cardiovasculares (CVD). Embora as MSC produzam o factor de crescimento endotelial vascular (VEGF), que é uma proteína envolvida na estimulação da angiogénese, a sua sobre-expressão pode melhorar as propriedades terapêuticas das MSC na regeneração cardíaca.

Quanto aos métodos de introdução de genes, os sistemas não-virais são uma prioridade no campo da terapia genética. Como uma alternativa ao plasmídeo convencional, esta tese de mestrado explorou a tecnologia associada aos minicírculos. Minicírculos que codificam para VEGF-GFP foram produzidos pela estirpe *Escherichia coli* BW2P através da recombinação *in vivo* induzida na fase exponencial que levou a eficiências de recombinação maiores do que 90%. Em relação à purificação, a população de minicírculo representa aproximadamente 15% da amostra e a sua recuperação a partir das cromatografias de permuta aniónica (AEC) e de interacção hidrofóbica (HIC) foram de 50-67% e 40-46%, respectivamente, e devem ser melhoradas.

As MSC transfectadas com minicírculos atingiram um máximo de 31±8% de células a expressar GFP, considerando os promotores CMV e mCMV+hEF1α CpGfree e não foi observada uma diferença significativa em comparação com pVAX-VEGF-GFP. No entanto, a maior sobrevivência das MSC transfectadas com minicírculos e os resultados de ELISA mostraram que a concentração de VEGF foi pelo menos 1,3 vezes maior do que nas MSC pVAX-VEGF-GFP, após 7 dias de transfecção. Os promotores hEf1α e hEf1α CpGfree mostraram baixos níveis de expressão.

Este trabalho demonstrou que os minicirculos têm potencial para melhorar a eficácia terapêutica das MSC no tratamento de doenças cardiovasculares através de angiogénese.

Palavras-chave: Células estaminais mesenquimais, angiogénese, doenças cardiovasculares, terapia génica não viral, minicírculo

Index

List of abbreviatures

ACE - Angiotensin-converting Enzyme
AEC – Anion Exchange Chromatography
ALS – Amyotrophic Lateral Sclerosis
APC - Antigen-presenting Cell
ASC – Adult Stem Cells
AT – Adipose Tissue
BAC – Bacterial Artificial Chromosome
BM - Bone Marrow
ButFF – Butyl Sepharose 4 fast flow
ButFFS – Butyl-S Sepharose 6 fast flow
CA – Number of viable cells
cAMP – Cyclic Adenosine Monophosphate
CCL- Chemokine (C-C motif) Ligand
CD – Cluster of Differentiation
CFU-F - Colony Forming Unit Fibroblast
CIM – Convection Interaction Media
CMV – Cytomegalovirus
CR – Cell Recovery
CSC – Cancer Stem Cells
C_T – Cycle Threshold
CT – Total cell number
CV – Cell Viability
CVD – Cardiovascular Diseases
CXCL - Chemokine (C-X-C motif) Ligand
DEAE – Diethylaminoethyl
DMD - Duchenne Muscular Dystrophy
DMEM – Dulbecco's Modified Eagle Medium
ds – double-stranded
ECM – Extracellular Matrix
EGF - Epidermal Growth Factor
EMA – European Medicines Agency
ESC – Embryonic Stem Cells
FBS – Fetal Bovine Serum
FDA – US Food and Drug Administration
FGF - Fibroblast Growth Factor
FHF – Fulminate Hepatic Failure
flk-L - fms-like tyrosine kinase Ligand
FSC – Fetal Stem Cells
G-CSF - Granulocyte Colony-stimulating Factor
GFP – Green Fluorescence Protein
GFP^+ - GFP-expressing cells percentage
GHRH – Growth Hormone Releasing Hormone
GM-CSF - Granulocyte Macrophage Colony-stimulating Factor
GMP - Good Manufacturing Practices
GVHD - Graft-versus-host-disease
HAC – Human Artificial Chromosome
hEF – Human Elongation Factor
HGF – Hepatocyte Growth Factor
HIC – Hydrophobic Interaction Chromatography
HLA - Human Leukocyte Antigen
HS – High Substitution
HSC - Hematopoietic Stem Cell
IDO - Indoleamine-pyrrole 2,3-dioxygenase
IFN – Interferon
IGF - Insulin-like growth factor
IL – Interleukin
IMDM – Iscove's Modified Dulbecco's Medium
iPSC – Induced Pluripotent Stem Cells
ISCT - International Society for Cellular Therapy
KGF - Keratinocyte Growth Factor
L- Linear
lacI – Lac Operon Repressor
lacO – Lac Operator
LB - Luria-Bertani
LIF - Leukemia Inhibitory Factor
LS – Low Substitution
MAC – Mammalian Artificial Chromosome
MC - Minicircle
mCMV – Mouse Cytomegalovirus

MCS – Multiple Cloning Site

M-CSF - Macrophage Colony-stimulating Factor

MHC – Major Histocompatibility Complex

miMC – Micro-minicircle

miRNA – Micro-RNA

MP – Miniplasmid

MS – Multiple Sclerosis

MSC – Mesenchymal Stem Cells

NCD – Non Communicable Disease

NK – Neutral Killer Cell

NMWL - Nominal Molecular Weight Limit

NSC – Neural Stem Cells

OC – Open Circular

OctFF – Octyl Sepharose 4 fast flow

OD - Optical Density

PBS - Phosphate Buffered Saline

PCR – Polymerase Chain Reaction

PDGF - Platelet-derived Growth Factor

pDNA – Plasmid DNA

PEI - Poly(ethylene imine)

PFA – Paraformaldehyde

PG – Prostaglandin

PheFF – Phenyl Sepharose 6 fast flow

PheHP – Phenyl Sepharose 6 high performance

PLA - Poly lactic acid

PLGA - Poly(lactic-co-glycolic acid)

PLGF - Placental Growth Factor

PP –Parental Plasmid

PPAR - Peroxisome Proliferator-activated Receptor

PRC - Progenitor Cell

RE – Endonuclease Restriction Enzyme

RTK - Tyrosine Kinase Receptor

RT-PCR – Real-Time Polymerase Chain Reaction

SC – Stem Cells

SC - Supercoiled

SCF - Stem Cell Factor

SDF – Stromal Derived Factor

SEM – Standard Error of Mean

siRNA - Small interfering RNA

ss – single-stranded

TGF - Transforming Growth Factor

TH – Helper T Cell

TIMP- Tissue Inhibitor of Metalloproteinase

TLR – Toll-like Receptor

TVC – Total viable cell number

UCB - Umbilical Cord Blood

VEGF - Vascular Endothelial Growth Factor

VEGFR - Vascular Endothelial Growth Factor Receptor

VPF - Vascular-permeability Factor

VVO - Vesiculovacuolar Organelle

YAC – Yeast Artificial Chromosome

YT – Yield of Transfection

Figures Index

Tables Index

1. Context

Among non communicable diseases (NCD), the cardiovascular diseases, which include heart and blood vessels diseases, are the major cause of NCD deaths [1]. For successful cardiac tissue regeneration as well as the treatment of ischemic cardiac tissue, a controlled angiogenesis is required. Using limb or myocardial ischemic models, differentiated cells, such as hematopoietic cells and myoblasts, have been shown to induce vessel formation by expressing angiogenic factors [2, 3]. However, their clinical application is hindered by the difficulty in obtaining a large cell number, their lack of ability to expand *in vitro* and poor engraftment efficiency to target tissue sites [2].

Stem cells are promising therapeutics for revascularization due to their special properties that overcome the main limitations of differentiated cells and can contribute directly to angiogenesis, by participating in new vessel formation or indirectly by secreting a broad spectrum of angiogenic and antiapoptotic factors [2]. However, effects of stem cell therapy are modest at best and often neither effective nor long lasting. This is because transplanted stem cells do not present high survival rates. These cells are transferred from their native niches, to which they are entirely adapted, to a hostile environment of low oxygen, poor nutrients and become prone to attacks by immune system and action of apoptotic agents [4].

To overcome this impasse, the emerging trend is genetic modification of stem cells. Gene therapy is a novel therapeutic branch of modern medicine. Still, gene therapy relies on similar principles as those of traditional pharmacologic therapy such as: regional specificity for the targeted tissue, specificity of the introduced gene function in relation to disease and stability and regulation of expression of the introduced gene [5]. Its emergence is a direct consequence of the discovery of the transduction process and the introduction of recombinant DNA methodology in the 1970s [6]. To achieve a successful therapy, all these features need to be integrated with the help of molecular and cell biology, genetics and virology knowledge in addition to bioprocess manufacturing capability and clinical laboratory infrastructure [5]. Gene therapy is progressing over time and has a great potential to become an important treatment regimen.

Stem cells can be modified to withstand apoptosis and inflammation and even be activated by low oxygen to switch on protective genes to make them survive longer as grafts [5]. Also, stem cells can be genetically modified to deliver proteins encoding for hormones, growth factors and homing factors. Genetically modified stem cells could be a new step forward in stem cell therapy when designed to enhance their native properties and utility in the treatment of a variety of diseases. Particularly, stem cells expressing angiogenic factors can be applied for treatment of myocardial ischemia and heart failure.

2. Stem cells

Stem cells (SC) are undifferentiated cells common to all multicellular organisms. They do not have the phenotypic characteristics of cells from any known adult tissue (epithelial, connective, muscle, neural or immune) but are able to generate different differentiated cells of the body. Also, stem cells retain the ability to renew themselves through cell division, maintaining the undifferentiated state, and show *in vivo* engraftment ability [7, 8].

According to the plasticity of these cells, they can be classified as (Figure 1) [7, 9]:

- **Totipotent** – can give rise to all cells/tissues that contribute to the formation of a whole organism, including the extra-embryonic structures. The zygote and the cells produced by its cleavage during the first few divisions (morula) are the only totipotent cells known.
- **Pluripotent** – have the potential to generate all cell types from the three germ layers (endoderm, mesoderm or ectoderm) but are not able to give rise to the extra-embryonic trophoblast lineage.
- **Multipotent** – can generate different cell types from the same germ layer.
- **Unipotent** – can only originate one type of cell but have the property of self-renewal which distinguishes them from non-stem cells.

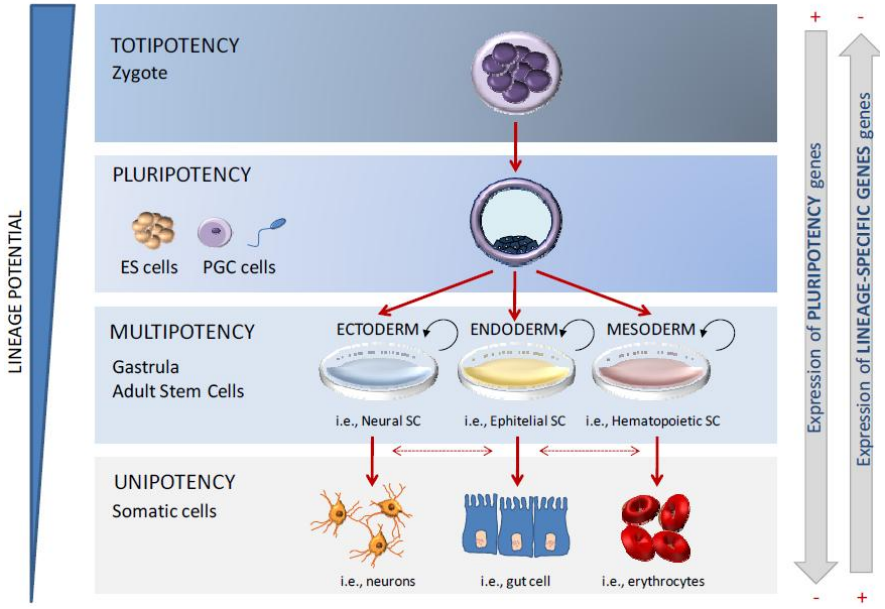

Figure 1 – Different differentiation potential and gene expression profile of stem cells [10].

Two broad categories of stem cells can be presented: embryonic stem cells (ESC) and adult stem cells (ASC), which are present at different stages of life. Within ASC, there is still one pathological cell type present in cancers that have some stem properties (cancer SC (CSC)) [8]. Regarding the source, beyond embryonic and adult stem cells, fetal stem cells (FSC) can be also addressed [11]. Lastly, there is a genetically manipulated type of stem cells which present pluripotency potential, named as induced pluripotent stem cells (iPSC) [8].

Stem cells have emerged as an important part of regenerative medicine, representing the best and most straightforward option for bioprocesses to produce cells and tissues in order to restore or establish normal function to damaged parts of the body. Besides the challenging application of stem cell research in order to discover the path to destroy the malignancy seeding cancer stem cells in blood and solid tumors, curing or ameliorating the damages of HIV/AIDS, blindness, Type I diabetes, spinal cord injuries, other motor neuron and demyelinating diseases are also goals under development. Moreover, strong expectations for the application of stem cell therapies in neurodegenerative diseases were created. Finally, stem cells can also be genetically manipulated to introduce the therapeutic sequence and be applied in gene therapy [12, 13].

Stem cells applied in transplantations can be derived from autologous, syngeneic, allogeneic or xenogeneic sources. Autologous cells are derived from the person on whom they are used. Highly plastic adult stem cells from the umbilical cord blood or bone marrow are good sources of autologous cells. Syngeneic cells are collected from a genetically identical individual. In case of allogeneic transplant, stem cells can be derived from bone marrow, peripheral blood or cord blood of family donors or HLA (human leukocyte antigen) typed or untyped unrelated donors. Xenotransplantation happens when there is a transplant of live cells, tissues or organs between two different species. Regarding allogeneic and xenogeneic sources, histocompatibility is a prerequisite for a successful transplantation [12, 14].

Beyond stem cells application in clinical treatments, the understanding of stem cells biology is essential for progress in the field, not only regarding the development of new products but also because they are the origin of life which means that some birth defects can be demystified and consequently prevented or treated (Figure 2) [4, 11, 15]. Moreover, stem cells can be a reliable source for testing safety and efficacy of human drugs and for identification of drug targets (Figure 2) [15, 16]. For example, new drugs are not directly tested on the human body. Instead, researchers rely on an animal model. However, there is pressure against animal testing, regarding the ethical and economic points of view, and important interspecies differences between animal and human tissues are observed. Therefore, there is a demand for the development of new robust and economic *in vitro* models using human cells. Stem cells, specially the pluripotent ones such as hESC and iPSC, might be a useful source for the different stages of pathological and toxicology modelling, by providing physiological models for any human cell type at the desired amount [17].

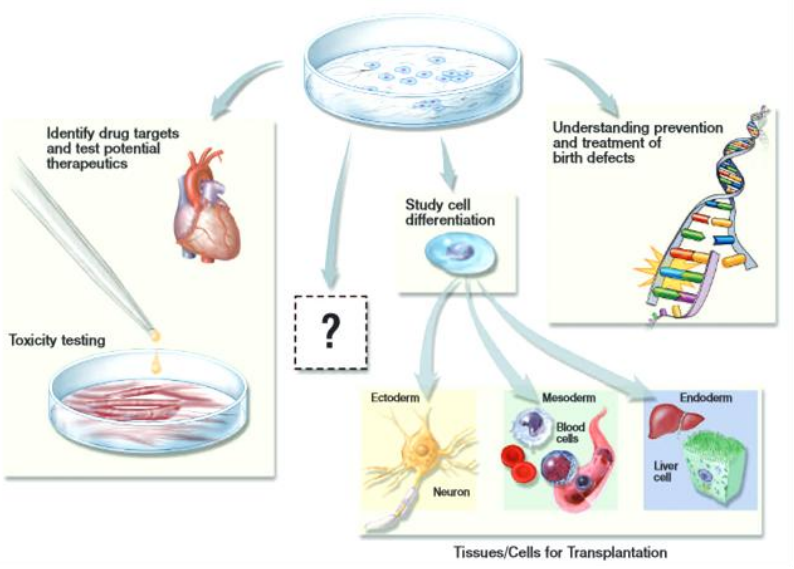

Figure 2 –Stem cells applications [15].

2.1 Adult Stem Cells (ASC)

ASC are postnatal derivatives of ESC present in different tissues of the body, which act as a repair system for the body replacing specialized damaged cells. They are also known as somatic stem cells which can be found in children as well as adults [8]. In comparison with ESC, ASC maintain co-expression of at least three of the four transcription factors characteristic of ESC (*OCT4*, *KLF4* and *SOX2*) and reveal high expression of ABC transporters and alkaline phosphatase but telomerase expression is not clear. Also, they demonstrate the overexpression of structural genes (E-cadherin, vimentin and β-catenin) but unlike ESC, ASC show a more restricted proliferation and differentiation capacity, being only multipotent cells [8].

There is no evidence of how many markers are common to all ASC but according to the tissue, ASC express a set of markers which are organ specific [8]. Additionally, more research is required to demonstrate if populations of ASC expressing different sets of genes may coexist in the same organ. Some ASC markers are also expressed by differentiated somatic cells, although with different levels of expression and not in a balanced way as described for ESC [8].

ASC can be divided into parenchymal and mesenchymal stem cells (MSC), which generate new somatic non-connective and connective tissue, respectively [8]. While MSC are extensively distributed throughout the body, parenchymal ASC aggregate in the organs in a structure called the niche. In these niches, ASC are maintained in a quiescence state or at a low basal rate of division. The number of ASC in the niche is maintained through symmetric division, while asymmetric division gives rise to one daughter ASC and one daughter progenitor cell (PRC), with limited self renewal capacity. After proliferation of PRCs, they differentiate into somatic cells [8].

Within ASC, hematopoietic stem cells (HSC), neural stem cells (NSC) and MSC are the most extensively studied [12].

2.1.1 Mesenchymal Stem Cells (MSC)

MSC were firstly described by Owen and Friedenstein[18] and can alternatively be defined as multipotent mesenchymal stromal cells. Minimal criteria to universally define human MSC was developed by the Mesenchymal and Tissue Stem Cell Committee of the International Society for Cellular Therapy (ISCT), establishing that MSC are distinguished, besides the surface antigens (positive expression for CD105, CD73 and CD90 and negative for CD45, CD34, CD14 or CD11b, CD79α or CD19 and HLA-DR), by their ability to adhere to plastic (when maintained in standard tissue culture flasks these cells should adhere to the bottom of the flask) and by their capability to differentiate into osteoblasts, adipocytes and chondroblasts, under standard differentiating conditions *in vitro* [19].

MSC have a fibroblast-like morphology and a clonogenic potential with CFU-F (colony forming unit fibroblast) ability, which means that they have the potential to proliferate and give rise to a colony and some daughter cells from each generation retain the potential to proliferate [20-22].

MSC have been characterized by many markers depending on their location. There is no specific and unique single marker for *ex vivo* cultured MSC. Currently, for clinical application, each *ex vivo* MSC expanded cells are characterized but the use of a definitively phenotyped MSC population remains an unmet goal since they form a heterogeneous population [20, 21]. Considering the perivascular origin of MSC, the discrepancy of MSC CD marker expression is reasonably explained by taking into account the potential differences in the perivascular microenvironment of the various tissues in the body [23].

MSC can be readily and easily isolated and *ex vivo* expanded from a wide range of tissues, are capable of undergoing multilineage differentiation, show hypoimmunogenicity and immunomodulatory properties, have migration behaviour to injury sites, trophic ability and no ethical limitations [20, 21].

2.1.1.1 MSC Sources

It has been shown that MSC are present in almost every post-natal tissue, a larger view than what was previously expected. These cells reside in specialized niches within various tissues and a particular niche, related to their perivascular origin, is along blood vessel walls. In bone marrow (BM) and some other tissues, MSC can be found in perivascular zones, where they support blood vessels and contribute to tissue and immune system homeostasis [20, 24].

MSC can be isolated from many different organs and tissues. Most studies of MSC use cells derived from BM, where MSC are isolated after BM cell suspensions are layered onto a density gradient and the nucleated cell fraction is collected, washed, and resuspended in MSC culture medium. After 24h of culture, only individual colonies of fibroblast-like cells are allowed to expand, whereas non-adherent cells are removed [25]. Although, in this organ, MSC numbers are very low, representing just 0.0001% (1 per $1x10^6$ cells) of nucleated bone marrow cells. Moreover, BM harvesting is an invasive and painful procedure for the donor. Alternatively, MSC can also be isolated from adipose tissue (AT), blood vessels (as perivascular cells), placenta, amnion, umbilical cord blood (UCB), amniotic fluid, lung and liver. In some of these tissues' cases, the MSC access is not facilitated but, for example, placenta is readily and widely available [20, 24]. According to some studies, since there is no significant difference between BM MSC and placenta MSC, the use of placenta as a source of human MSC for clinical trials might be considered [20]. AT can also be an alternative source since isolated MSC appear to have higher frequencies than BM (100-1000X) and a higher potential for angiogenesis and vasculogenesis [24, 26, 27]. Additionally, UCB has no associated ethical considerations and UCB MSC are more primitive than BM MSC but lower yields of MSC are obtained [24, 28]. In addition to the aforementioned CD markers, they also express CD29, CD49b, CD58, CD166 and HLA-I. They are negative for CD3, CD7, CD33, CD40, CD49d CD80, CD86, CD117, and CD133 [28]. MSC from different sources share some common properties, however they can differ in their

differentiation potential and their gene expression profile according to their tissue of origin [22]. Considering the number of MSC throughout its lifetime, the total number *in vivo* of MSC decreases with individual's age [26].

2.1.1.2 Multilineage differentiation potential

Once MSC are derived from embryonic mesoderm and present multipotency, they are capable of differentiating into chondrocytes, adipocytes and osteocytes (Figure 3), making MSC suitable for a wide range of potential therapeutic applications [20, 21]. MSC differentiate into osteoblasts under the presence of β-glycerol-phosphate, ascorbic acid-2-phosphate, dexamethasone and fetal bovine serum (FBS). Selection of positive differentiated cells can be achieved by the observation of calcium accumulation in nodules with von Kossa staining [13, 29, 30]. On the other hand, in the presence of transforming growth factor-β (TGF-β), dexamethasone, sodium pyruvate, ascorbic acid-2-phosphate, proline and insulin-transferrin selenium, MSC originate chondrocytes, which can be identified by toluidine staining of glycosaminoglycans within the extracellular matrix [13, 30, 31]. To induce the differentiation into adipocytes, MSC cultures are incubated with dexamethasone, insulin, isobutylmethylxanthine and indomethacin. Peroxisome proliferator-activated receptor-γ (PPAR-γ) and fatty acid synthetase are key factors for adipogenic lineage differentiation which can be verified by oil red O staining [13, 30, 32].

Remaining as a controversial issue, several studies have reported that MSC have the ability to differentiate into cells from various lineages beyond the conventional mesodermal lineages (in a process known as transdifferentiation), namely into cells of ectodermal and endodermal origin, such as hepatocytes and neurons (Figure 3) [21]. Furthermore, they can differentiate into endothelial cells, form capillaries *in vitro* and secrete growth factors such as vascular endothelial growth factor (VEGF) to support angiogenesis [20]. Additionally, undifferentiated MSC express many lineage-specific genes other than those of the mesenchymal lineage. Due to the lack of specific MSC markers, *in vivo* transdifferentiation of MSC can not be well elucidated in comparison to *in vitro* MSC characterization [33].

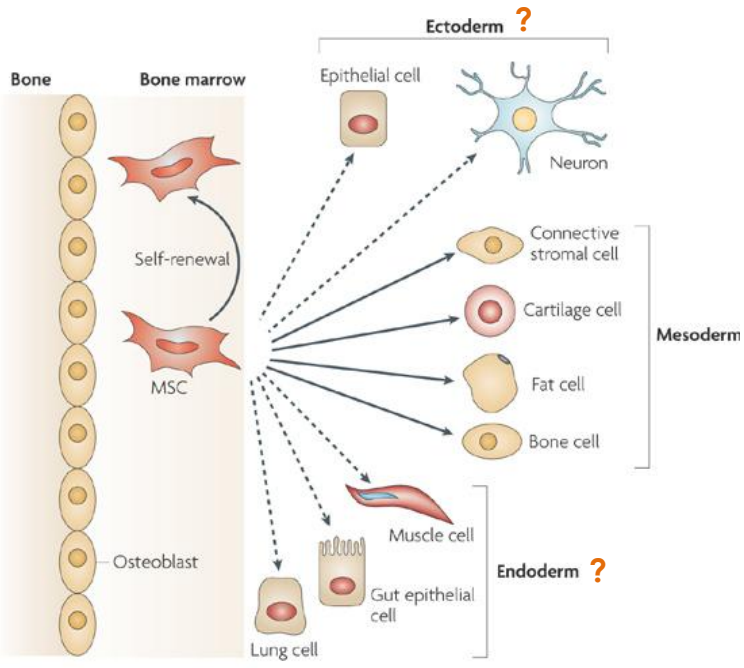

Figure 3 –MSC reported differentiation potential [21].

2.1.1.3 Immunosuppressive and Immunomodulation Capacity of MSC

Undifferentiated MSC express low to medium levels of HLA Class I and low levels of HLA Class II, thus they are considered MHC II (Major Histocompatibility Complex II) negative cells and additionally they lack co-stimulatory molecules such as CD40, CD80 and CD86 (involved in the activation of T cells in transplant rejection) [20, 21, 24]. Therefore, in theory, they could be used in allogeneic transplantation without the need of immunosuppression in adulthood, HLA matching and without it being immunologically rejected. Some studies have been made regarding the mechanism behind this hypoimmunogenicity, suggesting the inhibitory action of MSC over the proliferation of T cells, B cells functions, neutral killer (NK) cell proliferation and cytokine production and differentiation, maturation and activation of dendritic cells, however the full process remains unclear [20].

With evidence suggesting an immune-privileged status of MSC, the possibility of using these cells for therapeutic application without the need of HLA compatibility presents great advantage for having MSC available in a timely manner for patients in a variety of acute and chronic clinical settings. This constitutes a distinct clinical advantage over other cellular populations and a single allogeneic MSC donor, if it is qualified and well-characterized, can supply cells for several patients' treatment [34]. However, besides the potential loss in efficacy, the use of allogeneic cells presents a risk of a host immune response towards the donor cells if detected or as a reaction to cell culture and preservation reagents in the cell preparation. For example, the expression of induced functional HLA-DR in MSC was reported after exposure to culture media containing mitogenic growth factors such as FGF-2 (Fibroblast Growth Factor-2) and PDGF (Platelet-derived Growth Factor) [20, 23].

Associated with immunosupression, secretion of soluble factors and cell-to-cell contact molecules are important for immune-regulatory nature of MSC *in vitro* and *in vivo* (Figure 4). For instance, MSC demonstrate immunomodulatory properties especially in the presence of immune-related disorders, such as autoimmune diseases [20]. By producing and releasing a number of cytokines and chemokines and expressing specific receptors, MSC show both immune enhancing and suppressing potentials [20]. For example, under acute inflammatory conditions polarized by M1 macrophages and helper T lymphocyte (TH)-type-1 cytokines, especially the pro-inflammatory cytokine interferon (IFN-γ), the immunosuppressive capacity of MSC is enhanced and they act as antigen-presenting cells (APC) [20]. Additionally, under chronic inflammatory conditions, MSC are polarized by M2 macrophages and TH2 cytokines and can be recruited into the fibrotic process. On the other hand, when the level of IFN-γ increases above a given threshold, MSC inhibit antigen presentation and promote immune suppression [33] . In addition, MSC-induced immune suppression by IFN-γ is associated with an up-regulation of B7-H1, a co-stimulatory surface molecule on stem cells [20]. Therefore, depending on the inflammatory microenvironment, MSC action may protect against foreign antigens or limit damage caused by a disproportionate inflammatory response [20]. MSC constitutively or upon stimulation secrete large amounts of cytokines (Figure 4): mitogenic proteins as TGF-α, TGF-β, hepatocyte growth factor (HGF), epithelial growth factor (EGF), FGF-2 and insulin-like growth factor-1 (IGF-1) to promote fibroblast, epithelial and endothelial cell division; VEGF, IGF-1, EGF and angiopoietin-1 to enhance vascularization;

interleukin(IL)-1, IL-6, IL-8, IL-7, IL-8, IL-10, IL-11, IL-12, IL-14, IL-15, LIF (Leukemia Inhibitory Factor), G-CSF (granulocyte colony-stimulating factor), GM-CSF (granulocyte macrophage colony-stimulating factor), SCF (stem cell factor), M-CSF (macrophage colony-stimulating factor), flk-3L (fms-like tyrosine kinase-3 ligand), CCL2 (chemokine (C-C motif) ligand), TIMP2 (tissue inhibitor of metalloproteinase), CXCL1, CXCL2, CXCL6 (chemokine (C-X-C motif) ligand) to regulate immune responses [23, 24, 30]. Several groups have reported that IDO (indoleamine-pyrrole 2,3-dioxygenase) and PGE2 (prostaglandin E2) are key molecules involved in immunosuppression mediated by MSC [24]. Interestingly, MSC also express a particular peptide of the cathelicidin family LL-37 which is commonly secreted to eliminate Gram-positive and Gram-negative bacterial infections. In humans, MSC showed IDO overexpression in bacteria and protozoal elimination, thus MSC are also potential therapeutic agents for acute and systemic infections (Figure 4)[23].

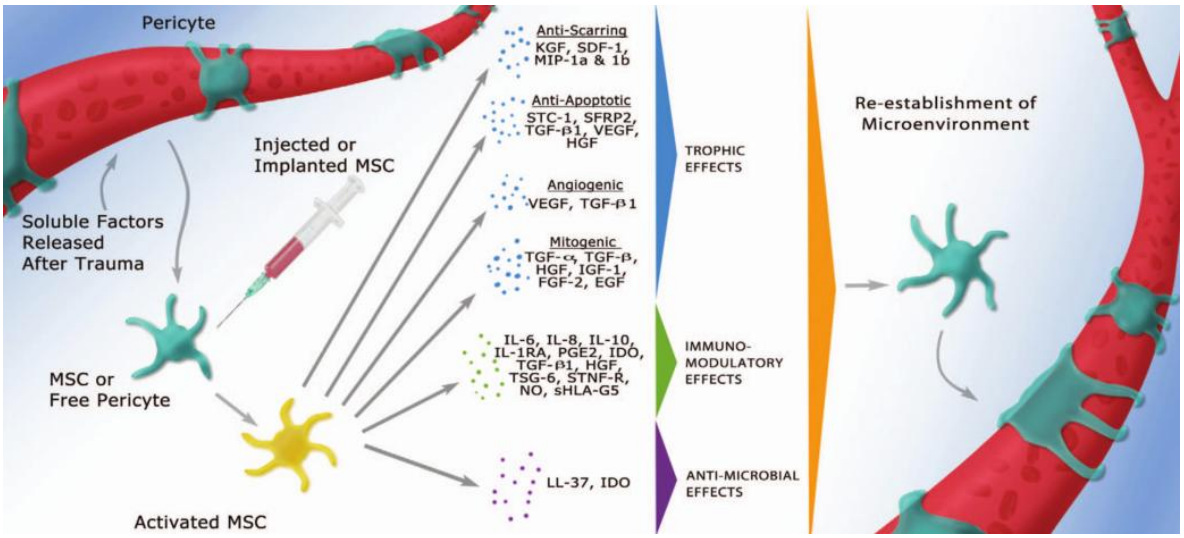

Figure 4 – MSC potential for secretion of trophic, immunomodulatory or antimicrobial factors [23].

2.1.1.4 Migration of MSC

Similar to immune cells, by the expression of adhesion molecules on MSC surface, these cells can extravasate from the blood vessels [21]. In the presence of an injury, such as an inflammation, when MSC are injected intravenously, after the passage through the lungs, where most of them get trapped, these cells migrate to the site of inflammation, instead of going to BM, the organ thought to be the traditional MSC homing site [13, 20]. The molecular mechanisms responsible for homing to the injured site are not fully elucidated, but some studies revealed that MSC trafficking depends on many signals, including growth factors, interleukins and chemokines secreted by the cells at the site of inflammation. For example, stromal derived factor-1 (SDF-1), released in diverse tissue injures, functions as a MSC chemoattractant [30, 35]. Also, PDGF or IGF-1 and CCR2, CCR3, CCR4 or CCL5 influenced the MSC migration as assessed by *in vitro* migration assays [36].

MSC express the receptors for several chemokines released after tissue damage, so chemokine/receptor interactions seem to be necessary to develop targeted MSC migration, for example, SDF-1/CXCR4 interaction [20, 35]. Also, the migratory capability of MSC cultured under hypoxic conditions seems to be enhanced in

contrast to that seen in normoxia environment [24]. MSC homing ability has already been demonstrated in several cases such as bone fracture, myocardial infarction and ischemic cerebral injury.

2.1.1.5 MSC applications

Regarding the clinical setting, MSC can be applied in local implantation of MSC for localized diseases, in systemic transplantations, in stem cell therapy associated with gene therapy and in tissue engineering applications [22]. Furthermore, due to special MSC tropism, these cells have been also used as delivery vehicles for targeted therapy.

The first clinical trial using culture-expanded MSC was performed in 1995 and involved 15 hematooncology patients who were treated with autologous cells [30, 37]. According to clinical trials' database, as of October 2014, there are 4214 clinical trials all over the world using MSC, but of which 2491 have an open status and, most of them are in North America and Europe (Annex 1)[38]. MSC are being explored in various conditions, including BM transplantation, orthopedic and spine injuries (fracture and cartilage repair, spine fusion, osteonecrosis, osteogenesis imperfecta, arthritis, degenerative disc disease), cardiovascular damages (acute myocardial infarction and vascular diseases), neural disorders and spinal cord injuries (multiple sclerosis (MS), amyotrophic lateral sclerosis (ALS), Parkinson's disease, stroke), autoimmune disorders (Duchenne muscular dystrophy (DMD), rheumatoid arthritis, Crohn's disease, type 1 diabetes, lupus, Graft-versus-host disease (GVHD), inflammatory and liver diseases (fulminate hepatic failure (FHF), cirrhosis), wounds, ulcers and burns [13, 23, 26, 30, 33]. Furthermore, genetic modification of MSC to overexpress antitumor genes has provided prospects for clinical use as anticancer therapy [13, 33].

3. Cardiovascular Diseases (CVD)

Non communicable diseases are the leading causes of death globally, killing more people each year than all other causes combined. Among NCD, CVD were responsible for the largest percentage of NCD deaths (39%) in individuals under the age of 70 in 2008 [1]. CVD are a group of disorders of the heart and blood vessels, which include hypertension (raised blood pressure), ischemic heart disease (or coronary heart disease), congestive heart failure, congenital heart defect, cerebrovascular disease (stroke), peripheral arterial disease, rheumatic arterial disease, deep vein thrombosis and pulmonary embolism. Ischemic heart disease is the most common type of heart disease and cause of heart attacks. It is characterized by reduced blood supply to the myocardium, caused by the obstruction in coronary arteries by atherosclerosis and thrombus. Plaque building up along the inner walls of the arteries of the heart narrows the arteries and reduces blood flow to the heart. If the patient is not aware of symptoms such as temporary pain (angina) and irregular heart beat (arrhythmia), due to the disruption of the capillary network surrounding heart muscle, permanent myocardium damage (myocardial infarction) and loss of muscle activity (heart failure) can take place [39]. In a myocardial infarction, 25% of the present cardiomyocytes are destroyed in a short period of time [40] and the human heart's

regenerative capacity is manifestly small, if it exists, in comparison to that observed in many other human tissues. While heart regeneration in lower vertebrates and developing mammals is a lifelong continuous process, in adult humans it is insufficient to repair the heart damage [41]. Cardiac remodeling includes ventricular shape and function changes followed by chamber dilation and interstitial and perivascular fibrosis. These phenomena are caused by cellular events: neurohormonal responses, cytokine activation, loss of cardiomyocytes due to necrosis or apoptosis, cardiomyocyte hypertrophy, disruption of extracellular matrix (ECM) and collagen accumulation followed by scar formation, leading to the chronic heart failure [39]. On the other hand, disorders of cardiac overload like hypertension or valvular disease result in a decrease in the number of cardiomyocytes throughout people's lives [42]. Aging is also associated with loss of cardiomyocytes even in the absence of a specific heart disease [41].

In Europe, CVD represent more than 50% of all deaths and cause 46 times the number of deaths and 11 times the disease burden caused by AIDS, tuberculosis and malaria combined, according to the World Health Organization in European region [43].

The most important behavioral risk factors of heart disease and stroke are tobacco use, unhealthy diet (malnutrition or obesity), physical inactivity, stress and alcohol abuse. Besides behavior risk factors, the person's genetic profile and age are also relevant regarding the probability of developing CVD and can contribute to high blood pressure, diabetes and cholesterol [1, 44]. Behavioral risk factors are responsible for about 80% of coronary heart disease and stroke [1]. The effects of an unhealthy diet and physical inactivity can result in raised blood pressure, raised blood glucose, raised blood lipids and obesity. Therefore, cessation of tobacco use, reduction of salt in the diet, higher intake of fruits, vegetables, whole grain breads, high fibre cereals, fish, low-fat dairy products, regular physical activity (approximately 30 min/day) and avoidance of harmful use of alcohol have been shown to reduce the risk of CVD. Also, in primary care facilities, hypertension, diabetes and cholesterol can be avoided, controlled and treated [1, 44].

Current treatment options for people at high risk include a combination of drug therapies such as aspirin, β-blockers, diuretics, statins, angiotensin-converting enzyme (ACE) inhibitors and anti-trombotic agents and surgical interventions like stents implantation [1, 39]. During a heart attack episode, if patients are immediately treated after the occurrence of the first symptoms, by restoration of patency of the infarct related artery, a successful reperfusion treatment will be expected. However, this positive effect of reperfusion treatment is roughly the same if the patient is only treated three to four hours after onset of symptoms or later after acute myocardial ischemia. Changing the shape of the left ventricle and implanting assistive devices such as pacemakers or defibrillators can help the heart function, however none of those procedures restore function to damaged tissue [1, 39]. Heart transplantation offers a viable option to replace damaged myocardium but organ unavailability and transplant rejection complications are well-known events [1].

The number of people who die from CVD, mainly from heart disease and stroke, will increase to reach 23.3 million by 2030 and CVD are projected to remain the single leading cause of death in world [1]. These trends suggest an unmet need for therapies to regenerate or repair damaged cardiac tissue, as well as, social

programs that encourage favorable environments for making healthy choices affordable and available. Especially in developing countries, where over 80% of CVD deaths exist and occur almost equally in men and women, these policies are extremely required to motivate people to adopt a healthy behavior [1, 44].

4. Angiogenesis and Vascular Endothelial Growth Factor

Angiogenic processes are the formation of new blood vessels and include angiogenesis, vasculogenesis and arteriogenesis [45]. Blood vessels are the first organ in the embryo and form the largest network in our body, the vascular system, also known as the circulatory system. Vascular vessels transport blood and lymph through the body, performing the crucial function of supplying tissues with oxygen and nutrients as well as removing carbon dioxide and diluting waste products, such as urea and lactic acid [46]. To accomplish these goals, the vasculature must be sufficiently permeable to allow free and bidirectional passage of small molecules and gases through the walls [46].

Table 1 – Stimulators and inhibitors of angiogenesis process [45].

Angiogenesis

Stimulators	*Inhibitors*
Vascular endothelial growth factor	Angiostatin
Fibroblast growth factor	Endostatin
Hepatocyte growth factor	Vasostatin
Platelet-derived endothelial cell growth factor	Canstatin
Transforming growth factor	Tumstatin
Angiogenin	Soluble VEGF receptor
Proliferin	Matrix metalloproteinase inhibitors
Interleukin-8	16-kDa prolactin fragment
Angiopoietin	Interleukin-12
Leptin	Arrestin
Granulocyte colony-stimulating factor	Platelet factor-4
Folistatin	Restin
Tumor necrosis factor-α	Maspin
Pleiotrophin	Interleukin-18

Angiogenesis consists in the formation of new capillary blood vessels from existent microvessels and is a multistep process involving many growth factors, ECM molecules, enzymes and several cell populations *in vivo*. The existence of angiogenic factors was initially proposed on the basis of the strong neovascularisation induced by transplanted tumors but angiogenesis occurs in physiological and pathological states and the balance between angiogenic and antiangiogenic molecules plays a crucial role in the development of vascular supply in normal tissue as well as in pathology (Table 1). Abnormal or excessive angiogenesis is involved in many ischemic diseases like heart disease, peripheral vascular disease, rheumatoid arthritis, psoriasis, tumor growth and metastasis, among others [45, 46].

Angiogenic processes comprise a complex cascade of events that begin with production and delivery of angiogenic factors by injured tissues (or tumor). These molecules bind to specific receptors located on the endothelial cells surface of pre-existing blood cells and activate them to proliferate and migrate to the injured tissues or tumor. Lastly, the emergent endothelial cells arrange themselves to create a blood vessel tube, loops and finally, matured vessels supported mainly by smooth muscle cells [45].

As present in Table 1 , VEGF is a positive regulator of angiogenesis. In mammals, VEGF gene family consists of five members: placental growth factor (PLGF), VEGFA, VEGFB, VEGFC and VEGFD. VEGFA is the key regulator of blood vessel growth and VEGFC and VEGFD regulate lymphatic angiogenesis. The human VEGFA gene is

organized in eight exons separated by seven introns. Alternative exon splicing generates at least five different molecular variants that differ from native protein in total aminoacid number: $VEGF_{121}$, $VEGF_{145}$, $VEGF_{165}$, $VEGF_{189}$ and $VEGF_{206}$, being $VEGF_{165}$ the predominant *in vivo* isoform. Like native VEGF, $VEGF_{165}$ is a heparin-binding homodimeric glycoprotein of 45kDa and its properties are similar to those of the native protein [47, 48].

VEGF was originally discovered as a vascular-permeability factor (VPF), based on its ability to induce vascular leakage. VEGF induces an increase in hydraulic conductivity of microvessels by increased calcium influx. Vascular permeability is a prerequisite for physiological processes such as wound healing, but might also aggravate pathologies such as cancer. Related to the role in the regulation of vascular permeability, VEGF induces endothelial fenestration, allowing leakage of small solutes, but larger molecules are still retained. Passage of small proteins has instead been attributed to VEGF-induced formation of caveolae, the assembly of caveolae into vesiculovacuolar organelles (VVO), and/or the induction of trans-endothelial pores (Figure 5) [46, 47].

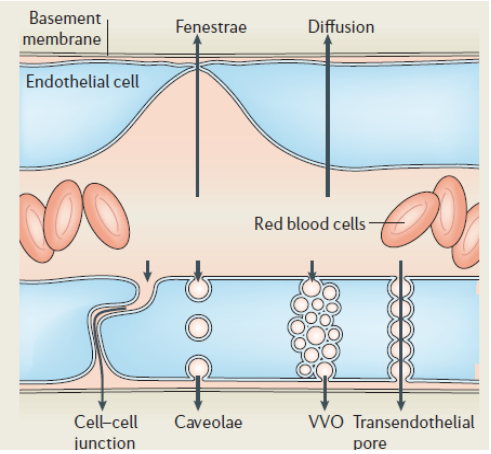

Figure 5 – VEGF regulation of vascular permeability [47].

Regarding other VEGF activities, as mentioned earlier, VEGF has the ability to promote the growth of vascular endothelial cells derived from arteries, veins and lymphatics and also to induce lymphangiogenesis in mice. VEGF is a crucial factor for endothelial cells' survival both *in vitro* and *in vivo*, mainly in developmental stages of life (embryonic and postnatal physiologic angiogenic processes), where VEGF inhibition results in extensive apoptotic changes in the vasculature of neonatal mice. Although endothelial cells are the primary target of VEGF, several studies have reported effects on other cell types. For example, VEGF stimulates surfactant production by alveolar type II cells, promotes monocyte chemotaxis, induces colony formation by mature subsets of granulocyte-macrophage progenitor cells, in adult mice, inhibits dendritic cell development, increases production of B cells and promotes the origin of immature myeloid cells [48]. Moreover, VEGF regulates vasodilatation *in vitro* in response to nitric oxide quantity released by endothelial cells [49].

Exposure to low oxygen tension induces VEFG mRNA expression under a variety of pathophysiological conditions and paracrine and autocrine release of several major growth factors, such as EGF, TGF-α, TGF-β, KGF (keratinocyte growth factor), IGF, FGF and PDGF, cooperates with local hypoxia to this upregulation. Inflammatory cytokines and oncogenic mutations also lead to VEGF upregulation [48].

VEGF signaling often represents a critical rate-limiting step in physiological angiogenesis and the biological effects of VEGF are mediated by two tyrosine kinase receptors (RTK), VEGFR-1 and VEGFR-2. VEGFR-3 is a member of the same family of RTK but is not a receptor for VEGF, binding instead to VEGFC and VEGFD (Figure 6 and Figure 7). Additionally, VEGF interacts with a family of co-receptors, the neuropilins [47, 48].

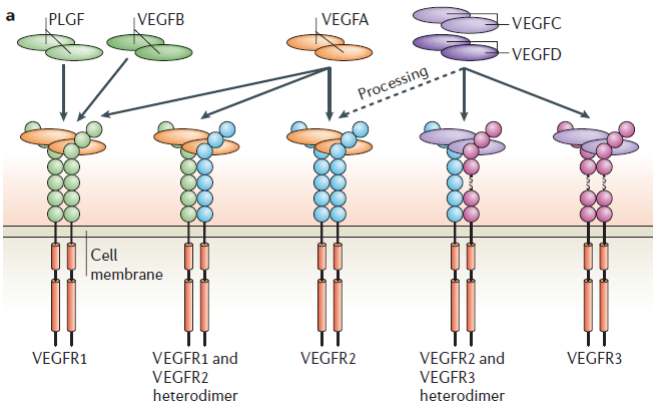

Figure 7 – Mammalian VEGF bindS to the three VEGFR tyrosine kinases, leading to the formation of VEGFR homodimers and heterodimers [48].

Figure 6 - Crystal structure of VEGFR-2 and VEGF-A complex (PDB code: 3V2A).

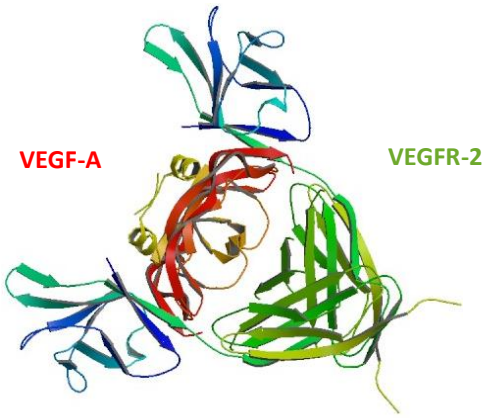

VEGF is a protein of great interest for therapeutic applications. In a wide variety of tumor models, when VEGF is inhibited, pathological angiogenesis do not occur, a phenomenon which has led to the clinical development of a variety of VEGF inhibitors with good results in clinical trials. On the other hand, the ability of VEGF and other angiogenic factors to promote collateral vessel growth in ischemia animal models, led to the application of VEGF in several clinical trials with patients with coronary and limb ischemia. Other activities of VEGF may have interesting clinical implications, such as blood vessel formation and ossification in models of bone damage [48].

5. Gene Therapy

The emergence of recombinant DNA technologies, combined with the human genome sequencing and genetic understanding of cellular processes and disease pathogenesis led to the application of engineering genetic material into therapeutic products [50, 51]. A gene therapy product is an active biological product which contains at least an exogenous recombinant nucleic acid used to regulate, repair, replace, add or delete a genetic sequence. When administered to human beings, the therapeutic, prophylactic or diagnostic effect is directly dependent of the nucleic acid sequence it contains or to the product of genetic expression of this sequence (Figure 8) [51].

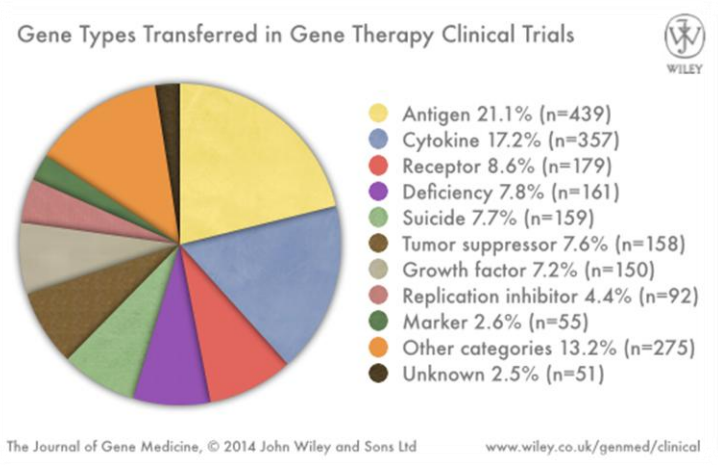

Figure 8 – Gene types transferred in gene therapy clinical trials. (*In* http://www.wiley.com/legacy/wileychi/genmed/clinical/ (19/09/2014))

Gene therapy was initially conceptualized as an ideal treatment for inherited monogenic disorders, such as hemophilia, human severe combined immunodeficiency, cystic fibrosis, among others, but over time gene therapy has been regarded as a promising treatment for many other diseases, for instance acquired diseases like AIDS or cancer [51]. Gene therapy clinical trials are mainly focused on cancer diseases, representing more than 50%, considering it is the sort of disease without an effective cure which affects lot of people throughout the world (Figure 9) [52].

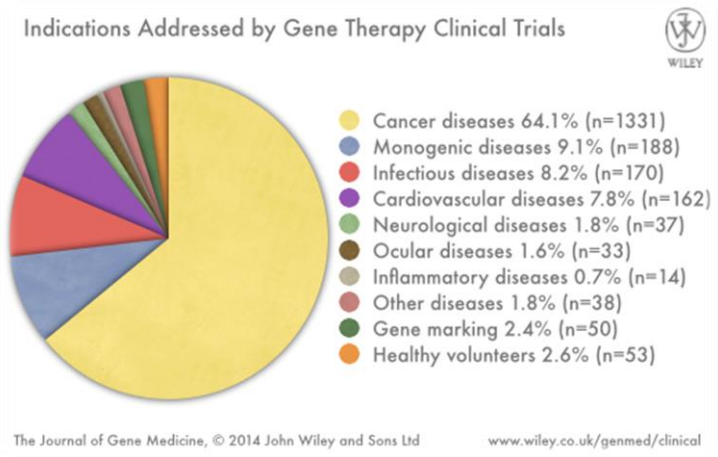

Figure 9– Indications addressed by gene therapy clinical trials. (*In* http://www.wiley.com/legacy/wileychi/genmed/clinical/ (19/09/2014))

Cardiovascular gene therapy is the fourth most popular application for gene therapy, representing 7.8% of trials (down from 9.1% in 2007). Therapeutic angiogenesis, myocardial protection, regeneration and repair, prevention of restenosis following angioplasty, prevention of bypass graft failure and risk-factor management are the main challenges for gene therapy in this field. Therapeutic angiogenesis to recovering ischemic regions, mainly myocardial ischemia, which is usually caused by coronary artery disease, and lower limb ischemia, as a result of peripheral artery disease, has been addressed by the vast majority of cardiovascular gene therapy trials. The FGF and VEGF gene families have been widely applied and a small number of trials have used PDGF to treat foot ulcers resulting from the microvascular disease of diabetes. The induction of hypoxia as a trigger to stimulate angiogenesis has been used in 11 trials until 2013 [52].

5.1 Gene delivery methods

Human body cells can be divided into somatic or germ cells. In theory, both of these cell types can be targeted for gene therapy but the transfection of germ cells raises a lot of controversy, since these genes could be inherited through generations. On the other hand, somatic cell therapy is viewed as a more conservative, safer approach because the therapeutic effect ends with the individual who receives the therapy [6].

The genes may be directly delivered *in vivo* into patients, often with the goal of targeting particular tissues or organs [53]. This method is accepted by its simplicity, however all the cells present in the injury site can be potentially affected and thus specific gene targeting cannot be assured [52]. Alternatively, patients' cells may be isolated, expanded and genetically modified *ex vivo* before reimplantation into the same subject for therapeutic purpose (Figure 10) [53]. In this strategy, it is particularly important to use cells that are able to recognize particular regions of the human body, according to their homing ability, which allows the specific delivery of the therapeutic gene. The use of cells as gene transfer vehicles has its advantages, because cells can be manipulated much more precisely in this manner than in the body. However, isolation of a specific cell type

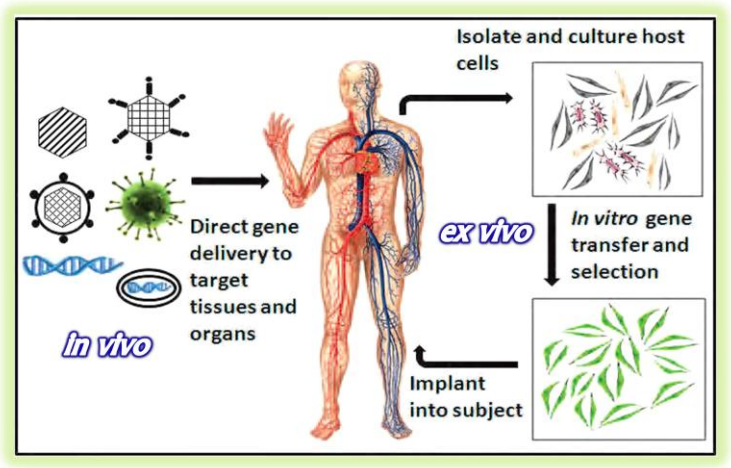

requires not only extensive knowledge of biological markers, but also insight into the requirements for that cell type to stay alive *ex vivo* and continue to divide. Unfortunately, specific biological markers are not known for many cell type and the majority of normal human cells can not be maintained for long periods of time without acquiring deleterious mutations [51].

Figure 10 – Mechanisms of gene delivery into patients (Adapted from [53]).

The most important and most difficult challenge in gene therapy is the delivery, since extracellular and cellular barriers need to be overcome to achieve the specific target. Where extracellular barriers are concerned, particle clearance mechanisms and nucleic acid degradation are the main obstacles. Regarding cellular barriers, cellular uptake, endosomal escape, nuclear entry and nucleic acid release should be observed. For these reasons, there is a need to optimize the gene therapy delivery vectors and strategies in order to obtain an effective, specific, transient and safe gene expression [51, 54].

Gene delivery systems can be divided into viral and non-viral. Currently, viral systems are considered the most effective because they frequently present high delivery efficiencies, broad tropism and stable gene expression, but their application is limited by their oncogenicity, pathogenecity, immunogenicity, the small size of the DNA they can transport and difficult and costly mass production. Therefore, the development and improvement of non-viral systems is a priority in gene therapy research field. Non-viral systems are safer with low or no immunogenicity and no risk of transmission of infectious diseases, industrially reproducible allowing easier pharmaceutical development, quality control and scalable production. Also, they do not present DNA size limit, however low transfection efficiencies are obtained and cell mortality can be also associated [25, 51, 53, 54].

5.1.1 Viral methods

The application of viral vectors for both *in vivo* and *in vitro* gene delivery is based on their natural ability to infect cells. Retroviruses, lentiviruses and adeno-associated viruses are the three main integrating virus types that are used for a transduction of mammalian cells for long-term transgene expression. On the other hand, adenoviruses and Sendai viruses are non-integrating types of virus that result in a transient expression of the transgene (Figure 11 and Table 2) [53-55].

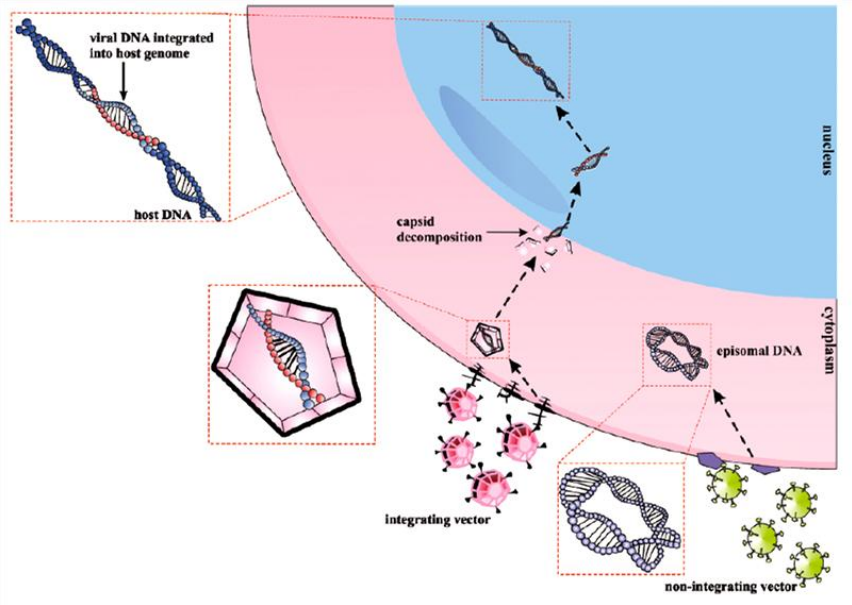

Figure 11 – Viral systems for gene delivery [55].

Table 2- Description of viral delivery systems for gene therapy [55].

Delivery System	Virus type	Characterization
Integrating viral vectors	**Retroviruses**	• Nucleocapsid with double-stranded RNA (dsRNA) and reverse transcriptase and a lipid envelope with receptor binding proteins. • Infect proliferating cells with high efficiency, however post-mitotic cells are not susceptible, which limits the spectrum of cells for targeting. • Random viral DNA integration into the host genome.
	Lentiviruses	• Subclass of retroviruses with a similar structure, including dsRNA, reverse transcriptase and genetic payload capacity of up to 9 kb. • Ability to efficiently infect the non-dividing or slow proliferating cells. • Random viral DNA integration into host genome.
	Adeno-associated viruses	• Small and single-stranded DNA (ssDNA) viruses. • Dependence on an adenovirus to replicate. • Specific DNA integration into the host genome on chromosome 19 (AAVS1 site). • Low immunogenicity.
Non-integrating viral vectors	**Adenoviruses**	• Non-envelope virus family with dsDNA as genetic material. • Icosahedral capsids, protein fibers situated on their surface for specific targeting and genetic payload capacity of up to 36 kb. • High immunogenicity • Usually stays in the cytoplasm in an episomal form. Gene expression is transient because the episomal DNA of an adenoviral vector is gradually lost during cell divisions.
	Sendai viruses	• Belong to the *paramyxviridae* family with negative-strand RNA. • Not pathogenic for humans • High transduction efficiency and very rapid onset of expression.

Biosafety improvements of viral vectors have emerged based on the scientific knowledge about viral life cycles biology and genotoxic risks that are inherent to them. They include modification of the viral genome by the deletion of some critical coding sequences to prevent spontaneous replication in target cells, targeted mutations of the integrase genes of integrating virus to achieve episomal forms of the vector, the use of viral vectors that do not integrate or that do so with a more selective integration spectrum, the inclusion of self-inactivating LTR elements and chromatin insulators to reduce neighborhood effects of integrated vectors on gene expression and the use of cell- or tissue-specific promoters for physiological and tissue-specific gene expression. Also, novel and hybrid viral vectors can be achieved through new designs and combination of positive traits of different viral vectors, respectively [53].

5.1.2 Non-Viral methods

Currently, non-viral delivery systems are based on inorganic particles, synthetic or natural biodegradable particles and physical methods (Table 3) [51, 54, 55].

Table 3 - Description of non-viral delivery systems for gene therapy [51, 55].

Delivery System	Description	Materials
Inorganic Particles	• Nanoparticles varying in size, shape and porosity; • Easily prepared and surface-functionalized; • Reticuloendothelial system evasion capacity and protection over entrapped nucleic acid from degradation or denaturation; • Good storage stability; • Not subject to microbial attack.	• Calcium phosphate • Silica • Gold • Magnetic (Fe_3O_4, MnO_2)
Synthetic or natural biodegradable particles	• Biodegradable carriers; • Particles composed by cationic polymers, cationic lipids or cationic peptides and also the combination of these components;	• **Polymeric-based non-viral vectors:** Most commonly used type of nano-scale delivery system using cationic polymers that condense DNA into small particles (polyplexes). DNA can be entrapped into the polymeric matrix or can be adsorbed or conjugated on the surface of the nanoparticles. ▪ Poly(lactic-co-glycolic acid) (PLGA) ▪ Poly lactic acid (PLA) ▪ Poly(ethylene imine) (PEI) ▪ Chitosan ▪ Dendrimers ▪ Polymethacrylates

<table>
<tr>
<td rowspan="2">Synthetic or natural biodegradable particles</td>
<td rowspan="2">• Protection over entrapped nucleic acid from degradation or denaturation;
• Reduced toxicity (degradation leads to non-toxic products);
• Low accumulation of the polymer in the cells.</td>
<td>• Cationic lipid-based non-viral vectors:
Cationic lipids condense nucleic acids into cationic particles, yielding a complex (lipoplex). Lipoplexes are partially condensed DNA complexes with an ordered substructure and an irregular morphology.
▪ Cationic liposomes
▪ Cationic emulsions
▪ Solid lipid nanoparticles</td>
</tr>
<tr>
<td>• Peptide-based non-viral vectors:
Cationic peptides rich in basic residues such as lysine and/or arginine are able to efficiently condense DNA into small, compact particles that can be stabilized in serum and overcome all the main cellular barriers.
▪ Poly-L-lysine
▪ Other peptides to functionalize cationic polyplexes and lipoplexes: SAP, protamine</td>
</tr>
<tr>
<td rowspan="4">Physical methods</td>
<td rowspan="4">• Employ a physical force to overcome the membrane barrier of the cells and facilitate intracellular gene transfer;
• Nucleic acid is not associated with any particulate or viral system (naked DNA).
• Simplicity;
• No use chemical reagents.</td>
<td>• Needle injection:
DNA is directly injected through a needle-carrying syringe into tissues. DNA vaccination is the major application of this gene delivery system. The efficiency of needle injection of DNA is low and transfection is limited to the needle surroundings.</td>
</tr>
<tr>
<td>• Balistic DNA injection:
This method is also called particle bombardment, microprojectile gene transfer or gene gun. DNA-coated gold particles are propelled against cells, forcing intracellular DNA transfer. The accelerating force for DNA-containing particles can be high-voltage electronic discharge, spark discharge or helium pressure discharge.</td>
</tr>
<tr>
<td>• Electroporation:
Through electric pulses, transient permeability on the cell membrane is created by pore formation. The efficiency is determined by the intensity of the pulses, frequency and duration. The number of cells transfected is low and surgery is required to reach internal organs.</td>
</tr>
<tr>
<td>• Sonoporation:
Ultrasounds are used to temporally permeabilize the cell membrane. The efficiency is also determined by the intensity of the pulses, frequency and duration. It is non-invasive and site-specific. Low-intensity ultrasound in combination with microbubbles has recently acquired much attention as a safe method of gene delivery.</td>
</tr>
</table>

Physical methods	• Employ a physical force to overcome the membrane barrier of the cells and facilitate intracellular gene transfer; • Nucleic acid is not associated with any particulate or viral system (naked DNA). • Simplicity; • No use chemical reagents.	• **Photoporation:** A single laser pulse is applied to generate transient pores on the cell membrane. The size of the focal point and pulse frequency of the laser determines the efficiency. The level of transgene expression reported is similar to that of electroporation. • **Magnetofection:** The magnetic nanoparticles (iron oxide coated with cationic lipids or polymers) complexed with DNA are concentrated on the target cells by the influence of an external magnetic field and the cellular uptake of DNA is due to endocytosis and pinocytosis.

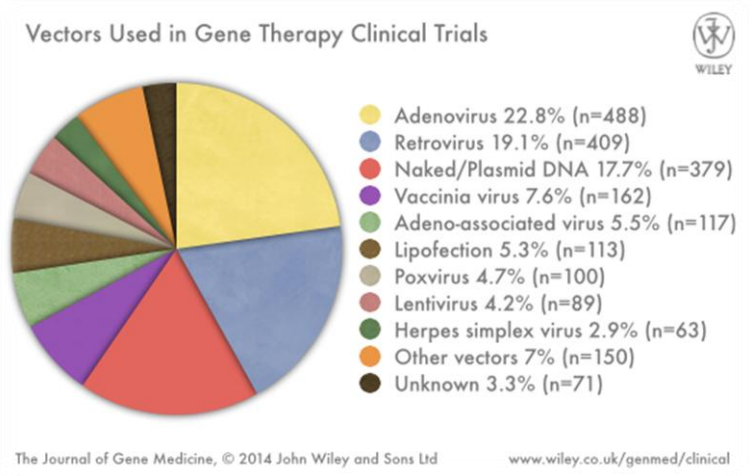

Figure 12 – Vectors used in gene therapy clinical trials.
(*In* http://www.wiley.com/legacy/wileychi/genmed/clinical/ (19/09/2014))

Nowadays, advances of non-viral delivery are still ongoing and have led to an increased number of products entering clinical trials. However, gene transfer via viral systems remains the most prevalent choice in clinical trials of gene therapy for its relatively high delivery efficiency (Figure 12) [52].

5.2 Gene delivery vectors

The application of non-viral vectors was initiated by Wolff and coworkers [56], who demonstrated that direct application of plasmid DNA (pDNA), encoding for a specific protein into animal muscle, led to the production of antibodies against this protein, which is actually the concept of the DNA vaccine. Besides vaccination, the development of highly safe and efficient vector systems for gene transfer in eukaryotic cells is the aim of gene therapy [57]. Gene therapy biosafety using non-viral vectors can be achieved if the positive traits of viruses are included and genotoxicity negative traits are eliminated. Therefore, two classes of non-viral vectors may contribute to this purpose, namely episomally maintained vectors and integrating vectors with safer integration profiles [51, 53].

Among DNA-based constructs, pDNA containing one or more therapeutic genes can be widely used. The success of pDNA gene delivery depends on its ability to overcome physical and metabolic barriers during

trafficking to the cell nucleus and also on the regulation of the transgene expression [55]. Conventional plasmid vectors can be subdivided into the bacterial backbone and the transcription unit. The bacterial backbone includes: the origin of replication, which is a particular sequence where replication is initiated and assures plasmid transmission to the progeny; the selection mark, which allows the specific selection of the cells containing the pDNA, for example an antibiotic resistance gene; the multiple cloning site (MCS), which is a short region containing several commonly used endonuclease restriction (RE) sites allowing the easy insertion of DNA of interest at this location; unmethylated CpG motifs and potentially cryptic expression signals. The transcription unit, in addition to the gene of interest, should have an efficient eukaryotic promoter for transcription initiation and polyadenylation signals (PolyA) for the transcription termination [57]. Insertion of these polyA sequences proved to improve pDNA nuclease resistance. It is especially important when administrated supercoiled (SC) pDNA is converted to the open circular (OC) and linear (L) forms within a few minutes [58]. Moreover, these DNA constructs can also contain some particular sequences that regulate the specific-site pDNA integration, such as integrase, transposase or recombinase genes [55].

Artificial chromosome technologies are another group of DNA-based constructs. YAC (yeast) and BAC (bacterial) systems have been used and new generation possibilities are becoming a reality, such as MAC (mammalian) and HAC (human), where an artificial chromosome does not integrate the host genome but is maintained in the nucleus as an extra chromosome, enabling almost unlimited possibilities to introduce multiple genes [55].

5.2.1 Minicircle System

Besides the lower gene transfer efficiency in comparison with viral systems, the short-lived transgene expression is one of the major obstacles to the development of non-viral vectors [59]. Firstly, it was proposed that the immune system responses were responsible for the loss of transgene expression caused by the hypothesized necrosis- or apoptosis-mediated cell death of transduced cells mediated by a cytotoxic immune response [60]. Unlike vertebrate DNA, the bacterial DNA is characterized by the presence and abundance of unmethylated CpG motifs. These motifs act as an alarm signal for the immune system, after binding to the Toll-like receptor 9 (TLR9) of APC, promoting a cascade of immunostimulatory events that results in the upregulation of cytokines and chemokines expression. Moreover, the binding of CpG motifs to TLR9 leads to the maturation, differentiation and proliferation of NK cells, macrophages and T cells, which themselves secrete cytokines that direct the immune system towards a TH1-dominated response [61]. For vaccination purposes, the induction of an immune response is required for the protective effect but, for therapeutic application in gene therapy, these immune reactions are clearly unwanted side effects [57, 61].

After this first hypothesis for short-lived transgene expression, a further study demonstrated that the covalent linkage of bacterial backbone DNA to a eukaryotic expression cassette is responsible for transgene silencing *in vivo*, because the co-application of bacterial backbone DNA not covalently connected to the expression

cassette had only a minor effect on transgene expression. Moreover, it was reported that three different viral and four different mammalian promoters were only silenced in the mouse liver when covalently connected to the expression cassette [62], instead of being directly inhibited by the production of IFN-γ and other cytokines, as proposed before[63].

Taken together, the results indicate that gene silencing takes place as a result of events that first occur at the bacterial backbone sequences and then spread to the expression cassette, when they are covalently linked [63]. Since transcription of genes in eukaryotic organisms is highly dependent on the chromatin structure, histone methylation was studied and the results indicated that the bacterial sequences are rapidly recognized by the mammalian cells and packed into a heterochromatic structure, characterized by the trimethylation of histone H3 Lysine 9 (H3K9me3) and low level of methylation of Lysine 4. Over time, the H3K9me3 to H3K4 ratio in the eukaryotic sequences increased gradually until it reached the value observed for the bacterial sequences, leading to the downregulation of the eukaryotic cassette expression [64]. The factors or patterns responsible for the remodeling of chromatin are still uncertain but some hypotheses have been discussed. For example, some bacterial backbone elements, namely CpG islands and other typical prokaryotic sequence elements, such as characteristic GC to AT ratios, are possible candidates for the stimulation of the remodeling of chromatin, since the recognition of prokaryotic DNA in mammalian cells may induce a defense mechanism that results in heterochromatin formation [62, 65]. On the other hand, more recently, DNA vectors with various lengths of extragenic spacer DNAs (nonbacterial, noncoding and non-genic sequences) between the 5′ and 3′ ends of the transgene expression cassette were compared in terms of their relative expression profiles after transfection into mouse liver. The results suggest that extragenic spacer reaching 1 kb or more in length, regardless of their origin, can silence transgene expression [66].

Regarding other pDNA properties, the bacterial backbone is highly rich in sequences associated with biosafety concerns, for example, antibiotic resistance markers, due to their dissemination via horizontal gene transfer. The regulatory agencies, specifically European Medicines Agency (EMA) and US Food and Drug Administration (FDA), recommend totally avoiding their use. Furthermore, it has been proposed that smaller plasmids lead to higher transfection efficiencies and have better bioavailability characteristics than larger ones, providing smaller plasmids with an advantage to overcome cellular barriers on their way to gene expression. Additionally, if a chemical transfection assay is performed, smaller plasmids minimize the amount of the transfection reagent required and the expression levels could be greatly increased by reducing the cytotoxicity of the DNA complexes [57, 67].

It seems obvious that the removal of bacterial backbone DNA, in order to overcome the silencing effects, to avoid unwanted immune responses and to reduce the vectors size, can greatly improve pDNA applied in gene therapy. Derived from conventional pDNA, supercoiled minimal expression cassettes were developed, minicircles (MC) no longer contain antibiotic resistance markers, the bacterial origin of replication and other inflammatory sequences intrinsic to bacterial backbone of pDNA (Figure 13). Besides the low risk of immunogenic responses that MC present, a number of studies have demonstrated that MC vectors greatly

increase the transgene expression in various *in vitro* and *in vivo* studies, in terms of high and persistent expression levels. Without integration into the host genome, these vectors also prevent unwanted genomic changes in the cells, demonstrating a great potential for the treatment of several diseases [57, 59, 67, 68].

A comparison between expression profiles of equimolar amounts of purified linear expression cassettes, a mixture of linearized expression cassette and the linearized bacterial backbone, uncut parental plasmid and minicircle DNA in its native structure demonstrated that supercoiled minicircle DNA was by far the most efficient form of an expression cassette to elicit persistent and high-level transgene expression [59]. Another study, based on angiogenic gene therapy application, revealed that a high VEGF expression generated by minicircle DNA stimulated efficient endothelial cell growth *in vitro*. Furthermore, minicircle DNA expressed higher VEGF compared to conventional plasmid in the tibialis anterior muscle of mice. Taken together, the results suggest that minicircle DNA encoding VEGF gene is an efficacious gene vector for angiogenic promotion [69].

Minicircle production technology is based on two steps: the recombination process and the purification methods. The first minicircle patent application belongs to Adhya and Choy from the US Department of Health (WO 94/09127, October 16, 1992). However this same application was subsequently withdrawn in November 1994. Despite the respective patent being based on MC concept, the inventors' intention was not to think about the application of MC as gene vector and for therapeutic ends. It was only in 1994 and 1995, that Seeber and Kruger (EP 0775203 and US Patent 6,573,100) and Cameron *et al.* (EP 0815214, US Patents 6,143,530 and 6,492,164 and CA 2211427) stated MC applications for gene therapy [70].

In *Escherichia coli* strains, the minicircles are the result of an *in vivo* site-specific intramolecular recombination process from a parental plasmid (PP). The parental plasmid carries the transcription unit flanked by two recognition sites of a site-specific recombinase. The *in vivo* induction of the expression of the respective recombinase results in the excision of the interjacent DNA sequences, dividing the parental plasmid into two supercoiled molecules: a replicative miniplasmid (MP) carrying the undesired bacterial backbone sequences and a minicircle carrying the therapeutic expression unit (Figure 13) [57, 67].

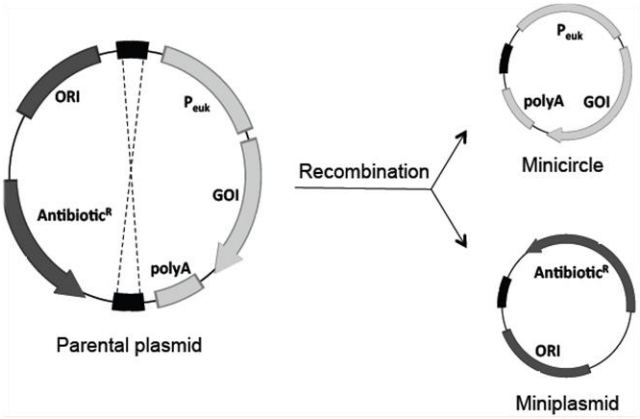

Figure 13 - MC production mechanism: MC and MP formation from the PP [71].

There are some recombination systems, which use different recombinases from different origins, recombination recognition sites and induction processes (Table 4). An efficient recombination process requires the stringent control of repression and expression of the site-specific recombinase in *E. coli*. For example, the expression system should efficiently silence gene expression before induction to avoid premature

recombination [57, 71]. The temperature-sensitive lambda *cI*857/p_R promoter [72] and the P_{BAD}/*araC* arabinose expression systems [59, 73] have been shown to be able to inhibit background expression of the recombinases in the uninduced state. Moreover, recombination efficiency as well as final MC yield are strongly influenced by the cell physiology at the time of induction, because the plasmid yield as an intracellular product is related to final biomass yield, but the recombinase expression and activity is diminished in the later stages of growth [71].

Table 4 – Recombination systems applied in minicircle production [57].

Recombinase Family	Recombinase	Origin	Recombination target sites	Type of Induction	Recombination Specifications
Tyrosine recombinase family	Cre Recombinase	Bacteriophage P1	*loxP*	Arabinose Induction	Intra and intermolecular recombination events
	FLP Recombinase	*Saccharomyces cerevisiae* (yeast plasmid 2-µm circle)	FRT	Heat Induction	Intra and intermolecular recombination events
	λ Integrase	Bacteriophage λ	*attB* and *attP*	Heat Induction	Intra and intermolecular recombination events
Serine recombinase family	φC31 Integrase	*Streptomyces* Bacteriophage φC31	*attB* and *attP*	Arabinose Induction	Unidirectional and intramolecular recombination event
	ParA Resolvase	Broad host range plasmids RK2 and RP4	MRS	Arabinose Induction	Unidirectional and intramolecular recombination event

Also some *in vitro* methods were developed for the MC production, claiming the elimination of residual sequences (scar) generated during the recombination process [74, 75]. One of these methods is based on PCR (Polymerase Chain Reaction) amplification and ligation, which takes less time, avoids the need for the specific bacterial strains and prevents the scar sequences [75]. However, the PCR process will increase the risk of mutation in the target gene [74]. More recently, another approach based on a series of enzyme-catalyzed reactions was developed. The recombination process was mimicked *in vitro* by the introduction of two mirror-symmetry pairs of restriction enzyme sites, which allow the digestion of the plasmid into bacterial backbone and transcription unit. Then, by the action of a phosphatase, the DNA segments cannot religate, unless the transcription unit is further single digested, having the phosphate groups to recircularize again in presence of T4 ligase. The linear fragments can be removed by digestion with an exonuclease and the MC is further purified. Therefore, the requirement of specific bacterial strains, culturing, inducing strategy and the mutation risk in MC caused by PCR amplification are eliminated. On the other hand, MC molecules are not in supercoiled form, which is a disadvantage for further therapeutic applications [70, 74].

Minicircle purification is one of the major limiting steps of industrial minicircle production, hence new strategies have been developed over time. Minicircle purification protocols aim to separate the MC from the MP and residual non-recombined PP, if it exists, which is a hard task since they have very similar physico-chemical properties. Most of the studies have been using a method where an enzyme restriction digestion is performed first. In the DNA mixture, only MP and PP are digested, once restriction sites are present in bacterial backbone of the initial pDNA, while the MC keeps its native structure. This strategy was first disclosed in US application 11/249929 by *Bigger et al.* priority date April 10, 2001, together with exonuclease treatment for the removal of restriction fragments deriving from MP or non-recombined PP [70]. After enzymatic digestion, MC can also be purified via CsCl-EtBr density gradient ultracentrifugation [57, 67]. The major disadvantages of this method are low yield of minicircle DNA, high costs of enzymes, toxicity and labor intensity, not suitable for large-scale minicircle purification. If the digestion step is not performed, supercoiled PP, MP and MC would not be successfully separated. Another developed approach consists on the PP and MP degradation *in vivo* by co-expression of a homing endonuclease (I-*Sce*I) with the φC31 integrase, after addition of arabinose (US Patent 7,897,380 to Kay and Chen based on an application with priority date August 29, 2002) [70, 76]. This restriction enzyme does not recognize sequences in the bacterial genome, only in the backbone sequence in PP. MP as well as PP are degraded by linearization and the activity of bacterial exonucleases (Figure 14) [76]. MC lower yields were observed with this method, so insertion of more copies of P_{BAD}-φC31 and P_{BAD}-*I-SceI* into chromosome of BW27783 strain was implemented, leading to better yields and fewer impurities [76].

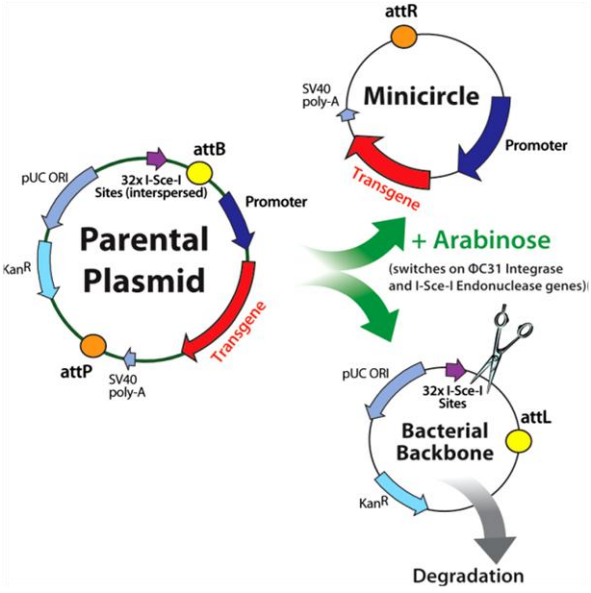

Figure 14 – Recombination and degration of MP and PP *in vivo* by co-expression of a homing endonuclease (I-*Sce*I) and the φC31 integrase via arabinose induction (*In* http://www.systembio.com/downloads/SBInsights_vol5.pdf)

Alternatively, excellent selectivity, speed and scale-up possibilities can be achieved with chromatography methods: anion exchange chromatography where negatively charged DNA will establish more or less interactions with the positively charged solid support depending on their size and structure [71]; and affinity chromatography in the presence of a recognition sequence in the PP that, after the induction and recombination, is located in the MC in a way that makes it possible for this sequence to interact with a solid support for purification [70, 77, 78]. One example is based on the interaction of a direct tandem repeat of modified lactose operator (lacO) sites present in pDNA with the repressor of the lactose operon (LacI) immobilized on the solid support [78]. This system assumes highly efficient recombination, because if it does not occur, MC and PP cannot be efficiently separated [57]. Other example refers to a specific affinity binding of an oligonucleotide to a recognition sequence in the MP, which is retained by the formation of a triple-helix with the oligonucleotide. This interaction was also used to immobilize MC on a chromatography column during

purification [70]. Furthermore, a method for purification of the MC is described in EP 1620559, wherein the minicircle is immobilized by a protein in the plasma membrane of the producing bacteria upon induced lysis and can be then isolated by chromatographic step [70]. Regarding the recent *in vitro* production of aforementioned, the purification of MC products can be achieved by a simple DNA precipitation method, which provides good potential for manufacturing the minicircle DNA vectors, without complex and expensive purification techniques [74].

Nowadays, the lack of efficient technologies for large scale production of MC is limiting the application of this system to gene therapy and DNA vaccination, because quantities on the order of grams and kilograms are necessary to perform preclinical and clinical trials. Currently, in contrast with the pDNA production, the MC production does not exceed the concentration of 9mg/L [79]. Once a high ratio of recombinase to plasmid is necessary to yield high recombination rates, these lower yields can be explained to a small number of recombinases or their reduced activity in the growth phase of maximum production of PP. Moreover, for the clinical use of minicircle become a reality, improved purification methods are required [80].

5.2.2 Other therapeutic systems

In addition to the DNA-based methods, mRNA-based strategies are an option if a transient presence of therapeutic proteins is required. The genes of interest can be transcribed *in vitro* into mRNA and then mRNA is delivered into the target cells and translated into the desired proteins. Nuclear transport is not required and there is no risk of an insertional mutagenesis because genome integration does not happen. Also, due to the high transfection efficiency, it is possible to efficiently transfect cells that are resistant to transfection. However, once mRNA is unstable and vulnerable to intracellular degradation, its transfection is temporary and gradually declines over time. New strategies have been employed to stabilize exogenous mRNA molecules in the cytoplasm [55].

Non-viral gene transfer is not only of interest for transfection of protein-encoding plasmids [67]. In addition to direct gene expression based on the induction of DNA or mRNA, there also exist a number of regulatory RNAs, which are highly interesting in a gene therapy setting. It is possible to apply regulatory RNA sequences, to regulate native gene expression. These short, non-protein-coding RNA sequences, microRNA (miRNA) and small interfering RNA (siRNA), interact with mRNA molecules, causing the inhibition of their translation and posterior cleavage, which results in the silencing of gene expression (Annex 2) [15, 55]. This solution permits the silencing of selected genes, which causes some beneficial biological effects. Recently, micro-minicircles (miMC), which consists of MC vectors encoding short regulatory RNAs were produced and their properties *in vivo* and *in vitro* were tested [81].

5.3 MSC as gene therapy vehicles

Stem cell therapy is a promising strategy for overcoming the limitations of current treatment methods. In gene therapy, stem cells hold great potential for successful use, since repeated administrations can be reduced or probably eliminated, due to their ability of self-renewal. To fully exploit stem cells' potential, the modification of their properties may be required. The increasing knowledge about stem cell and molecular biology has opened up new strategies for manipulating the fate and the functionality of stem cells. Genetic engineering methodologies to induce gene expression in stem cells in an accurate and well-controllable manner are particularly attractive and offer several advantages over conventional gene therapy, namely avoiding direct administration of vectors and complexes into the recipient organism [55, 82]. Manipulation of stem cells' properties by gene transfer can be used for many purposes: to reconstruct organs, to deliver factors in order to retard regenerative processes or to deliver molecules for therapeutic use [82].

MSC have been explored as a vehicle to deliver genes into tissues for gene therapy applications, particularly due to their unique biological properties which were previously analyzed: migration ability to sites of ischemia or injury and their immunomodulatory and immunosuppressive properties in the host upon local transplantation or systemic administration [20-22, 33]. A gene therapy with Adenovirus-transduced MSC, due to anti-inflammatory properties of these cells, is less immunogenic than direct administration of Adenovirus vectors [25]. Gene transfer efficiencies above 50% are achieved when viral vectors are used to transduce MSC, however very high viral titres seem to be required [25, 83]. Although MSC are less accessible to transfection using non-viral vectors, from the current non-viral methods available, liposome carriers and electroporation-based gene transfer techniques were determined to be the most efficient for transfecting MSC. Despite being effective in transfecting stem cells, electroporation leads to high cell death. Some lipofection reagents were able to successfully introduce transgenes into MSC, while these cells maintained their proliferation capacity and ability to differentiate into different mesodermal lineages without loss of transgene expression [84, 85]. Some modifications of lipoplexes can further enhance gene expression, such as recombinant peptides, for example, TAT peptides or nuclear localization sequence (NLS) peptides, because they allow the overcoming of cellular and nuclear barriers [86, 87].

These improvements to non-viral gene delivery systems hold substantial prospective to replace viral vectors, still a successful gene therapy based on MSC depends not only on the delivery method and the adopted gene therapy strategy but also on the cells, the vector, the therapeutic genes to be delivered and the promoter. It has been reported that the efficiency of MSC transfection decreases with the cell passage number [54]. At the end, all these systems will also require certifications for immunogenicity, duration of expression and other toxicities in *in vivo* testing [25].

5.3.1 VEGF-expressing MSC for cardiac repair

The main beneficial mechanism of MSC for cardiac repair is the enhanced production of anti-inflammatory and pro-repair factors, although cardiomyocytes production *via* MSC differentiation was initially considered [25, 88]. MSC have demonstrated to express VEGF and other proteins which promote angiogenesis [2, 20, 24]. However, these proteins are not found naturally in cultured MSC, but rather are expressed when MSC are exposed to specific microenvironments, for example cardiac tissue. Many studies have shown that VEGF expression is upregulated in hypoxic conditions [48]. In preclinical studies, MSC were shown to engraft and improve cardiac repair after administration. Clinical trials using MSC to improve cardiac function have also yielded encouraging results [89]. However, the MSC regenerative capacity is limited partly by the insufficient expression of angiogenic factors and low survival rate of the transplanted cells [2, 49]. As a result, a combination of cell and angiogenic gene therapies would improve this poor viability [58, 90]. For example, transplant of MSC modified with an Adeno-associated viral vector to overexpress VEGF under hypoxic conditions increased MSC cell survival, induced angiogenesis and improved overall heart function [49]. Also, MSC-based VEGF gene therapy in rat myocardial infarction model using a non-viral delivery system (facial amphipathic bile acid-conjugated PEI conjugates) improved cell viability, particularly during severe hypoxic exposure *in vitro* and enhanced the capillary formation in the infarction region after transplantation [91]. In another study, in agreement with the fact that MSC do not express VEGF receptors, the overexpression of VEGF in MSC did not exert any significant effects in the receptor-mediated autocrine processing, but the migration of endothelial cells, which are well known for being responsive to VEGF, increased when exposed to supernatant of MSC overexpressing VEGF. Moreover, control MSC showed only a limited improvement of blood flow on *in vivo* ischemic limb, whereas MSC overexpressing VEGF showed a clear improvement in revascularization over time by restoration of blood flow [92]. Thus, MSC overexpressing VEGF cell populations seem to be the best preclinical candidate to be considered for further testing in revascularization studies. Additionally, a combination of overexpression of VEGF and more genes with complementary mechanisms of action has already revealed benefic effects in acute myocardial infarction compared to the expression profile to MSC transduced with each gene individually (VEGF and stem cell homing/retention factor SDF-1 cassete) [93]. Pro-VEGF therapy may also be an effective approach to prevent occlusive artery and ischemic heart and limb disease.

6. Transient engineered human MSC to promote angiogenesis: Master Thesis Overview

More research is needed in order to determine the mechanisms and biological properties of MSC to enhance their therapeutic efficacy in various diseases, particularly in cardiovascular diseases since they represent a worldwide emergency. The genetic modification of MSC seems to be an interesting option to improve their therapeutic potential and short-term therapeutic gene expression conjugated with the transient paracrine effects of MSC may be sufficient to promote cardiac damage repair. Besides the need to generate an

environment that mimics the niche of MSC *in vivo* and the optimization of serum-free culture conditions for large-scale therapeutic MSC production, finding a safe and highly efficient non-viral gene delivery system for MSC is also a priority [25].

Therefore, this master thesis project aimed to overexpress VEGF in a sustained and transient manner through genetic manipulated human MSC from BM in order to promote controlled angiogenesis in further *in vivo* studies, where cardiovascular diseases have led to the damage and injury of the cardiac tissue. These human MSC at different cell passages were genetically engineered through the application of a non-viral delivery system using minicircles and are expected to represent an interesting tool for therapeutic purposes.

In our laboratory, a new minicircle system, believed to be robust and scalable to industry, has been undergoing development. The recombinase chosen was the ParA resolvase. This is considered to be the most effective recombinase among all site-specific recombination systems and it catalyzes the *in vivo* recombination between two sites for the resolution of multimers (MRS) [94]. In our strategy, this recombinase is under the transcriptional control of the P_{BAD}/AraC system. In presence of arabinose in culture media, this sugar binds to AraC protein stimulating the mRNA transcription from P_{BAD}, whereas in absence of arabinose, the AraC protein acts negatively to repress transcription by forming a locking loop [95]. The first times this system was used, an unwanted recombination of the PP in MC and MP in the initial phase of replication was observed due to the leaky expression of the ParA resolvase by the P_{BAD} promoter. As a result, MP species dominate the plasmid population in the cell before the recombination induction, since it contains an origin of replication. Although the addition of glucose would prevent this leaky expression of ParA from P_{BAD} through low cAMP (Cyclic Adenosine Monophosphate) levels [95], in conditions wherein the pH is not controlled, this sugar also leads to the pH decreasing, resulting in an inhibition of cell growth and PP production, and subsequently the MC production being compromised [71, 96]. Therefore, buffering solutions or minimal pH control solutions, for example, bromothymol blue pH indicator should be used during the fermentations [71, 96].

Apart from the choice of the recombinase, to achieve better expression levels, it was essential to define where the recombinase gene should be located (*E. coli* chromosome or plasmid). Thus, three different systems for recombination were created: the ParA gene was placed in the PP; the resolvase gene was expressed from a low-copy helper plasmid and the gene was inserted in a single copy in the chromosome of the host strain. Furthemore, the ribosome binding site (RBS) was modified, in order to increase the expression of ParA, due to the greater efficiency of the translation of the resolvase transcript in the host [71].

For the construction of these three systems, the *E. coli* BW27783 strain (*F^-, Δ(araD-araB)567, ΔlacZ4787(::rrnB-3),$λ^-$, Δ(araH-araF)570(::FRT), ΔaraEp-532:FRT, ϕP_{cp8}araE535, rph-1, Δ(rhaD-rhaB)568, hsdR514*) was used and modified [97]. This strain is capable of more easily uptaking arabinose present in the culture medium due to the constitutive expression of a low-affinity high-capacity arabinose transporter AraE, being more sensitive to the arabinose induction [97]. To create the BWAA strain, which is capable of producing high amount of plasmids and easily absorbing the arabinose, the *E. coli* BW27783 strain was modified by the deletion of *endA* (responsible for non-specific digestion of pDNA) and *recA* (responsible for DNA homologous recombination) genes. On the

other hand, *E. coli* strains BW1P and BW2P were designed to express ParA resolvase from a chromosome's single copy by disrupting the *endA* gene via the insertion of the P_{BAD}*/araC-parA* (BW1P) or P_{BAD}*/araC-RBS-parA* (BW2P) cassettes into the *E.coli* BW27783 chromosome, followed by *recA* knockout [71].

For the construction of the parental plasmid backbones used in this study, commercially available pVAX1 plasmid (Invitrogen), which contains the human cytomegalovirus (CMV) immediate-early promoter and a kanamycin resistance gene for bacterial selection, was modified thourgh the insertion of the Green Fluorescence Protein (GFP) gene, giving the pVAX-GFP [58]. Then, the pVAX-GFP was modified through the insertion of the P_{BAD}*/araC-parA* cassette and two MRS flanking the eukaryotic expression cassette, giving the pVAXmini [96]. By deleting the P_{BAD}*/araC-parA* region of the pVAXmini, pMINI was obtained [71].

The results of the three production systems showed relatively similar recombination efficiencies (Table 5), except when the resolvase transcript did not present the optimized RBS and the gene was inserted into a single copy in the chromosome. This exception showed that improvements made in the *parA* gene RBS in strain BW2P effectively led to a more accurate and efficient translation of the corresponding mRNA [71].

Table 5 – Recombination efficiencies in the constructed systems based on the resolvase gene localization and the RBS sequence (Adapted from [80]).

***E. coli* Strain**	***ParA* gene localization**		**RBS**	**Parental Plasmid**	**Recombination Efficiency (%)**
BWAA	Parental Plasmid		Original	pVAXmini	88
BWAA	Low-copy Helper Plasmid (≈10 copies)	pMMBparA	Original	pMINI	88
		pMMBpar2A	Optimized		91
BW1P	Chromosome (1 single copy)		Original		33
BW2P			Optimized		90

A quantitative real-time PCR analysis showed that *E. coli* BWAA cells contained more *parA* gene copies than BW1P and BW2P cells and consequently the recombination of pMINI proceeded faster when ParA resolvase was expressed from the low copy number plasmids [71, 98]. However, the BW1P and BW2P strains are advantageous in terms of minicircle purification over systems relying on helper plasmids due to the presence of fewer plasmid species in the process streams. Therefore, the BW2P strain (Figure 15) was selected for further studies, namely high cell density fermentation process for minicircle production, which led to volumetric titers of 53.7mg/L total pDNA which were at least 10 times higher than those described in the literature [71].

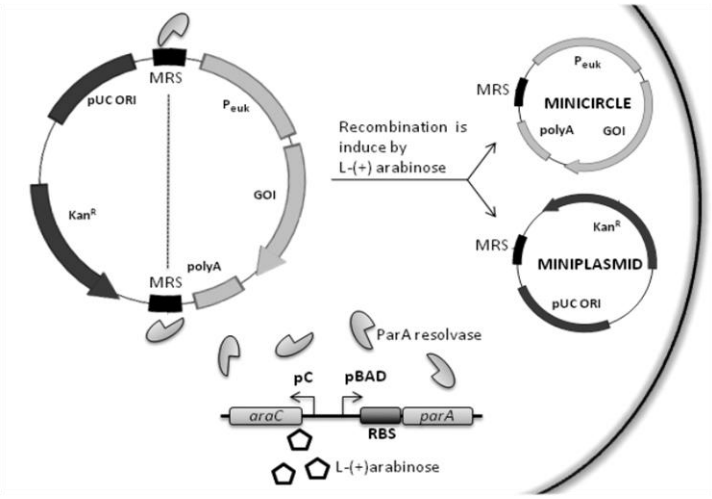

Figure 15 - Minicircle production in BW2P strain[80].

Regarding the purification methods developed in our laboratory, the PP were designed to have some PvuII restriction sites in the bacterial backbone, which would allow the specific digestion of the PP and MP. Plasmids pMINI5, pMINI7 and pMINI8 were constructed by adding PvuII restriction sites to the original pMINI, which already contains two restriction sites for PvuII. Afterwards, the DNA mixture is separated by monolith anion exchange chromatography (AEC), according to the exposed negative charges and their respective electrostatic interactions with a DEAE (diethylaminoethyl) monolith. Optimized separation resulted in two distinct peaks, one containing digested linear fragments and the other representing MC [71]. In parallel with this master thesis, another purification method was optimized for MC separation, namely the hydrophobic interaction chromatography (HIC), using a Phenyl Sepharose 6 Fast Flow resin [99]. This was proposed since the bacterial backbone of pMINI and its derivatives also contain a Nb.BbvCI DNA nickase site, which provides the relaxation of MP molecules and PP, if it exists, by the formation of one nick in their double-stranded chains. Subsequently, due to the different hydrophobicities and interaction with the matrix, in the presence of a kosmotropic salt, the separation of MC from the MP and PP relaxed species is possible.

Using the minicircle system developed in our lab and previously described, four different parental plasmids, based on pMINI8 without P_{BAD}/*araC-parA* cassette (pMINILi), were constructed. Once the single copy of P_{BAD}/*araC-parA* with optimized RBS in *E.coli* BW2P strain demonstrated to be sufficient to control the efficient *in vivo* site-specific recombination to the minicircle production, the P_{BAD}/*araC-parA* cassette from parental plasmid pMINI8 was deleted. The constructed plasmids, besides the origin of replication, the kanamycin resistance gene, the two MRS, the BGH (Bovine Growth Hormone) polyadenilation signal and the PvuII restriction sites, include the VEGF and GFP genes regulated by different promoters. Based on the reported different strengths of some promoters, four were chosen: the human cytomegalovirus immediate-early (CMV) and human elongation factor 1 alpha (hEF1α) promoters and two alternative versions of CMV and hEF1α promoters: one is composed by a CpG free version of mouse CMV enhancer and hEF1α core promoter (mCMV+hEF1α CpG free) and the other containing only the hEF1α CpG free core promoter.

After the *E. coli* transformation with the different parental plasmids, the MC were produced as a result of the *in vivo* site-specific recombination process induced by the presence of arabinose. Subsequently, MC were purified by two different chromatographic methods: AEC and HIC. In order to assess the bioactivity of all molecules after purification, evaluate transfection efficiency and quantify gene expression by the different promoters throughout the time, BM MSC were transfected, using microporation protocols previously optimized for this type of cells [100]. In contrast to standard cuvette based electroporation methods, microporation is a unique electroporation technology that uses a pipette tip as the reaction chamber and a capillary type of electric chamber. The pipette tip maximizes the gap size between the two electrodes while minimizing the surface area of each electrode. This special design and characteristics lead to a high but more uniform electric field, minimal pH variation, less metal ion formation and insignificant heat generation in the biological sample. As a result, higher transfection efficiency and cell viability are achieved in comparison with the conventional electroporation [100-102].

7. Materials and Methods

7.1 Plasmids construction

All designed primers that were used for vector construction or confirmation were synthetized by Stabvida (Lisbon, Portugal), with exception of GFP_Fwd, GFP_Rev and BGH_Fwd, which are from Sigma® (Annex 3). The PCR amplifications were performed using a KOD Hot Start Master Mix (Novagen®) according to the manufacturer instructions (Table 6 and Table 7) and using PCR Thermocycler Biometra® TGradient.

Table 6 – PCR mixture composition according to the KOD Hot Start Master Mix (Novagen®).

Component	Volume	Final Concentration
10X Buffer for KOD Hot Start DNA Polymerase	5µL	1X
25mM $MgSO_4$	3µL	1.5Mm
dNTPs (2mM each)	5µL	0.2mM (each)
Forward primer (10µM)	1.5µL	0.3mM
Reverse primer (10µM)	1.5µL	0.3Mm
KOD Hot Start DNA Polymerase (1U/µL)	1 µL	0.02U/µL
DNA template	Equivalent volume to 10ng	0.2ng/µL
H_20	Remaining volume	
Total reaction volume	50µL	

Table 7 – PCR conditions according to the KOD Hot Start Master Mix (Novagen®).

Step	Target Size			
	<500bp	500-1000bp	1000-3000bp	>3000bp
1. Polymerase activation	95°C for 2min			
2. Denaturation	95°C for 20s			
3. Annealing	Lowest Primer T_m (°C) for 10s			
4. Extension	70°C for 10s/kb	70°C for 15s/kb	70°C for 20s/kb	70°C for 25s/kb
N° of cycles	20-40 Cycles			

Plasmid purifications were performed according to the High Pure Plasmid Isolation Kit protocol (Roche). Purified plasmids were used directly after purification or stored at -20°C. The respective plasmid concentrations were determined using Nanodrop Spectrophotometer (Nanovue™ Plus, GE Healthcare).

DNA digestions with restriction enzymes for pattern confirmations were performed, when possible, in a total volume of 20µL for 1h30 at the corresponding incubation temperature. The mixtures included the volume relative to 500ng of pDNA, the desired restriction enzyme, the corresponding restriction enzyme buffer and water to complete the total volume. Restriction mixtures were loaded onto 1%(w/v) agarose gels (Seakem® Agarose, Lonza) and electrophoresis was carried out at 100V or 120V for a suitable period of time, with TAE buffer (40mM Tris base, 20mM acetic acid and 1mM EDTA, pH 8.0). Gels were stained in ethidium bromide and

visualised with an Eagle Eye II image acquisition system from Stratagene. Gel band extractions were performed according to the NZYGelpure kit instructions (NZYTech).

DNA ligations were performed using 0.5µL T4 ligase enzyme (3U/µL, Promega), 1µL T4 ligase buffer 10X, a certain quantity of vector and insert considering a 3:1 insert/vector molar ratio and water to complete the total volume of 10µL. The ligation mixtures were incubated for 3 hours at room temperature and overnight at 4°C.

E.coli DH5α and BW2P transformations were performed by heat shock protocol, wherein 50 µL of chemically competent cells were gently thawed on ice and mixed with 5 pg-100 ng (less than 5µL) of DNA. After 20 min of incubation on ice, the mixture was submitted to 42°C for 1min and then cells were immediately incubated for 2 min on ice. After that, the mixture was resuspended with 800µL of LB (Luria-Bertani, Sigma®) medium and after 1 hour of recuperation at 37°C, transformed cells were plated on LB agar plates with the antibiotic (30µg/mL of kanamycin) and, in the case of the BW2P strain, also with 0.5% (w/v) glucose (Fisher Scientific). The *E.coli* DH5α plates were incubated overnight at 37°C and the BW2P plates at 30°C. Glucose was prepared at a concentration of 20%(w/v).

E.coli DH5α cell banks were prepared from single colonies picked from LB agar plates containing the appropriate antibiotic (30µg/mL of kanamycin). Then, colonies were inoculated in 5mL of liquid LB medium supplemented with the antibiotic. Cultures were grown to reach the exponential phase (OD_{600nm}≈1.0) at 37°C, 250rpm and frozen at -80°C in a final concentration of 50% (v/v) of glycerol 30% (v/v). BW2P cell banks were prepared on the same conditions as *E.coli* DH5α cell banks, but the LB agar plates contained additionally 0.5% (w/v) glucose and the liquid LB medium was supplemented also with 0.5% (w/v) glucose. Moreover, the growth temperature was 30°C instead of 37°C.

The expected plasmid and minicircle constructions were confirmed by DNA sequencing of modified regions by Stabvida (Lisbon, Portugal) and their representation was performed using SnapGene® Viewer 2.5.

7.1.1 pMINILi construction

pMINILi plasmid (3987bp) is derived from the parental plasmid pMINI8 (4702bp)[71] by deletion of the P_{BAD}/*araC-parA* cassette (715bp). Firstly, using a directed mutagenesis strategy, one AgeI restriction site was inserted in pMINI8 via PCR amplification. The PCR conditions included the annealing temperature of 56°C, the extension time of 2min and 30 cycles. Then, 1 µL of restriction enzyme DpnI 10U/µL (Promega) was added directly to the PCR mixture to digest the methylated and non-mutated supercoiled dsDNA template for 1h30 at 37°C. Competent *E.coli* DH5α were transformed with the digested PCR mixture and plated on LB agar supplemented with kanamycin (30µg/mL) overnight at 37°C. Some colonies were selected and grown at 37°C, 250rpm in 5mL of liquid LB medium supplemented with kanamycin until reaching an OD_{600nm}≈2.0. After pDNA

purification, positive colonies were screened by AgeI and BamHI restriction pattern analysis of mutated pDNA. Using the same methodology and conditions, another AgeI restriction site was created in pMINI8. After these modifications and pDNA purification, AgeI digestion was performed, leading to the division of the modified pMINI8 into two fragments, the P_{BAD}/*araC-parA* cassette (715bp) and the remaining vector (3987bp). The band corresponding to the plasmid fragment without the P_{BAD}/*araC-parA* cassette was excised from the gel and purified. Subsequently, the purified linear fragment was religated by the action of the T4 ligase, giving the pMINILi vector. *E.coli* DH5α and BW2P strains were transformed with this new parental plasmid and after pDNA purification, SalI restriction pattern as well as DNA sequencing with the BGH_Fwd primer were confirmed.

7.1.2 pMINILi-CMV-VEGF-GFP construction

pMINILi-CMV-VEGF-GFP plasmid (4563bp) was constructed by the insertion of VEGF gene fragment into the pMINILi. The VEGF gene fragment was obtained by double digestion of the pVAX-VEGF-GFP (4273bp) with EcoRI and KpnI restriction enzymes. After gel electrophoresis, the band corresponding to VEGF gene fragment (611bp) was excised from the gel and purified. At the same time, pMINILi was also digested with the same enzymes and the resulting vector band (3952bp) was excised from the gel and purified. Afterwards, the digested pMINILi and the VEGF gene fragment were ligated and *E.coli* DH5α and BW2P strains were transformed. After bacterial growth and pDNA purification, NcoI and EcoRI+KpnI restriction patterns as well as DNA sequencing with the T7_Fwd primer were confirmed.

The pVAX-VEGF-GFP was constructed previously in our laboratory by the insertion of the synthesized VEGF gene (present in a pUC vector, NZYTech) into the pVAX-GFP [58], using EcoRI and KpnI restriction enzymes for the digestion of both vectors (João Trabuco personal communication).

7.1.3 pMINILi-hEF1α-VEGF-GFP construction

pMINILi-hEF1α-VEGF-GFP plasmid (4475bp) was constructed from pMINILi-CMV-VEGF-GFP by changing the CMV to the hEF1α promoter. After the growth at 37^{o}C and 250rpm of *E.coli* XL10-Gold strain containing the phEF1α (7889bp), the respective plasmid was purified and used to obtain the hEF1α promoter fragment (587bp) by PCR amplification, using the primers Ef1a_Fwd and Ef1a_Rev. The PCR conditions included the annealing temperature of 56^{o}C, the extension time of 1min and 30 cycles. After digestion of the hEF1α promoter fragment with KpnI and SpeI restriction enzymes, the DNA fragment was purified in a miniprep column using the protocol steps for pDNA purification after the cell lysis. In parallel, pMINILi-CMV-VEGF-GFP was also digested with the same enzymes and after electrophoresis, the resulting vector band (3895bp) was excised from the gel and purified. Subsequently, the digested pMINILi-VEGF-GFP and the hEF1α promoter fragment were ligated and the mixture was used to transform *E.coli* DH5α. After the growth of some

transformed *E.coli* DH5α colonies, plasmid purification and EcoRI digestion were perfomed to confirm the presence of the right plasmid. Since MC AEC purification method requires a initial PvuII enzimatic digestion, which will only digest MP and PP, the PvuII restriction site on hEF1α promoter sequence was eliminated by directed mutagenesis via PCR amplification, as described for pMINILi, using the primers hEF1a_PvuII_Fwd and hEF1a_PvuII_Rev. The PCR conditions included the annealing temperature of 56^{o}C, the extension time of 2min and 30 cycles. *E.coli* DH5α and BW2P strains were transformed with pMINILi-hEF1α-VEGF-GFP and DNA sequencing with the Promoter_Fwd primer confirmed the correct plasmid.

7.1.4 pMINILi-mCMV+hEF1α(CpG free)-VEGF-GFP construction

pMINILi-mCMV+hEF1α(CpG free)-VEGF-GFP plasmid (4560bp) was constructed from pMINILi-CMV-VEGF-GFP by changing the CMV to the mCMV+hEF1α(CpG free) promoter. The *E.coli* GT115 strain, containing the pCpG free-mcs plasmid (3049bp, InvivoGen), which includes the required promoter, was grown in liquid LB medium supplemented with zeomycin (25μg/mL, stock solution 100μg/mL) at 37^{o}C and 250rpm. The respective plasmid was purified and used to obtain the promoter fragment (761bp) by digestion with PstI restriction enzyme. After electrophoresis, the promoter fragment band was excised from the gel and purified. At the same time, pMINILi-CMV-VEGF-GFP was digested with the same enzyme and after electrophoresis, the resulting band (4563bp) was excised from the gel and purified. Subsequently, the linearized pMINILi-CMV-VEGF and the promoter fragment were ligated and the mixture was used to transform *E.coli* DH5α. After growth of some transformed *E.coli* DH5α colonies, plasmid purification and HindIII digestion were perfomed to confirm the presence of the promoter and its correct orientation. Because the initial promoter fragment had approximately unnecessary 100bp, previous HindIII digestion was used to achieve the proper sized promoter fragment (671bp) which was then cloned into pMINILi-CMV-VEGF-GFP plasmid digested also with HindIII, obtaining the provisional pMINILi-CMV-mCMV+hEF1α(CpG free)-VEGF-GFP plasmid (5234bp). After *E.coli* DH5α transformation, growth and plasmid purification, KpnI digestion was performed to confirm the ligation. Finally, NheI and MluI digestions removed the original CMV promoter and by S1 nuclease action, the sticky ends were eliminated and the pMINILi-mCMV+hEF1α(CpG free)-VEGF was religated. *E.coli* DH5α and BW2P strains were transformed and after plasmid purification, NcoI digestion confirmed the expected band pattern and DNA sequencing with the Promoter_Fwd primer was required.

7.1.5 pMINILi-hEF1α(CpG free)-VEGF-GFP construction

Derived from the aforementioned provisional pMINILi-CMV-mCMV+hEF1α(CpG free)-VEGF-GFP (5234bp), the pMINILi-hEF1α(CpG free)-VEGF-GFP (4125bp), was constructed by deletion of the original CMV promoter and the enhancer mCMV using a single SpeI restriction digestion. After agarose gel electrophoresis, the plasmid band was excised from the gel, purified and religated by T4 Ligase. *E.coli* DH5α and BW2P strains were

transformed and after plasmid purification, NcoI digestion confirmed the expected band pattern and DNA sequencing with the Promoter_Fwd primer was ordered.

7.2 Plasmids and Minicircles production

5mL of LB medium supplemented with kanamycin (30µg/mL) and 0.5% (w/v) glucose were inoculated with a loop of frozen *E.coli* BW2P from each cell bank and incubated overnight at 37°C, 250 rpm. Next, an appropriate volume of the first seed culture was used to inoculate 30mL of LB media also supplemented with kanamycin (30µg/mL) and 0.5% (w/v) glucose up to an initial OD_{600nm} of 0.1. Before the inoculation, the specific culture volume was centrifuged at 6000g to remove the exhausted culture medium and to obtain a cell pellet, which was resuspended in fresh culture media. Cultures were then incubated at 37°C and 250rpm until reaching an OD_{600nm} close to 2.5 (mid-exponential phase). At that moment, an appropriate volume of seed culture was once again used to inoculate in 2L erlenmeyers 250mL of LB medium supplemented only with kanamycin (30µg/mL) and to achieve an initial OD_{600nm} of 0.1. Cultures were then incubated at 37°C and 250rpm. Monitoring the OD_{600nm} during the growth, in this study, recombination induction was performed at OD_{600nm} between 2.4 and 3.6. Also, the pH was checked whether the values were between 7.0 and 8.5. The recombination was induced by adding 0.01% (w/v) of 20% (w/v) L-(+)-arabinose (Merck Millipore) directly to the medium and recombination was allowed to proceed for 2 or 5 hours. 2mL culture samples at the induction time and during induction (2h or 5h) were withdrawn hourly to allow recombination characterization on agarose gel electrophoresis. The final culture was centrifuged to obtain cell pellets that were stored at -20°C for further purification. The same protocol was performed for cell cultures in 500mL of LB medium.

7.2.1 Analysis of recombination efficiency by densitometry

2mL culture samples collected before and after recombination induction were used to isolate the respective pDNA. Specifically, purified plasmids relative to the final culture time were digested with SacII, a restriction enzyme with only one restriction site on the MP and, respectively, on the PP. After gel electrophoresis of the SacII restriction mixtures, the recombination efficiency was calculated on the basis of band intensities obtained with the ImageJ software (peak areas) and normalized for molar amounts using the following equation [71, 96]:

$$E_r(\%) = \left(1 - \frac{PP_{mol}}{MP_{mol}+PP_{mol}}\right) \times 100 \quad \text{(Equation 1)}$$

where E_r is the efficiency of recombination, PP_{mol} is the molar amount of parental plasmid and MP_{mol} is the molar amount of miniplasmid.

7.3 Minicircle purification

The cellular lysis and purification of the total pDNA was performed with Endotoxin-free Plasmid DNA Purification NucleoBond® XtraMidi kit (Macherey-Nagel), according to the manufacturer protocol and also using half of the columns suggested by the manufacturer.

After the determination of the concentration of the purified pDNA mixture, the recombined and purified plasmids were subjected to enzymatic digestion for 3h at 37^{o}C. Since two different chromatographic purification protocols were performed, two different enzymatic digestions were also realized. For AEC, total pDNA was digested by adding 1U of PvuII (50U/µL,Thermo Scientific™) per µg of recombinant products, 1X of the Buffer G and water to complete the total volume of 1mL. On the other hand, for HIC, total pDNA was digested by adding 10µL of Nb.BbvCI DNA nickase enzyme (10U/µL, New England BioLabs®), 1X of the provided buffer and water to complete the total volume of 240µL.

Regarding AEC, the Convective Interaction Media Diethylaminoethyl (weak anion exchanger) monolith disk CIM®-DEAE (0,34mL, BIA Separations) was used in the AKTA Purifier 10 (GE Healthcare) system. The mobile phase consisted of the buffer A (20mM Tris-HCl, pH 9.0-9.2) and the buffer B (1M NaCl in 20mM Tris-HCl, pH 9.0-9.2). Sample volumes were injected manually in the column previously equilibrated. The mixture was separated firstly using a linear gradient at flow rate of 1mL/min (20-80% buffer B, gradient slope of 2%/min, 90CV(column volumes)) and then by a step gradient at flow rate of 1mL/min, which included four or five steps. The salt concentrations of steps were established according to the correspondent linear gradient. The absorbance of the eluate was continuously measured at the disk outlet at 260nm. Fractions of 0.1mL for minicircle and 0.2mL for impurities were collected in a 96-well plate and the significant peak fractions were visualized on gel electrophoresis.

Regarding HIC, a Phenyl Sepharose 6 Fast Flow(High Sub) resin (10mL, GE Healthcare) was used in the AKTA Purifier 100 (GE Healthcare) system. The mobile phase included buffer A (2.2M $(NH_4)_2SO_4$ in 10mM Tris-HCl, pH 8.0) and buffer B (10mM Tris-HCl, pH 8.0). In this technique, DNA mixture was firstly conditioned in 2.5M of ammonium sulphate ($(NH_4)_2SO_4$) and then injected manually in the column previously equilibrated as in AEC. The species were separated by a step gradient at a flow rate of 2mL/min, which included three steps: 17%B (4CV), 35%B (2CV) and 100%B (2CV). The absorbance of the eluate was continuously measured at the column outlet at 260nm and fractions of 1.5mL were collected in eppendorfs. The significant peak fractions were previously dialysed to eliminate the salt and afterwards, were visualized on gel electrophoresis.

All buffers were filtrated before their use in AKTA Purifier systems, using 0.45µm filters (Merck Millipore). At the end of the purification, both columns were cleaned to remove the remaining column impurities. 1M NaCl and 10mM Tris-HCl were used, respectively, in AEC and HIC. Then, the column was equilibrated with MilliQ water for at least one hour, until constant UV and conductivity baselines were obtained.

The MC pure fractions were collected and processed in Amicon® Ultra-2 30k (volume of 2mL and 30,000 NMWL cutoff, Merk Millipore), according to the respective protocol, in order to diafiltrate and concentrate the sample. Since the BM MSC microporation protocol recommends concentrations 1–5 μg/μL, MC samples were concentrated by Savant™ DNA120™ SpeedVac Concentrator (Thermo Scientific™) at low drying rate and their concentrations were determined.

7.4 Human BM MSC culture

The different donor cryopreserved cells were thawed by submerging the cryovials in a 37ºC water bath and resuspended in 4mL of Iscove's Modified Dulbecco's Medium (IMDM, Gibco®) supplemented with 20%FBS (Gibco®). After a centrifugation at 1250rpm for 7min, the pellet was resuspended in Dulbecco's Modified Eagle Medium (DMEM, Gibco®) supplemented with 10%(v/v) MSC-qualified FBS (Hyclone®). Both media have 1%(v/v) of a mixture of antibiotics (Antibiotic-Antimycotic, 10,000 units/mL of penicillin, 10,000 μg/mL of streptomycin and 25 μg/mL of Fungizone® (amphotericin B) Antimycotic, Gibco®). The determination of total viable cell number (TVC, Equation 2) and cell viability (CV, Equation 3) was performed using the Trypan Blue (0.4%, Gibco®) dye exclusion method and a hemacytometer under an optical microscope (Olympus). According to the cell number, they were plated at cell culture flasks considering the more appropriate cell densities using DMEM+10%(v/v)MSC-FBS+1%(v/v)AA medium and kept in an incubator at 37ºC, 19.5% O_2, 5% CO_2 and 98% humidity. The medium was replaced every 3-4 days.

$$TVC = \frac{Number\ of\ viable\ cells}{Number\ of\ squares\ counted} \times 10000 cells/mL \times Dilution\ factor \times Final\ volume \quad \text{(Equation 2)}$$

$$CV(\%) = \frac{Number\ of\ viable\ cells}{Total\ number\ of\ cells} \times 100 \quad \text{(Equation 3)}$$

The cell passages were performed when 80% cell confluence was observed by microscope. This procedure first included a cell wash with Phosphate Buffered Saline buffer (PBS, Gibco®), followed by the cell detachment from the flask surface with Accutase solution (Sigma®) for 5min at 37ºC. Inactivation of the accutase was completed by adding IMDM+10%(v/v)FBS+1%(v/v)AA in a proportion of at least 2:1. Collected cells were concentrated by centrifugation and cell number and viability were accessed by the Trypan Blue dye exclusion method. At least one cell passage was done after thawing and before transfection experiment.

7.5 CHO cells culture

The culture of CHO cells (Chinese Hamster Ovary cells) was carried out using the same conditions of the human BM MSC with exception of the fact that the medium contained a less specific FBS, instead of the MSC-qualified FBS, and it was replaced every 2 days. Also, cell detachment from the flask surface was performed with Accutase solution but just for 2min at 37ºC.

7.6 Human BM MSC transfection by microporation

For each transfection experiment using the Neon™ Transfection System, in one reaction, equivalent to a time point, $1.5x10^5$ BM MSC cells were resuspended in resuspension buffer (RB) supplied by the microporator manufacturer at a density of $1.5x10^5$cells/10µL and incubated with a specific amount of vector (pDNA or MC) followed by electroporation using a Microporator MP100 (Digital Bio/(Neon™) Invitrogen). The microporation conditions used were: 1 pulse with 1000V of pulse voltage and 40ms of width. After microporation, each 10µL of cell suspension was introduced into an eppendorf containing the proper amount of Opti-MEM®I medium (Gibco®), which helped the cells to recover from the transfection shock. Afterwards, 25µL of the previous mixture was transferred to a well, from 6-well plates, containing 3mL of DMEM medium with antibiotics and FBS. The cells were subsequently incubated under static conditions at 37ºC and a 5% CO_2-humidified atmosphere until the established time points, namely, days 1, 4 and 7, after which they were collected for further analysis. All transfection experiments were performed using cells at passages P5-P7 and in all experiments, non microporated cells were used as control.

Simultaneously, supernatants were harvested at the mentioned different time points after transfection and stored at -80ºC for further VEGF quantification with RayBio® Human VEGF ELISA Kit (RayBiotech), according to manufacturer's instructions. The number of GFP-expressing cells(GFP^+ cells) was monitored at the same time points by flow cytometry and transfected cells were frozen for determination of plasmid internalization by real-time polymerase chain reaction (RT-PCR) by Fast SYBR® Green Master Mix kit (Applied Biosystems). Non-transfected cells were again used as a control.

7.7 CHO cells transfection by microporation

Two different CHO cell microporation experiments were performed with the same transfection system used for human BM MSC cells but for this cell line the microporation conditions recommended are 10 pulses with 1560V of pulse voltage and 5ms of width. In the first experiment, 1 day time point was established and in the second one, the analyzed time points were days 1 and 4. In these first screenings, there was only the collection of transfected cells for flow cytometric analysis.

7.8 Fluorescence Microscopy Imaging

Transfected and control cells were visualized using a fluorescence optical microscope Leica DMI3000B and Leica EL6000 compact light source (Leica Microsystems CMS GMbH) and digital images were obtained with a digital camera Nikon DXM 1200F. Fluorescence images were acquired with blue filter at 100X and 200X magnifications.

7.9 Flow cytometric analysis

For monitorization of the GFP-expressing viable cells at the previously established time points, the transfected and control cells were first harvested after the incubation for 5min (BM MSC cells) and 2min (CHO cells) with accutase, centrifuged and resuspended in a cell fixative solution (1% paraformaldehyde (PFA, Sigma®)). Then, considering the acquisition of a minimum of 10 000 events, the number of GFP^+ cells was determined using BD FACSCalibur™ equipment (BD Biosciences) and statistically evaluated by CellQuest™ Software (BD Biosciences). The level of GFP protein expression was given by mean fluorescence intensity (MI) also measured during the flow cytometry procedure. Non-transfected cells were used to determine the control cell population and the non-specific fluorescence. The results from flow cytometry were analyzed through Flowing Software 2.5.1.

Besides the previous described calculations of the cell number and cell viability, for each micro-electroporated sample (m), cell recovery (CR) was calculated by Equation 4, where CA is the number of viable cells and c is the non-transfected control cells. Yield of transfection (YT) was determined by Equation 5, where GFP^+ is the percentage of GFP-expression cells and CT is the number of total cells [100]. Moreover, two combined transfection parameters can be evaluated, which takes into account not only the percentage of cells expressing the protein (YT and GFP^+) but also the level of protein expression (GFP MI) resultant from the microporation.

$$CR_m\ (\%) = \frac{CA_m}{CA_C} \times 100 \text{ (Equation 4)} \qquad YT(\%) = \frac{CA_m \times GFP^+}{CT_c} \times 100 \text{ (Equation 5)}$$

7.10 Quantification of plasmid copy number by RT-PCR

Plasmid DNA copy number quantification was carried out with Fast SYBR® Green Master Mix kit (Applied Biosystems). The reaction was performed by amplification of a 108 bp sequence within the GFP gene using GFP_pVX_Fwd and GFP_pVX_Rev primers. The reaction mixture and amplification conditions applied are present on Table 8 and Table 9.

The experiment was conducted by StepOne™ Real-Time PCR detection system, which includes StepOne™Software v.2.2.2 (Applied Biosystems™).

Table 8 – RT-PCR mixture composition according to the Fast SYBR® Green Master Mix (Applied Biosystems™).

Component	Volume	Final Concentration
Fast SYBR® Green Master Mix 2X	10µL	1X
Forward primer (5µM)	1µL	0.25µM
Reverse primer (5µM)	1µL	0.25µM
Cell sample	5µL (Equivalent volume to 10 000 cells)	500cell/µL
H_20	3µL	
Total reaction volume	20µL	

Table 9 – RT-PCR conditions according to the Fast SYBR® Green Master Mix (Applied Biosystems™).

Step	Temperature	Time
AmpliTaq ® Fast DNA Polymerase, UP Activation	95°C	10min
DNA Denaturation	95°C	15s
Annealing/Extension	58°C	1min
N° of cycles	40 Cycles	

A calibration curve for each plasmid and MC vector was constructed by adding serial dilutions of DNA vector standards (3000, 1000, 300, 30 and 3 pg) to a suspension of non-transfected cells (10 000 cells per reaction) and the other PCR reagents as described in Table 8. One negative control was always included containing PCR grade water instead of control cells to detect undesired contamination.

7.11 VEGF quantification by ELISA

MSC culture supernatants were harvested on days 1, 4 and 7 and frozen at -80°C until the analysis was performed. VEGF quantification was performed using RayBio® Human VEGF ELISA kit (RayBiotech), according to manufacturer instructions. Reagent and standard solutions preparation was performed according to kit protocol and samples were centrifuged to remove cells in suspension and diluted 1:1 in the Assay Diluent supplied. 100µL of each standard and samples were added to the respective wells and then the microplate was covered and incubated for 2hours. Afterwards, the wells were aspirated and washed with 300µL of wash buffer, repeating the process for a total of four washes. The next step was 1hour of incubation with 100µL of biotinylated antibody and afterwards, for a second time, the microplate wells were aspirated and washed as previously described. After addition of 100µL of Streptavidin solution and incubation for 45min, a third washing step was performed. Protected from light, 100µL of TMB One-Step Substrate reagent was added to each well and after 15 minutes of incubation, the reactions were stopped by the addition of 50µL of Stop Solution. To obtain the results, OD_{450nm} was measured on Infinite® 200Pro microplate reader (Tecan). All steps of incubation were performed at room temperature and with gentle shaking. The standard curve was generated and the concentration of each sample was determined based on that calibration curve. The values were expressed as the mean of duplicates of one single experiment.

7.12 Data analysis

Results involving more than two independent cell experiments are present as mean ± standard error of mean (SEM), whereas experiments that resulted from two independent experiments present only the mean values without SEM.

8. Results and Discussion

To obtain MSC genetically modified to overexpress VEGF, several plasmids were constructed, produced and purified in order to evaluate VEGF expression levels of each one. All the plasmids are pMINI8 and pMINILi plasmid derivatives.

8.1 Plasmids construction

8.1.1 pMINILi construction

For the construction of pMINILi 3987bp (Figure 16), P_{BAD}/*araC-parA* cassette was deleted by AgeI restriction digestion after the genetic modification of the pMINI8 vector (4702bp). The first directed mutagenesis to introduce one AgeI restriction site was confirmed by AgeI and BamHI digestions. On agarose gel electrophoresis, one band of 4702bp for AgeI digestion was observed, since it only linearizes pMINI8, and two bands (3948bp and 754bp) proved the correct BamHI digestion (Figure 17). The second directed mutagenesis step which added another AgeI restriction site to pMINI8 was analysed by AgeI digestion. Two distinct bands were observable in agarose gel electrophoresis (Figure 18). The lower molecular weight band (715bp) corresponds to P_{BAD}/*araC-parA* cassette and the higher is the rest of the pMINI8 vector (3987bp). Gel extraction and religation of the vector fragment were performed and after *E.coli* DH5α transformation and plasmid purification, the correct plasmid was confirmed by SalI digestion, obtaining 3525bp and 462bp bands on agarose gel electrophoresis (Figure 19). The sequencing results corroborated the deletion of P_{BAD}/*araC-parA* cassette from pMINI8, leading the pMINILi plasmid. Moreover, this deletion also led to the elimination of two PvuII restriction sites present in P_{BAD}/*araC-parA* cassette, thus the pMINILi is only composed by six PvuII restriction sites (Figure 16).

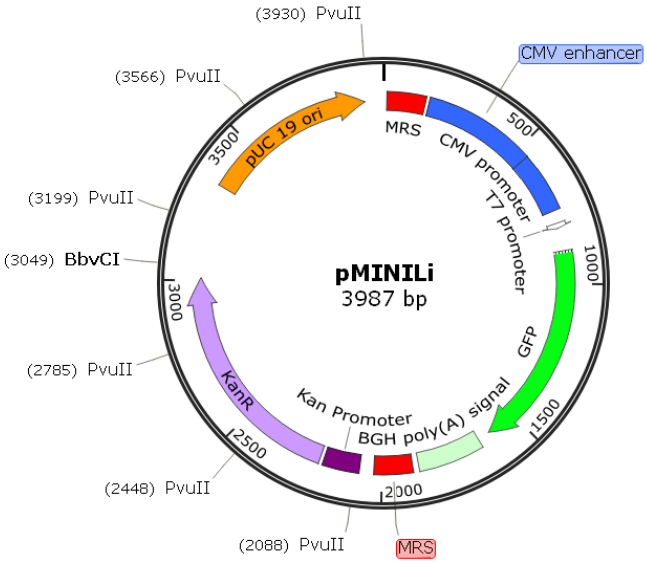

Figure 16 - Schematic diagram of pMINILi plasmid.

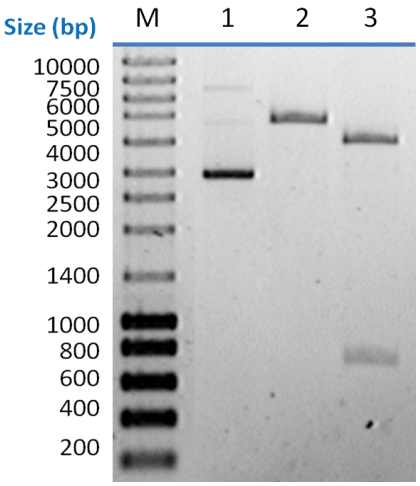

Figure 17 - AgeI and BamHI restriction digestion of pMINI8 with one AgeI restriction site: NZYTech Ladder III (Lane M), undigested pMINI8 (Lane 1), AgeI digested pMINI8: 4702bp band (Lane2) and BamHI digested pMINI8: 3948bp and 754bp bands (Lane 3).

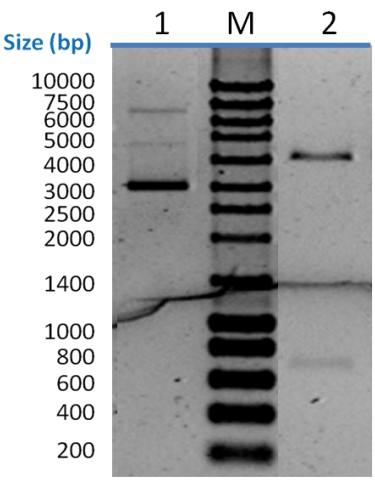

Figure 18 - AgeI restriction digestion of pMINI8 with two AgeI restriction sites: undigested pMINI8 (Lane 1), NZYTech Ladder III (Lane M), AgeI digested pMINI8: 3987bp and 715bp bands (Lane2).

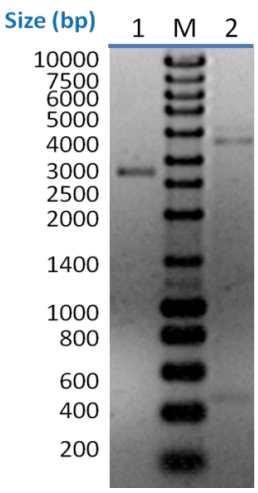

Figure 19 – SalI restriction digestion of pMINILi: undigested pMINILi (Lane 1), NZYTech Ladder III (Lane M), SalI digested pMINILi: 3525bp and 462bp bands (Lane2).

8.1.2 pMINILi-CMV-VEGF-GFP construction

For the construction of pMINILi-CMV-VEGF-GFP 4563bp (Figure 20), VEGF gene fragment was obtained from pVAX-VEGF-GFP after a double digestion with EcoRI and KpnI restriction enzymes. As a result, in agarose gel electrophoresis (Figure 21), two distinct bands are observable, one corresponding to VEGF gene fragment (611bp) and the other band is the rest of the pVAX-VEGF-GFP vector (3662bp). pMINILi was also digested with the same enzymes, resulting two DNA fragments, 3952bp and 35bp. The lower molecular weight band cannot be observable in the gel. The confirmation of the ligation between pMINILi and VEGF gene fragment, before sequencing submission, was performed by two restriction digestions, one with EcoRI and KpnI, originating 3952bp and 611bp bands and the other with NcoI, which has three restriction sites on this plasmid, leading to the appearance of 2398bp, 1746bp and 419bp bands in the gel (Figure 22). The sequencing results corroborated the insertion of VEGF into pMINILi.

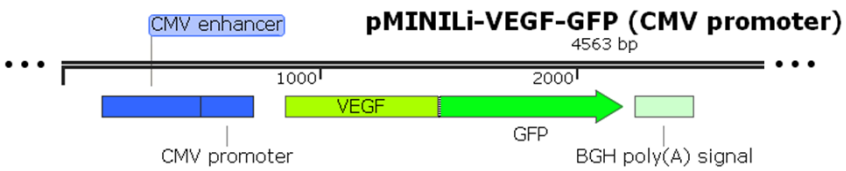

Figure 20 - Schematic diagram of pMINILi-CMV-VEGF-GFP plasmid.

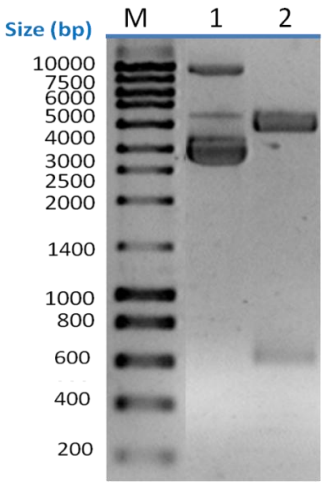

Figure 21 - EcoRI and KpnI double restriction digestion of pVAX-VEGF-GFP. NZYTech Ladder III (Lane M), undigested pVAX-VEGF-GFP (Lane 1), EcoRI+KpnI digested pVAX-VEGF-GFP: 3662bp and 611bp bands (Lane 2).

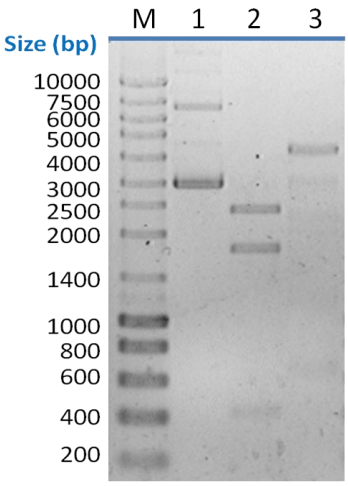

Figure 22 - NcoI and EcoRI+KpnI restriction digestions of pMINILi-CMV-VEGF-GFP. NZYTech Ladder III (Lane M); undigested pMINILi-CMV-VEGF-GFP (Lane 1); NcoI digested pMINILi-CMV-VEGF-GFP (Lane 2): 2398bp, 1746bp and 419bp bands; EcoRI+KpnI digested pMINILi-CMV-VEGF-GFP (Lane 3): 3952bp and 611bp (not well visible) bands.

8.1.3 pMINILi-hEF1α-VEGF-GFP construction

For the construction of pMINILi-hEF1α-VEGF-GFP 4475bp (Figure 23), hEF1α promoter fragment was obtained by PCR amplification from phEF1α plasmid isolated from *E.coli* XL10-Gold strain. This amplification was verified by agarose gel electrophoresis, where the hEF1α promoter band (597bp) is present (Figure 24). pMINILi-CMV-VEGF-GFP was digested with KpnI and SpeI restriction enzymes, leading to the deletion of CMV promoter, which can be observable in agarose gel electrophoresis where the lower molecular weight band corresponds to CMV promotor fragment (668bp) and the higher molecular weight band is the rest of pMINILi vector (3895bp) (Figure 25). After digested pMINILi purification and hEF1α promoter fragment digestion with the same enzymes and subsequent purification, the pMINILi vector and hEF1α promoter were ligated. Confirmation of the correct ligation was made with EcoRI restriction digestion where two bands were expected: 628bp and 3847bp. These bands can be observable in Figure 26. After directed mutagenesis of pMINILi-hEF1α-VEGF-GFP to remove the PvuII restriction site of the promoter, the mutation was confirmed by DNA sequencing results.

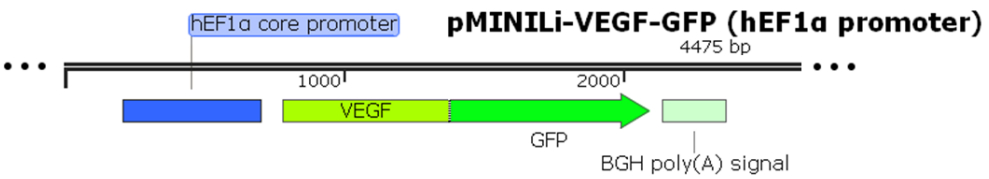

Figure 23 - Schematic diagram of pMINILi-hEF1α-VEGF plasmid.

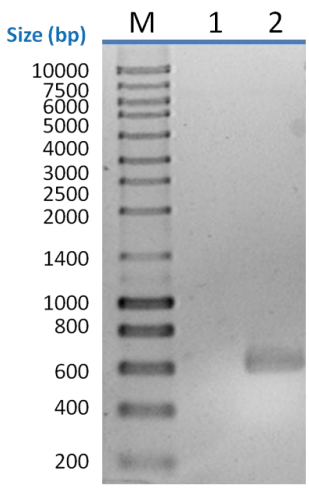

Figure 24 - PCR amplification of hEF1α promoter fragment by KOD Hot Start Polymerase: NZYTech Ladder III (Lane M), PCR negative control (Lane 1) and hEF1α promoter 597bp band (Lane 2).

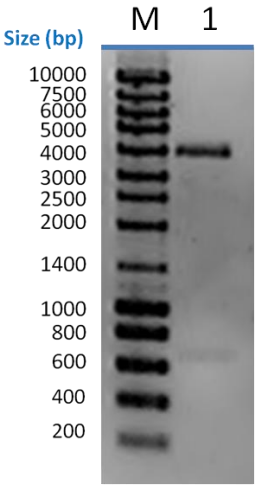

Figure 25 - KpnI and SpeI restriction digestion of pMINILi-CMV-VEGF-GFP: NZYTech Ladder III (Lane M), KpnI and SpeI digested pMINILi-CMV-VEGF-GFP: 3895bp and 668bp (Lane 2).

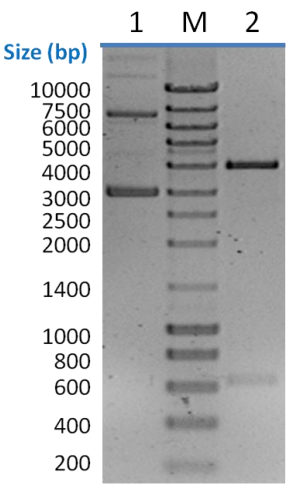

Figure 26 - EcoRI restriction digestion of pMINILi-hEF1α-VEGF-GFP: undigested pMINILi-hEF1α-VEGF-GFP (Lane 1), NZYTech Ladder III (Lane M), EcoRI digested pMINILi-hEF1α-VEGF-GFP: 3847bp and 628bp bands (Lane 2).

8.1.4 pMINILi-mCMV+hEF1α(CpG free)-VEGF-GFP construction

For the construction of pMINILi-mCMV+hEF1α(CpG free)-VEGF-GFP 4563bp (Figure 27), firstly the pCpG free plasmid was produced and digested with PstI restriction enzyme, leading to three observable bands in agarose gel electrophoresis: 1771bp, 517bp and the desired 761bp, which corresponds to the mCMV+hEF1α(CpG free) promoter fragment (Figure 28). Since pMINILi-CMV-VEGF-GFP has only one restriction site for PstI, its digestion with PstI revealed just one band on agarose gel electrophoresis with 4563bp. The digested pMINILi-CMV-VEGF-GFP and the promoter fragment were ligated and after *E.coli* DH5α transformation and plasmid purification, HindIII digestion of the resultant plasmids confirmed the samples with the correct orientation of the insert, since both fragments had the same PstI sticky ends and the insert could be inversely orientated. Therefore, only the bacterial cultures with 671bp and 4563bp bands pattern in agarose gel electrophoresis were selected as positives (Figure 29). The 671bp band of HindIII digestion, which corresponds to proper sized mCMV+hEF1α promoter, was excised from gel and after purification was ligated to pMINILi-CMV-VEGF-GFP plasmid digested also with HindIII that just cut once at the plasmid. Confirmation of the pMINILi-CMV-mCMV+hEF1α(CpG free)-VEGF-GFP was performed with KpnI restriction digestion that revealed on gel electrophoresis two bands: 4563 bp and 671bp. NheI and MluI double digestion was performed to delete the original CMV promoter, which is the 667bp band in the gel present in Figure 30**.** The other band (4567bp) was purified, S1 nuclease digested and religated, giving the final pMINILi-mCMV+hEF1α(CpG free)-VEGF-GFP. After *E.coli* DH5α transformation and plasmid purification, HindIII digestion confirmed the expected band pattern of the pMINILi-mCMV+hEF1α(CpG

free)-VEGF-GFP on gel electrophoresis: 3892bp and 671bp bands (Figure 31). The correct plasmid was confirmed by DNA sequencing results.

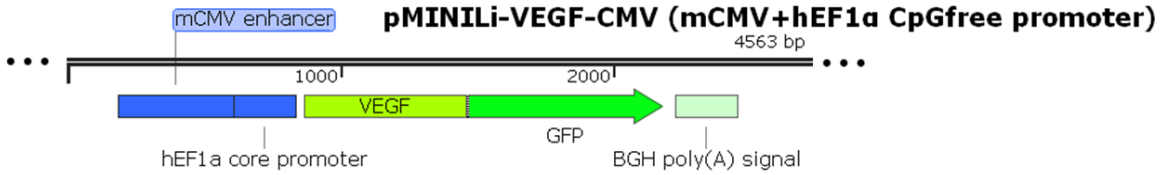

Figure 27 - Schematic diagram of pMINILi-mCMV+hEF1α-VEGF-GFP plasmid.

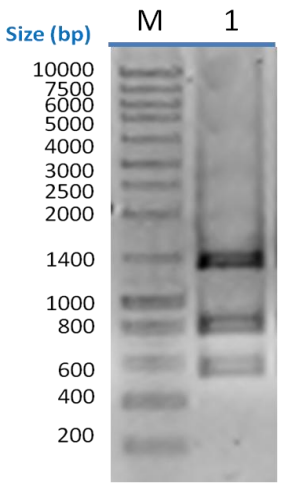

Figure 28 – PstI restriction digestion of pCpG free plasmid: NZYTech Ladder III (Lane M), KpnI digested pCpG free: 1771bp, 761bp and 517bp bands (Lane 2).

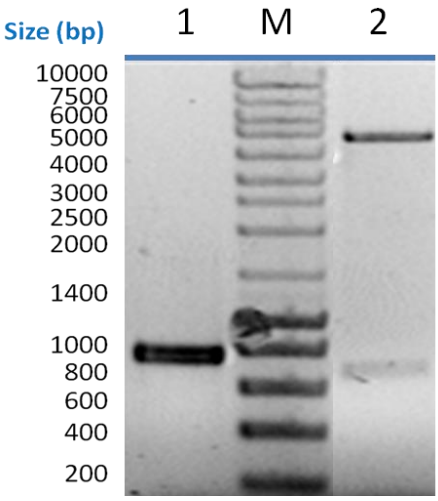

Figure 29 - HindIII restriction digestion of pMINILi-CMV-mCMV+hEF1α(CpG free): promoter fragment (761bp), NZYTech Ladder III (Lane M), HindIII digested pMINILi-CMV-mCMV+hEF1α(CpG free): 4653bp and 671bp bands (Lane 2).

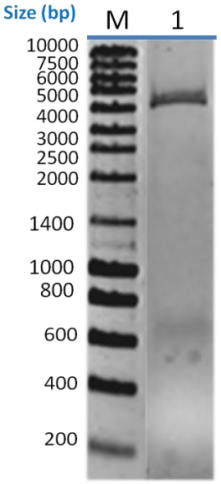

Figure 30 - NheI and MluI restriction digestion of pMINILi-CMV-mCMV+hEF1α(CpG free): NZYTech Ladder III (Lane M), NheI and MluI digested pMINILi-CMV-mCMV+hEF1α(CpG free): 4567bp and 667bp bands (Lane 1).

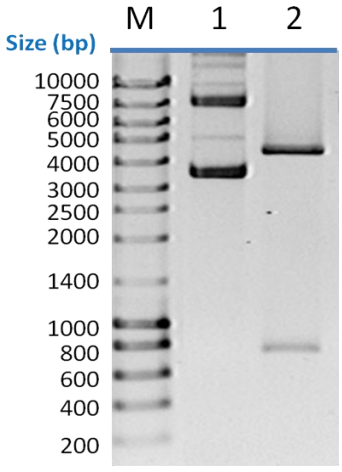

Figure 31 - HindIII restriction digestion of pMINILi-mCMV+hEF1α(CpG free): NZYTech Ladder III (Lane M), undigested pMINILi mCMV+hEF1α(CpG free) (Lane 1), NcoI digested pMINILi-mCMV+hEF1α(CpG free): 3892bp and 671bp bands (Lane 2).

8.1.5 pMINILi-hEF1α(CpG free)-VEGF-GFP construction

For the construction of pMINILi-hEF1α(CpG free)-VEGF-GFP (Figure 32), the provisional pMINILi-CMV-mCMV+hEF1α(CpG free)-VEGF-GFP (5234bp) was digested with SpeI restriction enzyme, in order to remove the original CMV promoter and the mCMV enhancer from the vector. After agarose gel electrophoresis, two bands were observed: 1109bp from CMV-mCMV fragment and the other 4125bp band from the rest of the plasmid (Figure 33). The digested plasmid without CMV-mCMV fragment was excised from the gel, purified and then religated. Confirmation of the correct ligation was made with NcoI restriction digestion where two bands were expected: 2398bp and 1727bp (Figure 34). The correct plasmid was confirmed by sequencing results.

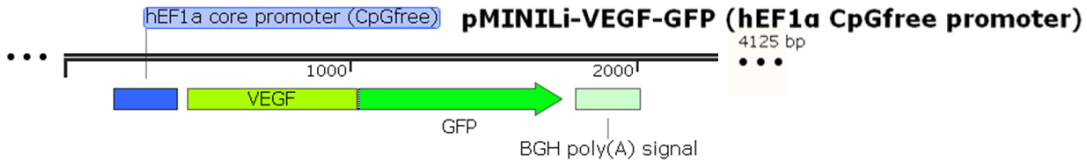

Figure 32 – Schematic diagram of pMINILi-CMV-hEF1α(CpG free)-VEGF-GFP plasmid.

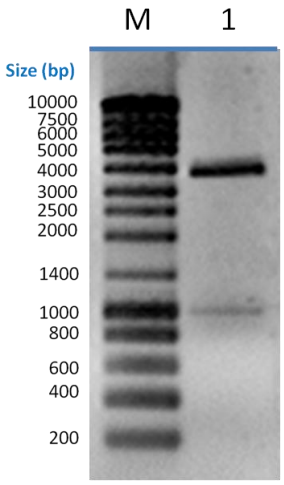

Figure 33 - SpeI restriction digestion of pMINILi-CMV-mCMV+hEF1α(CpG free): NZYTech Ladder III (Lane M), SpeI digested pMINILi-CMV-mCMV-hEF1α(CpG free): 1109bp and 4125bp bands (Lane1).

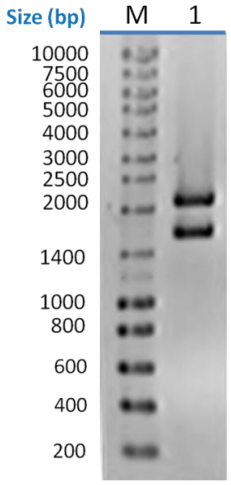

Figure 34 - NcoI restriction digestion of pMINILi-hEF1α(CpG free): NZYTech Ladder III (Lane M), NcoI digested pMINILi-hEF1α(CpG free): 2398bp and 1727bp bands (Lane 1).

8.2 Plasmids and Minicircles production

According to previous MC production from pMINI vector in *E.coli* BW2P, a recombination efficiency of nearly 100% was obtained when the induction with 0.01% (w/v) L-arabinose was performed in OD_{600nm} between 3.4 and 3.8 for one hour. These OD_{600nm} values correspond to late exponential phase and it would be advantageous because it allows the cell number and PP maximization before induction. A substantial decrease in recombination efficiency was also observed when induction was performed closer to the stationary phase [71].

In a first approach, the previous strategy was applied to pMINILi-CMV-VEGF-GFP production in *E.coli* BW2P, including 2h of recombination instead of 1h. However, low recombination efficiencies were obtained (Table 10). Then, the recombination efficiency and induction time were further studied by performing arabinose induction at a different stage of the growth and varying the induction time. Firstly, by increasing the induction time length to 5 hours, better recombination efficiencies were reached (Table 10). However, within fermentation and induction time, since MP contains the origin of replication, it becomes predominant in plasmid population which is less desirable. Afterwards, by recombination induction at a lower OD_{600nm} value during 5 hours, almost complete recombination was obtained after 2 hours of recombination (Figure 35). Therefore, the recombination time was reduced from 5 to 2 hours, maintaining the same range of OD_{600nm} and the recombination efficiency obtained was very similar to the previous experiment (Figure 36), decreasing the time required and hence the MP replication. At the time of induction, the pH was checked and the values were in desired range.

Table 10 - Recombination efficiencies according to the induction phase and time length. This recombination efficiency results from densitometry analysis of 500ng of SacII digested pDNA from one single experiment.

Strain/pDNA	$OD_{induction}$	Induction time	Recombination Efficiency
BW2P/ pMINILi-CMV-VEGF-GFP	3.63	2h	23.7%
	3.45	2h	47.2%
	3.58	5h	81.7%
	3.50	5h	89.9%
	2.58	5h	94.9%
	2.65	2h	96.2%

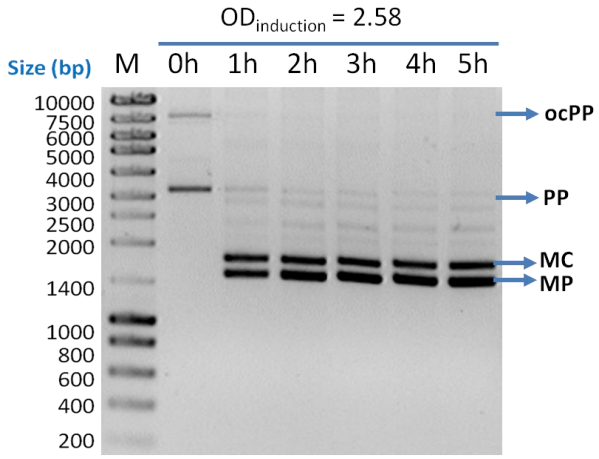

Figure 35- Agarose gel electrophoresis of the produced and purified plasmid population of *E.coli* BW2P/ pMINILi-CMV-VEGF-GFP, using NZYTech Ladder III (Lane M), at the moment of induction (Lane 0h) and during 5 hours of recombination (Lanes 1-5h). The induction OD_{600nm} in this experiment was 2.58. The unidentified bands are relaxed isoforms of MC, MP and PP.

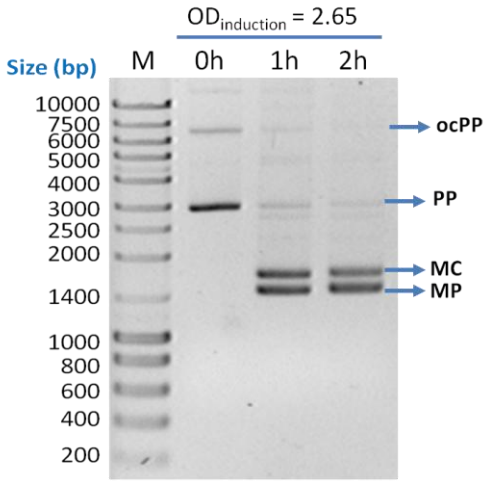

Figure 36 – Agarose gel electrophoresis of the produced and purified plasmid population of *E.coli* BW2P/ pMINILi-CMV-VEGF, using NZYTech Ladder III (Lane M), at the moment of induction (Lane 0h) and during 2 hours of recombination (Lanes 1h and 2h). The induction OD_{600nm} in this experiment was 2.65. The unidentified bands are relaxed isoforms of MC, MP and PP.

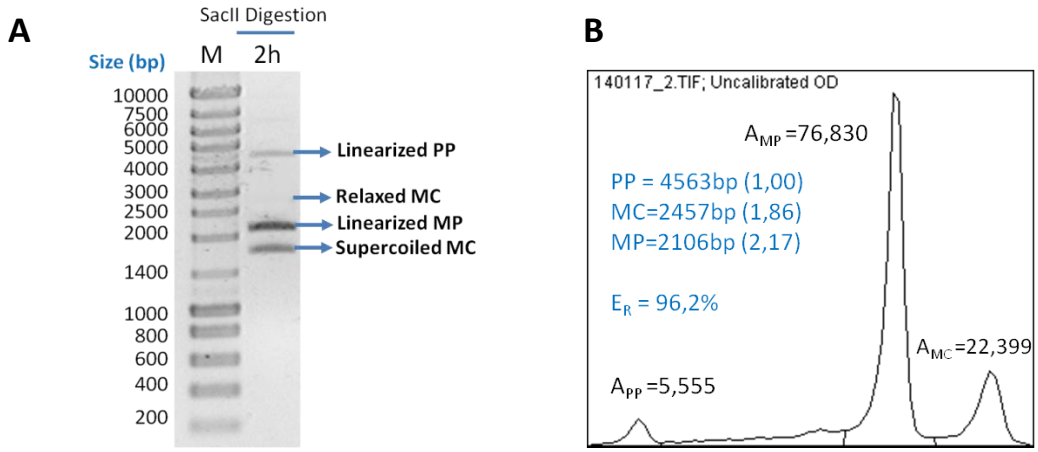

Figure 37 – Recombination efficiency: **(A)** Agarose gel electrophoresis, using NZYTech Ladder III (Lane M), of SacII restriction digestion of the produced and purified plasmid population of *E.coli* BW2P/ pMINILi-CMV-VEGF after 2 hours of recombination. The recombination induction OD_{600nm} in this fermentation was 2.65. The indicated bands correspond to the SacII digested form of parental plasmid (Linearized PP) and miniplasmid (Linearized MP) and minicircle is found in its supercoiled and relaxed form (Supercoiled MC and Relaxed MC). Relaxed MC band was not well visible. **(B)** Densitometry analysis, using the ImageJ software, of the SacII digestion bands pattern present in (A) for the recombination efficiency calculation with equation 1, that takes into account the density of the bands and MC and MP sizes relation to PP size.

Using the knowledge behind the previous experiments results, all the *E.coli* BW2P strains, containing four different plasmid constructions described before, were grown for MC production, according to the best conditions of induction established for *E.coli* BW2P/pMINILi-CMV-VEGF-GFP. The results of optical density of induction and the corresponding recombination efficiency from all the cell culture batches performed are presented in Table 11.

Table 11 – Average of optical densities of induction and correponding recombination efficiencies of all growths of strains constructed for MC production in 250mL LB medium.

Strain/pDNA	OD_{600nm} of Induction	Recombination Efficiency (%)
BW2P/pMINILi-CMV-VEGF-GFP	2.56 ± 0.17	96.44 ± 2.78
BW2P/ pMINILi-hEf1α-VEGF-GFP	2.49 ± 0.22	98.65 ± 1.68
BW2P/ pMINILi-mCMV+hEf1α(CpG free)-VEGF-GFP	2.51 ± 0.13	98.70 ± 1.32
BW2P/ pMINILi-hEf1α(CpG free)-VEGF-GFP	2.56 ± 0.15	92.68 ± 4.27

As present in Table 11, recombinations efficiencies above 92% in all strains were observed when the culture is inducted with 0.01% (w/v) L-arabinose in a OD_{600nm} close to 2.5.

These results can be supported by previous studies [71] and one important conclusion to this system can be accomplished, if the growth curves of both strains are analysed. Considering all performed growth experiments (data not shown), a regular and similar growth behaviour of *E.coli* BW2P with the different pMINILi plasmids was observed and the average logarithmic growth curves can corroborate this statement (Figure 38). According to these growth curves, the BW2P/pMINI growth curve described before [71] (Figure 39) and the induction time

that results in near 100% recombination efficiency for both strains, it is possible to conclude that the recombination efficiency in this system is determined by the induction growth phase. Higher recombination efficiency is achieved when the L-arabinose induction is performed in the period between mid-late exponential phase and before the stationary phase. Since BW2P/pMINI growth curve has a stationary phase with higher absorbance values in comparison with BW2P/pMINILi strains, the induction was performed with OD_{600nm}=3.4-3.8. In BW2P/pMINILi strains, recombination should be induced with absorbance around 2.5, since stationary phase is reached when absorbance values were below 5. This conclusion is particular significant for this MC production system, once the first step for any other cell growths using *E.coli* BW2P is the characterization of its logarithmic growth curve and allow the prediction of the induction time and respective induction OD_{600nm}.

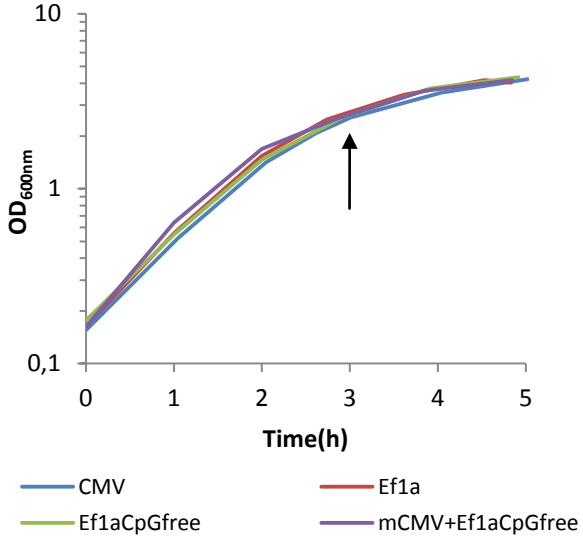

Figure 38 – Average logarithmic growth curves of the different *E.coli* BW2P/pMINILi strains in 250mL LB medium. The arrow illustrates the time of induction. SEM is not represented since the resolution of the graph is not enough to distinguish the differences between the different growth curves. Individual growth curves and standard deviations are present in Annex 4.

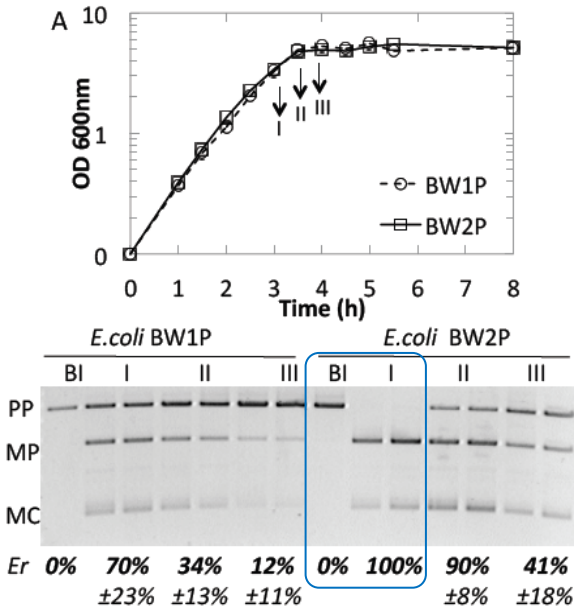

Figure 39 - Logarithmic growth curve of *E.coli* BW2P/pMINI (squares, solid line) and BW1P/pMINI (circles, dashed line) in 50mL LB medium [71]. The points I, II and III illustrate times of induction (OD_{600nm} I:3.4-3.8;II:4.4-4.8;III:5.0-5.2). The correspondent recombination efficiencies are represented by the agarose gel electrophoresis and densitometry analysis. The blue boxes highlight significant information and results for the discussion of the results of this thesis.

Moreover, Gaspar and coworkers, by monitoring in real time the dynamic recombination of PP to MC, concluded that kinetics of conversion event, using their strain and recombination system, is also dependent on the time of induction. In this study, different phase growth induction times were tested and the results showed that inducing recombination at the end of the exponential phase is a more valuable approach to achieve maximum yield and purity of MC, regardless of the growth temperature and inducer concentration used. On the other hand, induction times in stationary phase revealed not only that MC yield was markedly decreased, but also the presence of PP templates increased [79]. These are important findings that are in agreement with

the aforementioned results and have a great impact on the first stages of process development, downstream purification and consequently its applications.

Using the Equation 6, the average specific maximum growth rate (μ_{max}) of all constructed strains was calculated (Table 12). μ_{max} of all growths were determined considering the maximum number of OD_{600nm} values that were comprised in exponential phase and an average ± SEM was taken after.

$$ln(OD_{600nm}) = \mu_{max} \times t + ln(OD_{600nm})_i \text{ (Equation 6)}$$

Table 12 – Average specific maximum growth rate of all growths of strains constructed for MC production in 250mL LB medium.

Strain/pDNA	μ_{max} (h^{-1})
BW2P/pMINILi-CMV-VEGF-GFP	0.95 ± 0.07
BW2P/ pMINILi-hEf1α-VEGF-GFP	1.03 ± 0.09
BW2P/ pMINILi-mCMV+hEf1α(CpG free)-VEGF-GFP	1.02 ± 0.09
BW2P/ pMINILi-hEf1α(CpG free)-VEGF-GFP	0.94 ± 0.06

As it was expected by the analysis of Figure 38, there was not supposed to exist a significant difference in μ_{max} of the different genetically modified strains since their behavior during culture was very similar. This hypothesis can be supported by the μ_{max} values obtained that are all in the same range of values.

According to the previous work developed in our laboratory, the production of *E.coli* BW2P/pMINI in a 1L bioreactor batch mode, using Listner Complex medium [103] with 20g/L and 40g/L of glycerol as carbon source, yielded μ_{max} of $0.56h^{-1}$ and $0.39h^{-1}$, respectively [71]. These μ_{max} values are significantly lower to the ones obtained in present results, even using the same bacterial strain, since the growth conditions were different and the glycerol is slowly metabolised by cells, reducing the μ_{max} value, minimizing metabolites production and thus enhancing plasmid production. Regarding other MC-producing strains, such as *E. coli* strain ZYCY10P3S2T harboring a PP of 7.06kbp [79], higher μ_{max} values were obtained in present experiments, namely 10-fold higher. Besides the larger PP that this strain harbored, growth conditions and MC production system by the *E. coli* strain ZYCY10P3S2T were also different, since the *in vivo* degradation of MP and PP is dependent on the production and action of an endonuclease, which is encoded in PP and subsequently in MP.

The same type of results was analysed in BW2P/pMINILi cell growths performed in 500mL LB medium and no significant differences relatively to the 250mL growths were observed (Annex 5 - 7).

8.3 Total plasmid DNA purification

After lysis and column purification of total pDNA from the bacterial cultures selected for MC purification, the volumetric titers were calculated according to the Equation 7 and are present in Table 13.

$$Volumetric\ yield = \frac{Total\ mass\ pDNA}{Initial\ culture\ volume} \text{ (Equation 7)}$$

Table 13 - Total plasmid DNA titers reached in batch cultures using the manufacturer suggestions.

Strain/pDNA	BW2P/pMINILi-CMV-VEGF-GFP		BW2P/pMINILi-hEf1α-VEGF-GFP		BW2P/pMINILi-mCMV+hEf1α CpG free-VEGF-GFP		BW2P/pMINILi-hEf1α CpG free-VEGF-GFP	
Number of Columns	2	4	2	4	2	4	2	4
Volumetric yield (mg pDNA/L)	1.03*	0.55±0.11	0.97*	0.60±0.21	1.36*	0.82±0.02	1.77*	0.88±0.09

*Only one experiment was performed

As mentioned in Material and Methods, most of the pDNA purifications were realized according to the manufacturer recommendations, which means using 4 purification columns for our conditions of final OD_{600nm} (≈4.0) and culture volume (≤500mL) (Annex 8). In this case, the volumetric yields obtained (Table 13) did not exceed the value of 1mg pDNA/L and yields of constructions with CMV and hEf1α promoters and mCMV+hEf1α and hEf1α CpG free promoters were similar among them, respectively. BW2P/pMINILi-hEf1α CpG free was the strain that produced a higher volumetric yield and this was an expected result. Size has a crucial influence on pDNA yield and this PP is around 500bp smaller than the others, thus its replication within culture should be more pronounced (high number of pDNA copies).

According to the typical DNA yields of NucleoBond® Xtra Columns of MN Midiprep kit (400μg)[104] and the yields obtained with 4 columns, there was a finding that each used column was carrying, at maximum, half of the amount that it can bear. Taking into account the previous information and in order to reduce the costs associated with the pDNA purification, one purification experiment for each constructed strain, using only two columns for the same final conditions as before, was realized. Better volumetric yields were attained, specifically around 1.5-fold higher pDNA volumetric yields (Table 13). Even just one experiment was performed for each construction, these experiments were accomplished in different days, and therefore reproducibility is present. Also, the proportion within pDNA constructs in comparison with the 4 columns is relatively maintained. Moreover, quality of purified pDNA was not altered (data not shown) and, simultaneously, the costs can be reduced by using half of the recommended number of columns. Nevertheless, it is advisable to carry out more experiments using 2 columns to clearly conclude their advantageous use.

In previous work, 2.9 ± 0.5 mg pDNA/L was achieved using a 50mL (LB medium) shake flask system with BW2P/pMINI after 4.5hours of incubation [71]. Since the final OD_{600nm} was not specified in the previous study, no real comparison with the present results can be done because volumetric yields differ if final biomass production is different. Even so, since the strains are the same and the pMINILi plasmids are derivatives of pMINI, one possible explanation for the differences is based on the purification methods used. MN purification procedure is more stringent in order to obtain a high quality (A260/A280 between 1.80–1.90 and A260/A230 around 2.0) and endotoxin free (<0.05 EU/μg plasmid DNA) pDNA sample, thus a lower pDNA recovery can be observed. The use of this kit is particularly significant because these plasmid preparations should guarantee high transfection rates and high viability of transfected MSC, due to residual presence of endotoxins and other contaminants. For instance, pDNA purification using High Pure Plasmid Isolation Kit protocol (Roche) led to

much higher pDNA yields (data not shown) when 2mL of the same culture batch was purified to characterize the recombination event before and after induction in agarose gel electrophoresis.

8.4 Minicircle purification

The minicircle purification comprises four steps: enzymatic digestion, chromatography, dialysis and concentration and, finally, verification of the purified species.

8.4.1 Minicircle purification by Anion Exchange Chromatography

Anion-exchange chromatography is the most popular chromatography method for plasmid separation, since polynucleotides are negatively charged independent of the buffer conditions [105]. In this present study, AEC requires as a first and functional step, a PvuII enzymatic digestion of recombined and purified pDNA sample. Since pMINILi and its derivative constructions contain six PvuII restriction sites (Figure 16), the digested pattern using PvuII consists of short linear fragments varying in size between 337bp to 414bp from MP and unrecombined PP, and the undigested supercoiled and relaxed MC (Figure 40). If recombination was not complete, there is an additional band that is the linearized fragment corresponding to the remaining PvuII digested unrecombined PP, which is in practice the linearized form of MC. PvuII enzymatic digestion patterns of the remaining recombined constructs are present in Annex 9**.**

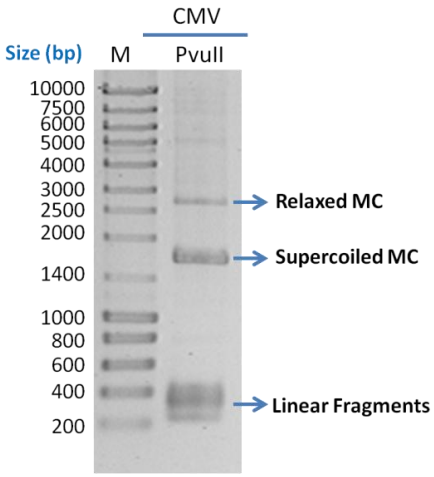

Figure 40 – PvuII digestion of purified recombination products derived from the *E.coli* BW2P pMINILi-CMV-VEGF-GFP growth. Lane 1- NZYTech Ladder III, Lane2 – PvuII digestion of recombination products present in purified sample.

The goal of AEC in this study was to eliminate the non-DNA impurities and the short DNA linear fragments derived from PvuII digestion of total pDNA mixture produced during fermentation and recover the maximum amount of pure MC. CIM®-DEAE Disk was successfully tested as intermediate step of the pDNA manufacturing process in one previous study [105] and consists of a monolithic stationary phase (poly(glucidyl methacrylate-co-ethylene dimethacrylate) modified with diethylamine to obtain a weak anion exchanger with diethylaminoethyl functional groups (Annex 10). T1his weak anion exchange matrix is positively-charged within a narrow pH range and binds DNA and other negatively charged species. A weak ion exchange support was chosen because it produces more resolution when charge differences between molecules are very small. Moreover, DNA is considered a labile molecule and more gentle conditions of pH and ionic strength can be used for elution with weak anion exchanger.

AEC relies on reversible exchange of anions in solution with anions groups of the molecules electrostatically bound to the support media. For that reason, the salt concentration required to elute the DNA impurities could vary depending on the sample (concentration and charge density differences) and buffer batches or on environmental factors which influence the conductivity, such as temperature. Consequently, a first separation of the digested recombination products, using a linear gradient increasing from 20 to 80% buffer B in 90CV was performed in all AEC purification experiments to define the salt concentration required for elution of the different DNA species in the mixture during the step gradient. For all PvuII digested plasmid constructs, in the chromatogram (Figure 41), a first set of peaks was observed, which included all molecules that have a low interaction with column and eluted in flow through. The protein PvuII used for enzymatic digestion is believed to elute in this phase due to its small size and low interaction potential with column [71]. During linear gradient performance, two main peaks were present in the chromatogram. According to the previous developed work in our laboratory [71], the first broad peak corresponds to the short linear fragments which have a lower negative charge density in comparison with the supercoiled and relaxed minicircle that are released in the second sharper peak (Figure 41). Moreover, the resolution of the two different groups of DNA molecules in these conditions was enough to comfortably design a step gradient. The salt concentration corresponding to the tail of the linear fragments peak end was used as a guide to set up the step gradient method (Figure 41). Considering the delay, meaning the time taken for gradient to reach column, the salt concentration to elute the impurities in step-gradient was adjusted as well as the salt concentration for MC elution.

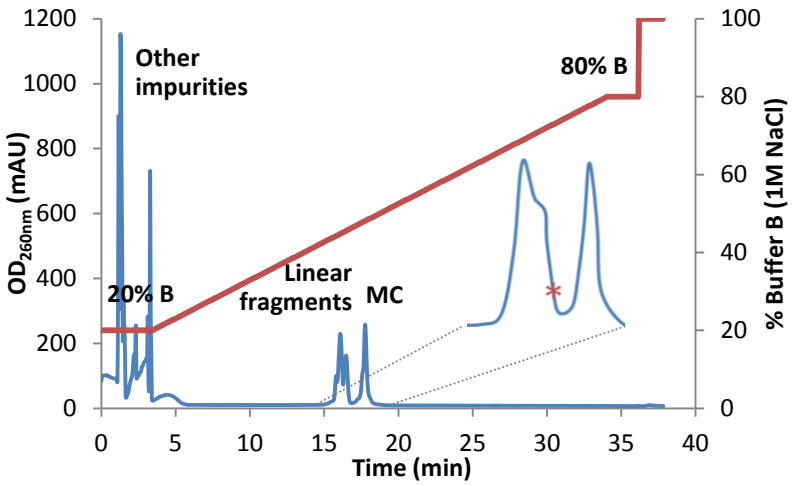

Figure 41- Chromatographic separation of pMINILi-CMV-VEGF-GFP recombined and digested products on a CIM®-DEAE disk using a linear gradient between 20% and 80% 1M NaCl and illustrative larger view of two significant peaks used to define the key salt concentration (represented by an asterisk) for purification using the step gradient.

In step-gradient chromatography, a first long elution step with a lower salt concentration was designed to allow the impurities elution, appearing as a first peak in the chromatogram. Then, a sharper peak during the elution step at a higher salt concentration appeared, as expected. At the end of the run, the final step of 100%B, which corresponds to 1M NaCl, for 5CV was applied to regenerate the column, eluting the remaining impurities from the column. Afterwards, gel electrophoresis of some peak fractions confirmed that the first peak consisted mainly in short linear fragments, having also some MC and the second peak is constituted by supercoiled and relaxed MC. One example of a step gradient of pMINILi-CMV-VEGF-GFP is represented on Figure 42.

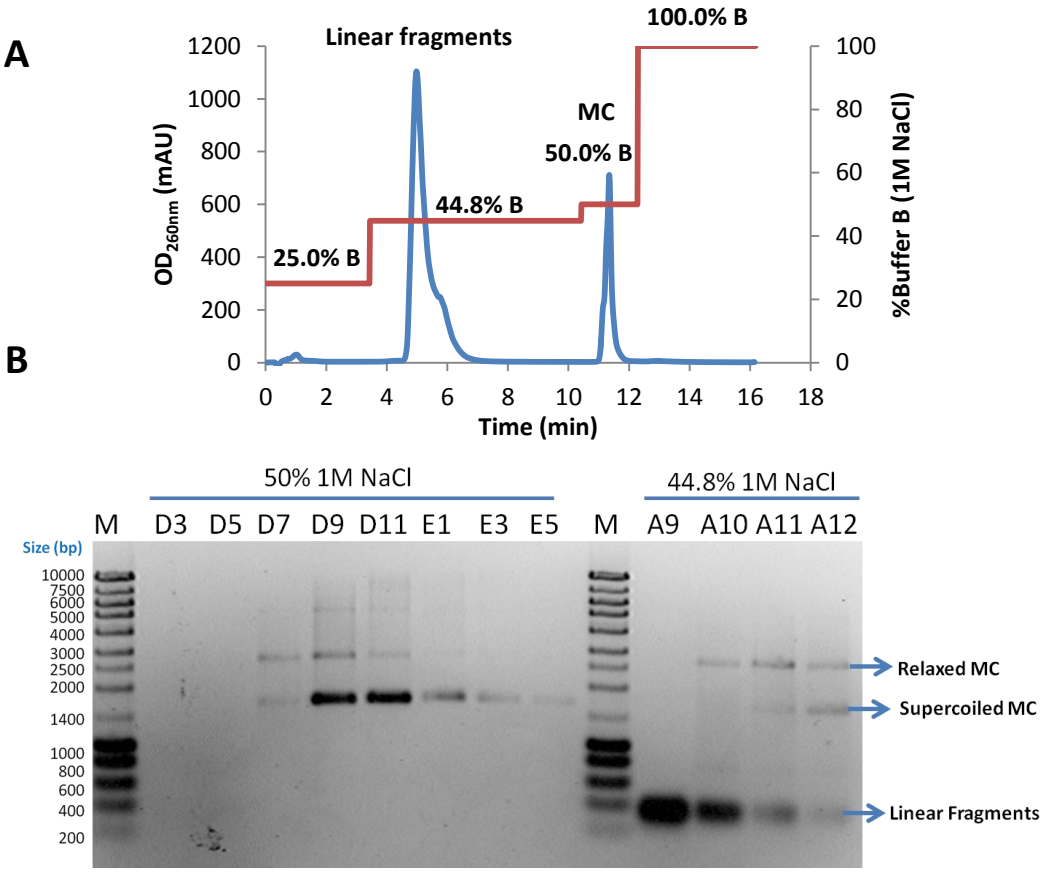

Figure 42 – Chromatographic separation of pMINILi-CMV-VEGF recombined and digested products on a CIM®-DEAE disk using a step gradient **(A)** and corresponding peak fractions on agarose electrophoresis gel **(B).**

The results from this step-gradient purification proved the ability of this method application for separation of impurities from MC. Moreover, in MC fractions, the supercoiled conformation was presented in higher quantity in comparison with the relaxed conformation, which is desirable to allow better efficiencies in cell transfection experiments [105-107]. In order to recover a higher final MC concentration in collected fractions, a higher salt concentration in the MC elution step (60%B) was used in other chromatography experiments, since it does not interfere in further downstream processes.

To ensure total impurity elution and as a consequence of contamination of MC peak fractions with linear fragments in more than one purification experiment, an optimization to the previous method was accomplished, namely the addition of a step of 20CV that corresponds to the second salt concentration in the method, relative to the higher absorbance of the linear fragments peak in the linear gradient chromatograph. An illustrative representation of the salt concentration of the additional step included in the optimized method is presented in Annex 11. By this modification, in this second step was possible to eliminate most of the linear fragments present in the loaded sample and if the elution conditions would not be enough to discard all linear fragments, the next step could be used for this purpose. There were some experiments where this additional step allowed the non-contamination of MC peak fractions, because all linear fragments eluted before the step of MC elution (Annex 12), and in most of them, this additional step was sufficient to elute all impurities and the next step peak fractions were composed only by pure MC (Annex 13).

There is the possibility of the used CIM-DEAE disk is damaged and not fully functional (resolution, binding capacity and back pressure affected) due to recurrent use and regeneration of column for purification of MC and other biomolecules that lead to progressive degradation of functional groups [108]. However, this new method allow better recovery of MC pure fractions, once at least one step had pure MC fractions, which could not be accomplished in the previous method if the two salt concentrations were not well set.

8.4.2 Minicircle purification by Hydrophobic Interaction Chromatography

When the PP was initially conceptualized and designed, the possible strategies for purification were also taken into account. Besides the introduction of the PvuII restriction sites, one Nb.BbvCI nickase site was also created to promote the cleavage of only one strand of DNA on a double-stranded DNA substrate, namely the MP and PP resulted from recombination induction. Typically pDNA molecules present hydrophilic nature since the majority of the bases are shielded inside the double helix. In the presence of high concentrations of a kosmotropic salt, to promote the interaction with the resin surface, the hydrophobicity of SC MC isoform increases as a consequence of the underwinding phenomena (negative supercoiling). On the other hand, nicked and relaxed MP and PP present a lower hydrophobic profile than MC isoforms. Since HIC purification of plasmids relies in varying strength of hydrophobic interactions due to different properties of pDNA isoforms, the relaxation of non-MC species by this enzymatic digestion is an important procedure to increase the differences in hidrophobicity and it is the first step after total pDNA purification and before the HIC chromatography (Figure 43) [109, 110].

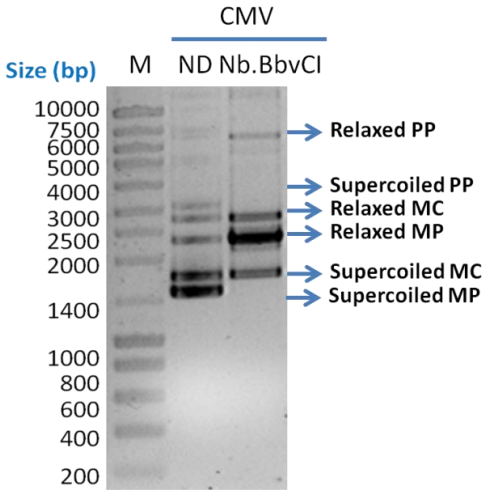

Figure 43 – Nb.BbvCI digestion of purified recombination products derived from the *E.coli* BW2P pMINILi-CMV-VEGF-GFP growth. Lane 1- NZYTech Ladder III, Lane 2 – Non-digested pMINILi-CMV-VEGF-GFP, Lane3 – Nb.BbvCI digestion of recombination products present in purified sample.

In the initial sample for purification, besides the pDNA species, other impurities can be present, such as RNA, genomic DNA and endotoxins. However, considering the experimental protocol used to purify the total pDNA after cell lysis, no RNA, genomic DNA and endotoxins are expected to be present in this study and even if they are, their concentrations are very low. Nevertheless, HIC chromatography allows their elimination. RNA and denatured genomic DNA, which are essentially single stranded molecules, have a high hydrophobic character due to the exposure of their hydrophobic bases, whereas highly hydrophobic endotoxins are even retained longer when compared with pDNA due to the lipid A portion of the molecule [109, 110].

Apart of the intrinsic biomolecule properties, the binding capacity to hydrophobic support is influenced by the structure of the ligand, the ligand density, the ionic strength of the buffer and the salt type used, the salting-out effect and the temperature, which are crucial factors for the success of HIC [109, 110].

A comparative study used six different commercial HIC resins from GE Healthcare for pDNA purification: phenyl Sepharose 6 high performance (PheHP), phenyl Sepharose 6 fast flow (low substitution) (PheFF-LS), phenyl Sepharose 6 fast flow (high substitution) (PheFF-HS), butyl Sepharose 4 fast flow(ButFF), butyl-S Sepharose 6 fast flow(ButFFS) and octyl Sepharose 4 fast flow (OctFF). This study concluded that aromatic phenyl ligand demonstrated the best selectivity for pDNA when the same mobile phase was used (ammonium sulfate 1.5 M)[109]. Concerning ligand density, a higher biomolecule binding capacity can be achieved by a higher ligand density since it leads greater possible number of interaction points but it is not necessarily true in all cases. A moderate ligand density enables the possibility to selectively bind the biomolecule of interest by adjustment of the binding buffer concentration [111]. Particularly, in the mentioned study, the PheFF-HS resin, which has higher ligand density (40µmol/mL medium), yielded better results when compared with the lower density (25µmol/mL medium) PheFF-LS and PheHP resins [109]. Thus, this was the selected resin for HIC purification of MC also in the present study.

PheFF-HS is a standard aromatic HIC support composed by highly cross-linked spherical agarose 6% beads modified with standard aromatic phenyl groups via uncharged, chemically-stable ether linkages. This resin was designed for capture and intermediate purification requiring low to medium hydrophobicity and its high ligand density substitution help to find the optimal selectivity and binding capacity [111]. Additional basic characteristics of this resin are present in Annex 14.

Regarding the salt type, the interactions ions-water and ions-biomolecules should be analyzed before choosing one. Based on ions surface charge density and water affinity, Hofmeister ordered ions from strongly hydrated (kosmotropic or anti-chaotropic ions) to weakly hydrated (chaotropic ions) [112]. Kosmotropic ions present a high water affinity and are considered “water structure makers” whereas chaotropic ions are weakly hydrated, and are known as “water structure breakers”. By these properties, anti-chaotropic ions are involved in stabilization and salting-out effects on macromolecules and on the other hand, chaotropic ions lead to salting-in effects (Figure 44) [109].

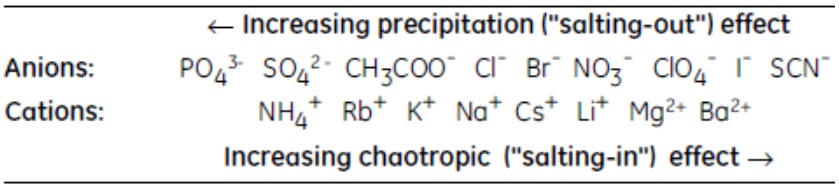

Figure 44 – Hofmeister series [111].

Increasing the precipitation salting-out effect supports the hydrophobic interactions and increasing the chaotropic effect weakens them. Ammonium sulfate, $(NH_4)_2SO_4$, at concentrations varying from 1.0 to 2.5M is the preferable salt to promote hydrophobic interaction due to its high salting-out ability, high solubility varying little in a range of 0–30°C, stability up to pH 8.0 and low cost. In the pDNA HIC purification study mentioned before, addition of ammonium sulfate up to 2.5M to the sample followed by HIC with 1.5M $(NH_4)_2SO_4$ in the binding buffer gave the best pDNA purification [109].

Additionally, hydrophobic interactions are weaker if the experiment is performed in a cold room, therefore the temperature should be controlled [111].

Taking into account all the previous variables, MC were purified by the PheFF-HS resin using a negative HIC strategy which begins by pre-conditioning samples with high salt concentration (2.5 M $(NH_4)_2SO_4$) and subsequent loading of the sample to HIC column. During chromatographic step, bound biomolecules, including MC and nicked MP and PP, are eluted by reducing the hydrophobic interaction and in this particular method, hydrophobic interactions were weakened by reducing the concentration of ammonium sulphate in the mobile phase. Firstly and according to the previous pDNA purifications using HIC, an isocratic HIC chromatography (1.5M $(NH_4)_2SO_4$ in 10mM Tris-HCl pH 8.0 followed by 10mM Tris-HCl pH 8.0 wash step) was performed and a reasonable separation of the MC from MP species was visualized in agarose gel electrophoresis. Therefore, an optimization process was realized. By performing a linear gradient chromatographic step between 2.2M $(NH_4)_2SO_4$ to 10mM Tris-HCl pH 8.0, different peak fractions species were observed on agarose gel electrophoresis and MC separation from MP species was possible [99]. After some adjustments and optimizations in salt concentrations in order to increase the resolution and purification, a step gradient method correspondent to the linear gradient peaks salt concentration was designed (17.0%B, 35.0%B, 100.0%B) [99] where the first peak is relative to relaxed forms of MP, the second one is composed by relaxed and supercoiled forms of MC and at 100%B, the remaining bound macromolecules are eluted (Figure 45).

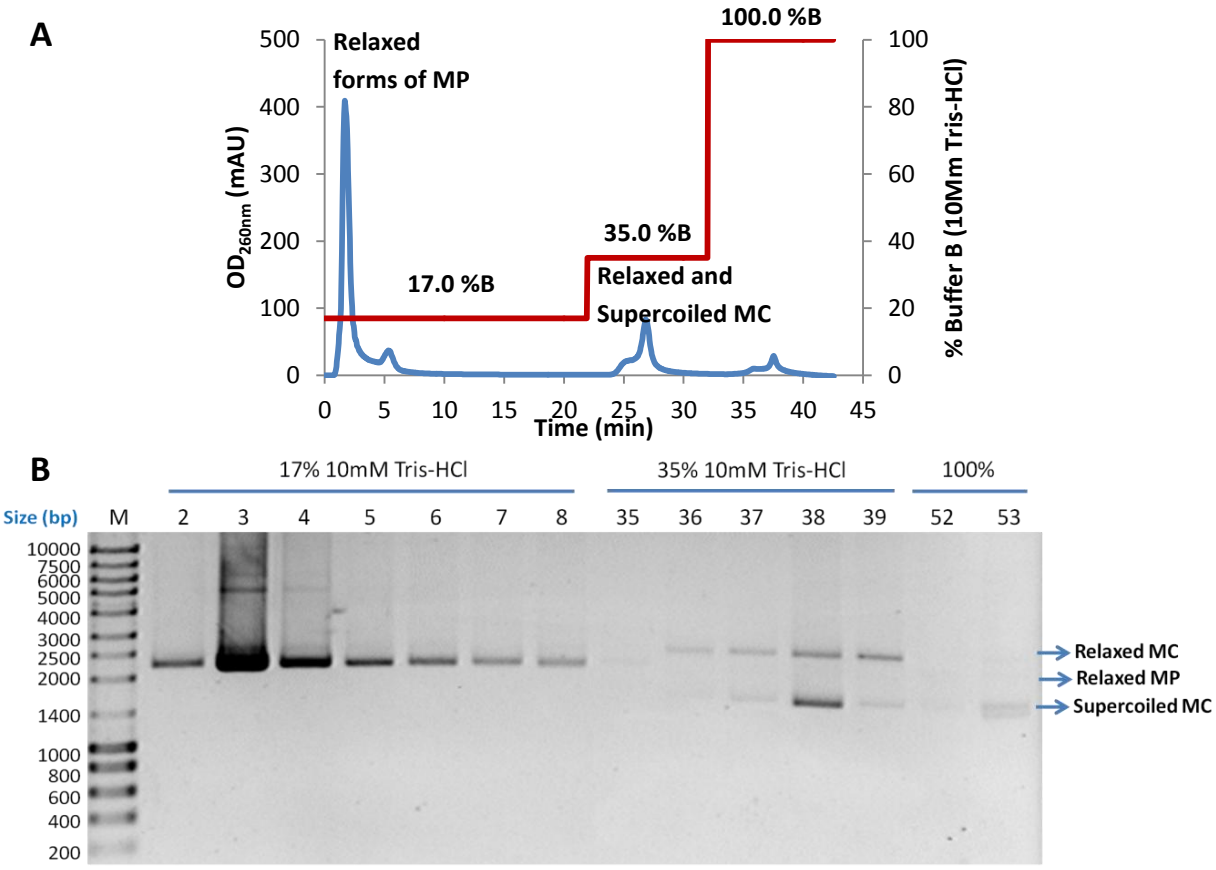

Figure 45 – Chromatographic separation of pMINILi-CMV-VEGF recombined and Nb.BbvCI DNA nickase digested products on a Phenyl Sepharose resin using a step gradient **(A)** and corresponding peak fractions visualized on agarose gel electrophoresis **(B).**

For all recombined, purified and digested pMINILi constructions, the same HIC method was applied and the reproducibility of HIC for MC purification in these conditions was proved (Figure 46). The individual chromatographs are present in Annex 15.

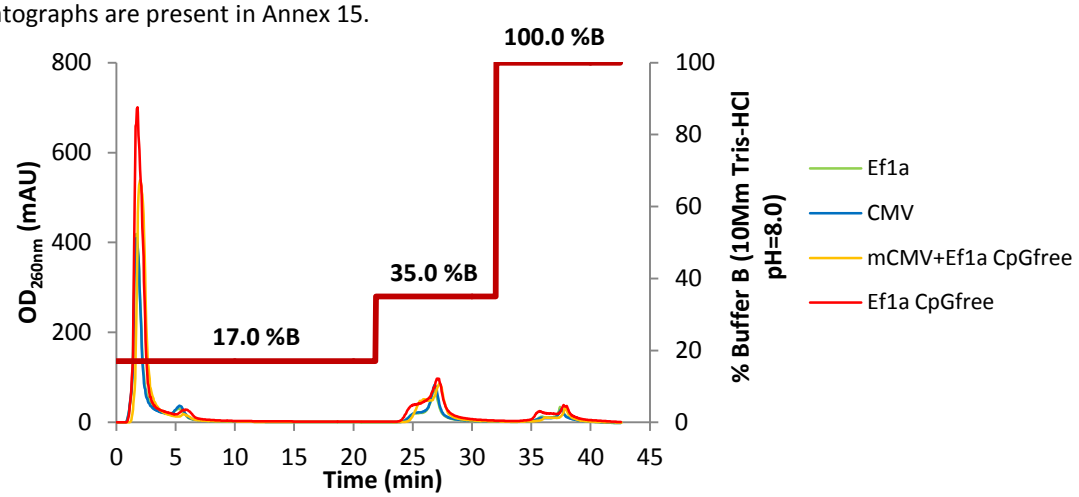

Figure 46 - Chromatographic separation of recombined and Nb.BbvCI DNA nickase digested pMINILi constructs on a PheFF-HS resin using a step gradient.

Other strategies of elution in HIC include increasing the concentration of chaotropic ions in the buffer in a positive gradient (linear or step), eluting with a polarity-reducing organic solvent as ethylene glycol, or including detergent in the eluent [111].

After chromatographic purification, dialysis and concentration of MC in MilliQ water was performed according to the manufacturer protocol. Finally, all MC were confirmed by enzymatic digestion (Figure 47) and DNA sequencing (Annex 16). In the DNA sequencing results, one point mutation was detected in the GFP gene sequence (G →A) that leads to an exchange of an arginine by a histidine. Since these aminoacids belong to the same group, which is aminoacids with positively charged R group, no negative consequences for GFP protein structure and activity were admitted.

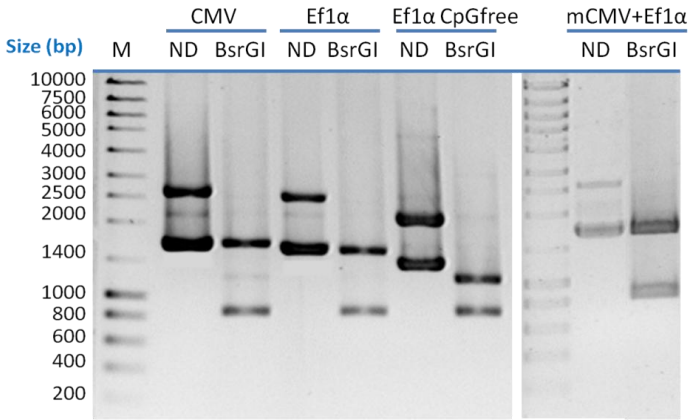

Figure 47 – BsrGI digestion of MC after all purification downstream processing: NZYTech Ladder III (Lane M); Non-digested MC (Lanes ND) and BsrGI digested MC (Lanes BsrGI) relative to the four promoters: MC CMV (1618bp+839bp), MC hEf1α (1531bp+839bp), MC mCMV+hEf1α CpG free(1618bp+839bp) and MC hEf1α CpG free (1180bp+839bp).

8.5 Minicircle purification methods comparison

In many areas, chromatography resins are the media of choice for chromatography applications and HIC is a well-established bioseparation technique at the laboratory and industrial scale [109, 110]. However, in some cases resin-based methods have limitations in purification of large molecules, such as DNA and viruses, due to their limited porous particle structure [113]. Particularly, PheFF-HS resin has 90µm of mean particle size and 45-165µm of bead size range [111]. Mass transfer between the mobile and stationary phase is essentially governed by diffusion, which is a slow process, especially for larger molecules that have a low mobility. Therefore, the separation is flow-dependent, which prevents work at high linear velocities. Also moderate flow-rates should be used to avoid back pressure. Moreover, resin pores are small which exclude large molecules from them. DNA molecules can only bind to the external particle surface and the internal surfaces of particles cannot be used. This results in a significantly reduced binding capacity and influences the process efficiency [113].

As an alternative to conventional resin supports, in monolithic chromatographic supports, all the mobile phase is forced to flow through the continuous and highly porous solid structure of the monolith. Methacrylate monoliths as CIM are characterized by a bimodal pore-size distribution, wherein macrochannels are composed by most of the void volume and the microchannels represent more than 80% of the monolith surface, which leads to high binding capacity. As a consequence, mass transport is enhanced by convection which is not limited by molecular size and dramatically reduces the long diffusion time required by conventional resins. These properties allow operations at high flow rates that do not affect mechanical stability, resolution and dynamic binding capacity for DNA, low back pressures and fast separations. Additionally, CIM Disks present simplicity of column filling and handling, no bubble entrapment problem and column length and monolith support can be changed by user according to their preferences because structure of the monolith is constant, regardless of the monolith volume, shape or design [105, 108, 113].

In this study, MC recoveries for HIC and CIM-DEAE purifications were determined using the Equation 8. According to the peak integration table of each chromatogram given by UNICORN software, the relative percentage of MC in the injected and original sample could be accessed and based on that, MC recoveries for both methods were calculated. These values are present in Table 14.

$$MC\ Recovery = \frac{m_{MC}}{m_{Load} \times \%MC\ peak\ area} \times 100 \quad \text{(Equation 8)}$$

Table 14 – MC Recovery results from CIM-DEAE and PheFF-HS chromatography.

Plasmid	Chromatographic method	Load		Peak areas		MC Recovery		
		m_{Load} (µg)	$V_{injection}$ (mL)	%MC	%Non-MC species	m_{MC} (µg)	MC Recovery (%)	Mean MC Recovery ± SEM (%)
pMINILi-CMV	CIM-DEAE	262.5	1.0	20.4	79.6	20.5	38.3	50.8 ± 8.9
		201.0	1.0	18.4	81.6	28.2	72.5	
		301.0	1.0	19.7	80.3	24.5	41.4	

pMINILi-CMV	PheFF-HS	493.9	1.0	20.8	79.2	46.8	45.6	45.6*
pMINILi-hEf1α	CIM-DEAE	513.0	1.0	11.8	88.2	26.9	44.4	63.8 ± 6.9
		104.6	0.5	8.3	91.7	7.2	82.6	
		365.0	2.0	16.7	83.3	41.4	67.9	
		227.0	1.0	17.6	82.4	24.0	60.2	
	PheFF-HS	466.8	1.0	18.6	81.4	37.7	43.4	43.4*
pMINILi-mCMV+hEf1α CpG free	CIM-DEAE	497.1	1.0	4.5	95.5	23.2	103.1	67.4 ± 17.4
		195.9	0.5	13.2	86.8	7.6	29.3	
		369.2	1.0	18.7	81.3	48.2	69.8	
	PheFF-HS	654.0	1.0	12.2	87.8	59.0	73.9	73.9*
pMINILi-Ef1α CpG free	CIM-DEAE	452.7	1.0	10.3	89.7	20.5	43.9	52.3 ± 6.2
		371.6	1.0	16.6	83.4	38.0	61.6	
	PheFF-HS	849.9	1.0	14.4	85.6	49.6	40.5	40.5*

*Only one experiment was performed

Regarding the percentage of MC in recombined, purified and digested samples, CIM-DEAE purifications revealed that MC occupied 14.69 ± 1.60% of the loaded sample and in HIC, this percentage was 16.50 ± 1.69%. Despite differences are not significant, it is important to notice that in CIM-DEAE purifications, some MC eluted during the steps of linear fragments elution, therefore a portion of MC was lost during this phase. These values were obtained taking into account all the MC constructions together for each purification method. Besides this comparison, the value of MC percentage in the original sample should be analyzed. Since these MC molecules are expected to be applied in biopharmaceutical applications, this range of percentages represents a very low MC amount produced during all the process. This low percentage can be associated to the low production of MC during *E.coli* BW2P growth or to MC loss during downstream processing.

HIC MC recovery was only verified by one experiment for each MC, but in three of four experiments, the HIC MC recovery was lower in comparison with the respective mean MC recovery obtained using monolithic CIM-DEAE method (Table 14). However, since MC recovery seems to decrease with higher mass loadings[71] and in HIC experiments, higher masses than in CIM-DEAE were loaded into the column, lower MC recoveries were obtained. All MC recovery mean values using CIM-DEAE monolith were similar and higher than the ones obtained with HIC purifications but if independent yields of the same MC purification experiments are analyzed, meaningful discrepancies are observed. These differences were also observed before, during the development of this CIM-DEAE purification method: values from 56.9 to 94.4% for MC recovery were obtained [71]. Despite the lower average MC recoveries in present study, these results demonstrate the possible variability of this method according to the sample load and established method.

With only one HIC experiment to each MC, no conclusions can be accomplished about which is the best method for MC purification, however some comments can elucidate pros and cons of each method for this purpose. In theory, CIM-DEAE monolith purification should be the preferred method and effectively, it led to a higher MC recovery. Nevertheless, high molecular weight smear in addition to the supercoiled and relaxed MC

bands were visualized in agarose gel electrophoresis, which are undesirable for further applications, even if they are isoforms of MC (Annex 12 and Annex 13). Considering MSC transfection experiments, CIM-DEAE purified MC samples led to MSC and CHO culture bacterial contamination, confirmed by bacterial growth in LB agar plates without antibiotics, whereas HIC purified MC samples did not promote this negative consequence. This bacterial contamination of CIM-DEAE samples was also negative for MC molecules, once in presence of bacterial nucleases, MC relaxation and degradation was notified (data not shown). Different strategies were adopted to eliminate contamination of the MC samples and MSC and CHO cultures, namely use of sterilized 96-well plates, cleaning in place of the monolith, addition of more antibiotic to MSC culture, and even the use of a new monolith, and only a decrease in bacterial concentration was observed. This difference between methods can be related with the different AKTA system that each one use, the salt concentrations applied to perform the purification that in HIC can be enough to kill bacteria or the presence of bacterial contamination in the CIM Disk support, which was not submitted to a cleaning protocol. Regarding the present HIC strategy, the use of ammonium sulphate is environmentally undesirable and should be replaced. The disposal of large quantities of this salt from large scale processes into the environment increase the eutrophication potential because it is a nitrogen-rich substance [109]. Results from a study revealed that sodium citrate is a viable alternative to replace ammonium sulfate in HIC, even though a smaller HPLC purity was obtained in the plasmid fractions. The study suggested a second purification step which could be considered as a final polishing step (usually size exclusion chromatography) to certify the purity and quality of the final pDNA sample required by GMP. The substitution of the ammonium sulfate by sodium citrate could reduce the environmental impact at least three times [109].

Despite these results and comments, both methods should be optimized. According to international regulations a content of plasmid supercoiled form higher than 90% is required for pharmaceutical applications but none of them achieved this goal because other undesired topological MC isoforms such as the open circular were present. These isoforms reduce the homogeneity and lead to less efficient transfections and expression rate in eukaryotic cells [105]. In the MC production market, there is at least one complete system that reported >99% of MC supercoiled form, endotoxin level of <4.9EU/mg DNA and <0.1% bacterial chromosomal DNA in final samples, suitable for *in vitro* and *in vivo* gene transfer [77].

An alternative to resins or monoliths is membranes. Membranes are very thin beds with an extreme aspect ratio. They provide a reduced pressure drop along the chromatographic unit, allowing higher flow rates and consequently higher productivity. The problems with membranes are uniform flow distribution, a relatively large dead volume and scalability. In order to scale-up the purification system, various membranes can be assembled into a column, but additional void spaces are created [105].

8.6 Transfections

The MC production and purification methods, which have been developed in our laboratory, were designed to achieve an efficient and effective non-viral gene delivery into human stem cells. In order to optimize the expression of the gene of interest in MSC, different promoter constructions with the same transcription unit (VEGF-GFP genes fusion), as described previously, were tested. The choice of these promoters was based on expression studies using similar or equal versions of them.

A quantitative comparison of some constitutive promoters' activity and stability in undifferentiated and differentiated hESC was performed [114]. In that study, lentiviral gene transfer was used to ensure stable integration of promoter-GFP constructs into the hESCs genome and promoter activities were monitored by the expression of GFP in long term culture of undifferentiated hESC and in cells differentiated into all three embryonic germ layers. The results showed that human β-actin and hEF1α promoters allowed stable activities during long term culture of undifferentiated hESC. The human β-actin promoter was superior by maintaining expression in 75–80% of the cells after 50 days in culture. Although the hEF1α promoter was downregulated in approximately 50% of the cells, it was the most stable promoter during differentiation. Whereas the human β-actin and hEF1α promoters were shown to mediate stable long term expression of GFP in hESC, the CMV promoter only mediated transient expression [114]. Another study showed that transduction of target cells with human CMV enhancer containing lentiviral vectors resulted in a multiple-log increase in GFP expression compared to corresponding vectors lacking the human CMV enhancer [115].

Regarding VEGF expression, MC DNA, containing the VEGF gene regulated by different promoters, including the CMV and chicken β-actin, were tested by *in vitro* and *in vivo* transfection studies. *In vitro* transfections, using a non-viral delivery strategy, the chicken β-actin promoter in MC DNA was found to show the higher VEGF expression. However, in skeletal muscle tissue, the CMV promoter showed higher VEGF expression compared to the chicken β-actin promoter. The discrepancy of promoter comparison *in vitro* and *in vivo* might be due to the different genetic environment between the immortal myoblast culture and differentiated myotubes in muscle tissue [69]. In the present study, human β-actin promoter was not included in the plasmid constructions due to cloning-associated difficulties and time constraints. However, it is integrated in the future perspective work.

Despite these reported experiments served as a guide for the selection of the promoters, it cannot be excluded that differences in methodologies and cell types as well as the possible interference between the promoter and reporter gene might influence transgene expression [114]. Also, *in vivo* evaluation of promoter activity is crucial and may not be substituted by an *in vitro* assay [69].

Regarding the present study transfection experiments, pVAX-GFP transfected cells were used as positive control (Annex 17), since literature about its behavior in similar studies is available. This plasmid was constructed from pVAX1 vector from Invitrogen™ [58]. Derived from pVAX-GFP, pVAX-VEGF-GFP (Annex 17)

transfected MSC were studied in order to evaluate the effect of vector itself in expression profile of VEGF and GFP.

Besides the plasmid size of the different vectors presented in plasmid construction section, there are other characteristics that should be mentioned for the analysis of transfection results, namely the number of CpG motifs, molecular weight and initial number of plasmid copies (Table 15). In all transfection experiments using CHO cells or MSC, equimolar amounts of the pDNA or MC DNA were used to ensure comparable initial copy numbers. The vector working amount was established based on pVAX-GFP reference working amount of 1µg.

Table 15 – Overview on the characteristics of the different vectors used in CHO and MSC transfections.

Vector	Length (bp)	CpG Motifs Content [116]	MW (g/mol) [117]	Working amount (µg)	Plasmid Copies
pVAX-GFP	3697	248	$2.40x10^6$	1.00	$2.51x10^{11}$
pVAX-VEGF-GFP	4273	266	$2.64x10^6$	1.10	$2.51x10^{11}$
pMINILi CMV	4563	285	$2.82x10^6$	1.17	$2.51x10^{11}$
pMINILi hEf1α	4475	303	$2.77x10^6$	1.15	$2.51x10^{11}$
pMINILi mCMV+hEf1α CpG free	4563	249	$2.82x10^6$	1.17	$2.51x10^{11}$
pMINILi hEf1α CpG free	4125	251	$2.55x10^6$	1.06	$2.51x10^{11}$
MC CMV	2457	132	$1.52x10^6$	0.63	$2.51x10^{11}$
MC hEf1α	2370	150	$1.46x10^6$	0.61	$2.51x10^{11}$
MC mCMV+hEf1α CpG free	2457	98	$1.52x10^6$	0.63	$2.51x10^{11}$
MC hEf1α CpG free	2019	98	$1.25x10^6$	0.52	$2.51x10^{11}$

8.6.1 CHO cell Transfection by Microporation

Due to the previously unexpected results of MSC transfection with MC, where MC attained lower VEGF production than conventional plasmids [118], a first screening using CHO cells was performed with the new promoter constructions. In this study, as previously described, some molecular modifications were made in PP and respectively in MC in order to evaluate if the theoretical hypothesis of better transfection and expression results of MC in comparison with the respective PP is correct. Two CHO cells transfection experiments were carried out using both MC and PP, and pVAX-GFP as positive control. Variables as cell viability and recovery, yield of transfection, percentage of GFP^+ cells attained by each vector were determined. Additionally, combined variables were also calculated in order to explore the results.

As described in methods section, the results from the first experiment were only assessed 24h after microporation and in the second CHO cells transfection, an additional time-point was included (day 4). Bacterial contamination was observed on day 4 and the experiment could not proceed. No supernatants or cells for RT-PCR were collected since it was not the goal of this screening.

8.6.1.1 CHO Cell Recovery

Regarding cell recovery calculations by Equation 4 (Figure 48), all CHO cells transfected with MC presented a higher cell recovery than transfection with their respective PP. However, this difference was less significant for MC CMV and MC mCMV+hEf1α CpG free constructions. Moreover, MC CMV demonstrated lower percentage value in comparison with other PP and even pVAX-GFP that was not expected. Since MC CMV is considerably smaller than these plasmids, its perturbation and entrance to the cells should be similar to the observed for the other MC constructions. Considering the pVAX-GFP and PP cell recoveries, the order from the highest to the lowest was: pMINILi hEf1α > pMINILi mCMV+hEf1α CpG free > pVAX-GFP > pMINILi CMV > pMINILi hEf1α CpG free. Also this tendency does not correspond to the expected result, considering that larger size pDNA molecules entrance into the cells cause more damage than the smaller ones [119]. The highest cell recovery was observed for MC hEf1α that is not the smallest MC and the major difference in cell recovery between MC and PP was noticed in hEf1α and hEf1α CpG free transfections.

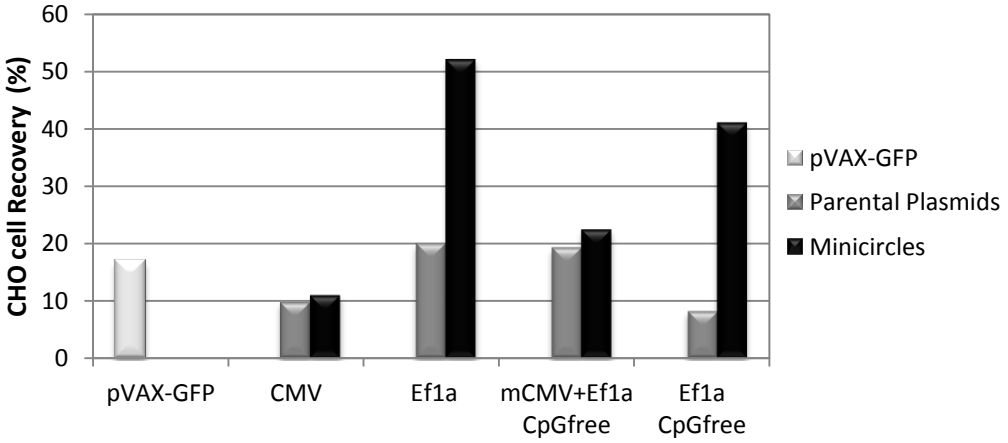

Figure 48 - Cell recovery of CHO cells after transfection with pVAX-GFP, VEGF-GFP encoding pMINILi vectors and their respective MC. Cell Data obtained from two independent experiments (n=2) 24h after transfection. Cell recoveries are presented as mean values.

8.6.1.2 CHO Cell Viability

Cell viability (Equation 3) is an important parameter to evaluate how cells handled the presence of a vector inside of them after transfection procedure. After media removal where dead cells were in suspension and were not considered for cell viability calculations, transfected and non-transfected cell viabilities were determined by trypan blue exclusion method (Figure 49). In literature, there is evidence that microporation does not affect significantly cell viability [101]. In fact, all CHO transfection experiments revealed cell viabilities above 80%. Moreover, all CHO cells transfected with MC presented viabilities values similar to non-transfected control cells (97.7% of cell viability) and above 90%. Additionally, no major differences were observed between the viabilities of cells transfected with the different MC vectors. On the other hand, CHO cells transfected with PP and pVAX-GFP attained slightly lower cell viabilities, with exception of PP hEf1α CpG free that presented higher cell viability in comparison with its MC. Similar cellular toxicity levels for pDNA and MC transfections

were already published in order to emphasize that greater MC efficiency is not related with cellular toxicity decrease[120, 121]. The only possible topic of discussion about these differences in cell viabilities is the negative influence of plasmid size during delivery to the cell that can have an impact in cell viability shortly after transfection [119].

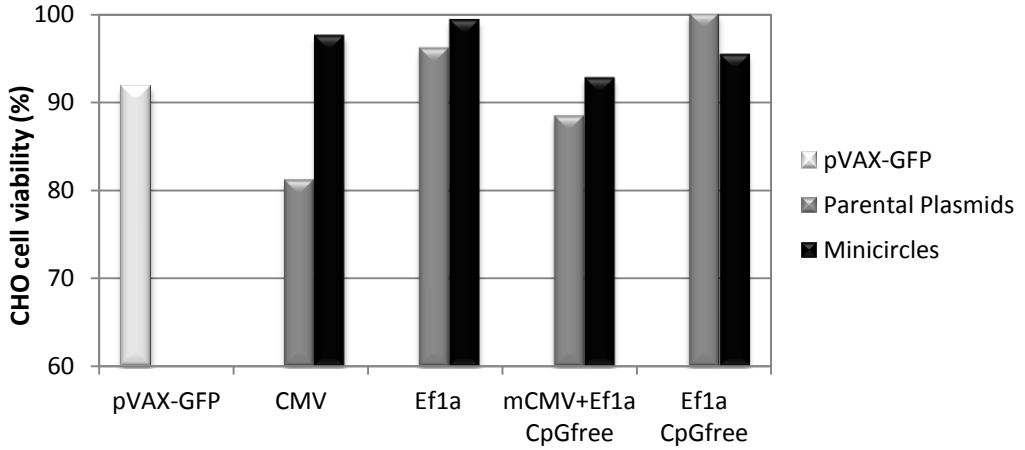

Figure 49 - Cell viabilities of CHO cells after transfection with pVAX-GFP, VEGF-GFP enconding pMINILi vectors and their respective MC. Cell Data obtained from two independent experiments (n=2) 24h after transfection. Cell viabilities are presented as mean values.

8.6.1.3 GFP$^+$ CHO cells percentage

Results of GFP$^+$ CHO cells percentage are present in Figure 50 and Figure 51. All CHO cells transfected with MC demonstrated a higher GFP$^+$ cell percentage on day 1 than transfections with their respective PP. The major difference was observed for hEf1α CpG free derived PP and MC transfections, wherein PP only led to around 20% of GFP$^+$ cells and the minor variation was for hEf1α promoter. Regarding the comparison between the GFP expression by different MC promoters, the highest and similar expression levels were observed for MC CMV and MC mCMV+hEf1α CpG free, followed by MC hEf1α and MC hEf1α CpG free respectively. The order of expression values for the PP promoters was similar to the observed in MC promoters, with exception of PP mCMV+hEf1α CpG free that demonstrated a higher percentage in relation to PP CMV. This result can be explained by the lower number of CpG motifs of mCMV+hEf1α promoter that might retard transgene silencing as previously described [60, 122].

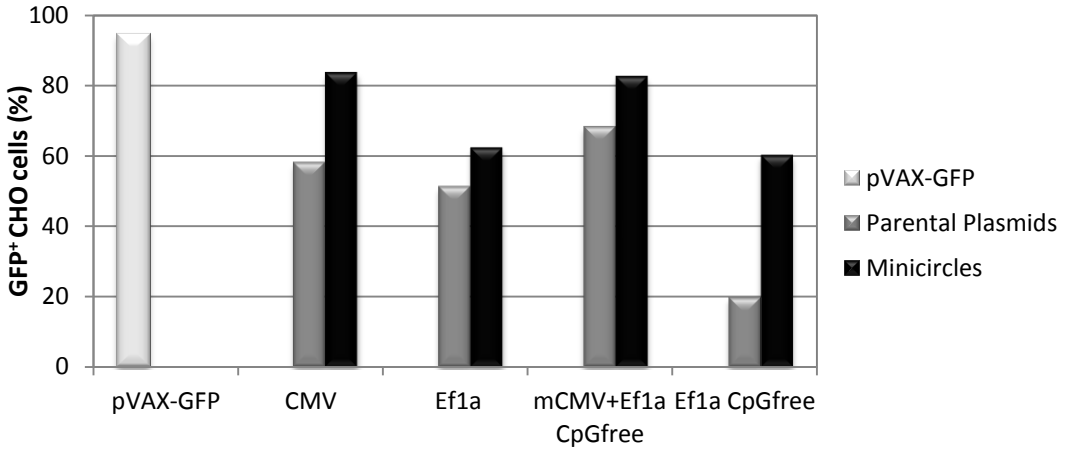

Figure 50 - GFP$^+$ cells percentage of CHO cells after transfection with pVAX-GFP, VEGF-GFP enconding pMINILi vectors and their respective MC. Cell Data obtained from two independent experiments (n=2) 24h after transfection. Percentage values are presented as mean values.

Regarding pVAX-GFP, one study reported an average value of 35.5 ± 12.8% of GFP$^+$ cells from three independent experiments of CHO cells transfected with pVAX-GFP by lipofection method. Furthermore, the same transfection experiments conducted in CHO cells using electroporation led to results similar to those obtained by lipofection [58]. Since microporation is described as an advanced and improved version of electroporation for transfection, the higher percentage of GFP$^+$ cell obtained in this study was expected.

Concerning day 4 after microporation (Figure 51), all of VEGF-GFP constructions showed a reduction in GFP$^+$ cells percentage. This decrease should be more significant for PP than MC because there is evidence that upon transfection, larger plasmids have less mobility inside the cytoplasm and are more exposed to the action of host nucleases for degradation. Moreover, PP contains the bacterial backbone which have immunogenic sequences, thus transgene silencing is more probable to occur. Therefore, not only the lack of bacterial genes and low CpG motifs content, but also the smaller size of MC might contribute to their improved expression profile [121]. However, this effect was not observed for MC CMV and hEf1α CpG free promoter transfections.

Analyzing individual promoters transfection results, MC CMV decreased by 41% in percentage of GFP$^+$ cells but still remained higher than PP percentage value; PP hEf1α decreased by 52% whereas its respective MC reduced only 20%; the minor expected reduction was observed in mCMV+hEf1α CpG free promoter, 30% and 9% for PP and MC respectively and finally, a diminution of 12% and 34% was reflected correspondingly in PP and MC hEf1α CpG free promoter.

The observed time-dependent slight increase of GFP$^+$ cells for pVAX-GFP might be attributed to the accumulation of intracellular GFP in transfected cells over time leading to elevated detection level [77]. The same event cannot be observed in MC and PP transfections since VEGF-GFP fusion protein is probably secreted to the medium, due to the maintenance of the secretion signal in the N-terminus of VEGF, which was not modified by the fusion with the GFP gene at its C-terminus [123]. Moreover, VEGF glycosilation, homodimerization and biological activity are not compromised by the GFP fusion [123].

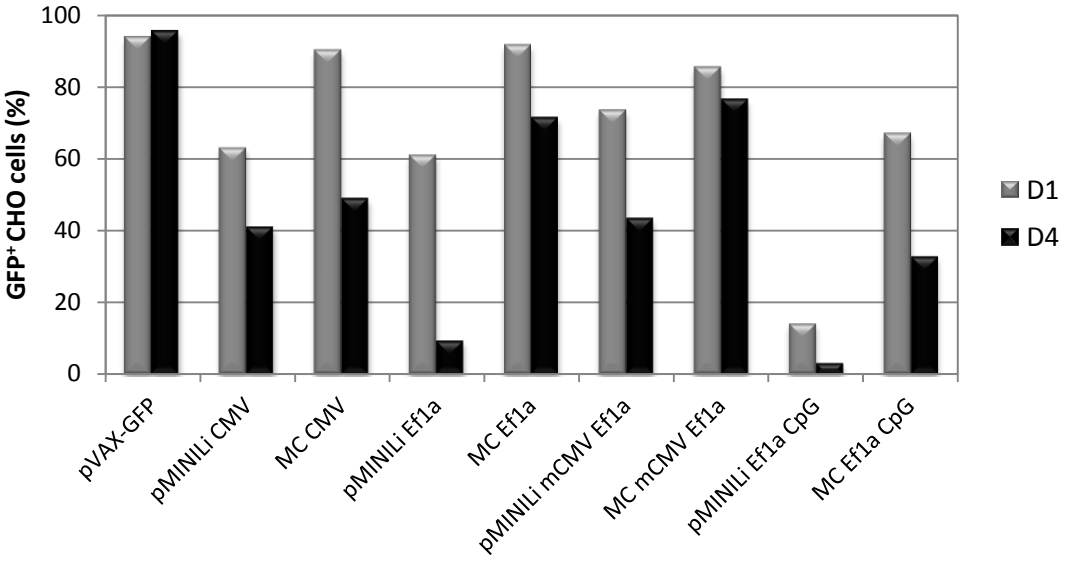

Figure 51 - GFP$^+$ cells percentage of CHO cells after transfection with pVAX-GFP, VEGF-GFP encoding pMINILi vectors and their respective MC. Cell data obtained from one single experiment (n=1) 24h and 4 days of culture after transfection.

8.6.1.4 CHO cell Yield of Transfection

According to Equation 5, yield of transfection takes into account the GFP$^+$ percentage in the transfected pool of cells in relation to the control cell number, 24h after transfection. Since all MC transfections demonstrated a higher GFP$^+$ cells percentage and in general a higher number of live cells than PP transfection experiments, superior MC transfection yields than PP were expected (Figure 52). The major difference between MC and PP yields was observed in hEf1α CpG free promoter because the CHO microporation with this PP led to the minor GFP$^+$ percentage and cell recovery values. pVAX-GFP had a superior transfection yield due to the high GFP$^+$ cells percentage achieved, represented in Figure 50.

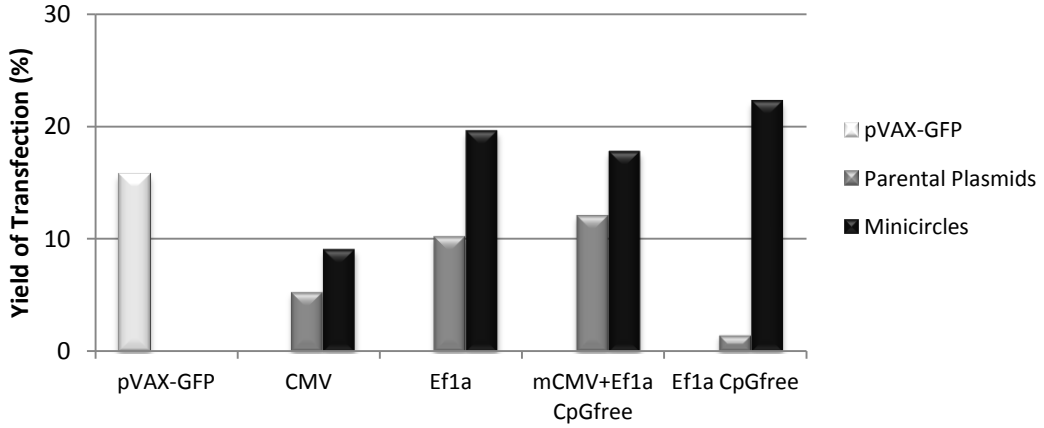

Figure 52 – Yield of transfection of CHO cells after transfection with pVAX-GFP, VEGF-GFP encoding pMINILi vectors and their respective MC. Cell Data obtained from two independent experiments (n=2) 24h after transfection. Cell recoveries are presented as mean values.

8.6.1.5 CHO cell GFP Expression Mean Intensity

GFP mean intensity is a parameter evaluated during flow cytometry analysis and from this methodology results, it is the more convenient measurement of GFP expression and, subsequently, promoter strength or transgene silencing over time due to the type of vector used. However, quantification of expression by mean intensity is not always straightforward and more techniques should be used to confirm or not the expression profile of a protein.

Regarding the results presented in Figure 53, pVAX-GFP mean intensity is much higher than all MC and PP transfections experiments (Figure 53 and Figure 54). However, this value cannot be comparable since the expression cassette of pVAX-GFP is only composed by one gene and accordingly to that, it is supposed that more mRNA transcripts of GFP are produced in comparison to the number of transcripts of VEGF-GFP expression cassette. Moreover in MC and PP, since GFP is transcript as a monocistronic mRNA and expressed as a fusion protein with VEGF, GFP protein structure and, consequently, fluorescent activity could be modified and reduced. Azzoni *et al.* [58] reported a GFP mean intensity in their study of around 500AU which is roughly 5 times lower to the one obtained in this study. The explanation for this difference can be the better transfection method used in our study, which also led to a higher %GFP^+ cells.

About the other experiments, CMV and mCMV+hEf1α CpG free constructions led to transfection results with the highest GFP mean intensity, whereas hEf1α and hEf1α CpG free resulted in half or less of those values. Every MC transfected CHO cells obtained a higher GFP mean intensity, excepting MC CMV experiment. This superior GFP mean intensity for MC is associated to a higher level of transcription and translation that can be associated to the lower MC degradation and subsequently more MC vector inside cells, or reduced transgene silencing process because they have less immunogenic sequences than PP that can trigger defense responses by CHO cells [121].

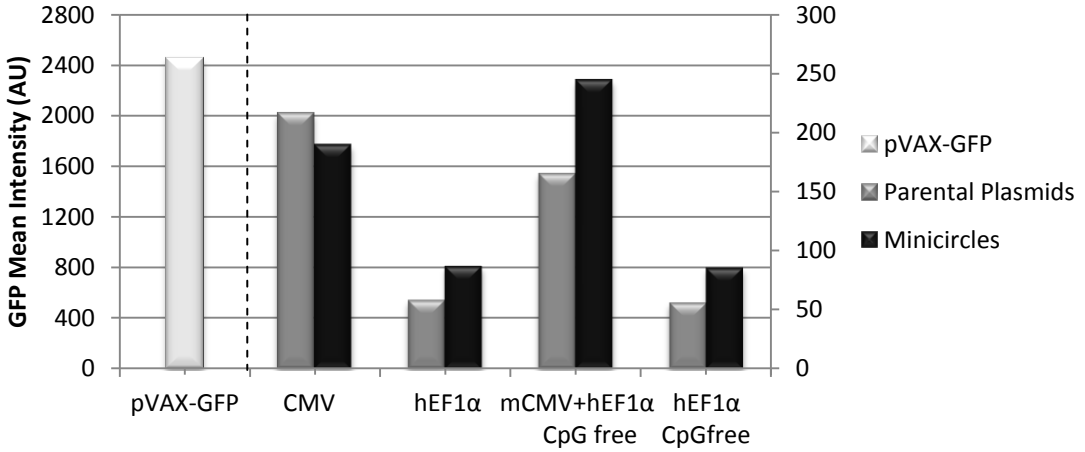

Figure 53 – GFP expression mean intensity of CHO cells after transfection with pVAX-GFP, VEGF-GFP encoding pMINILi vectors and their respective MC. Cell Data obtained from two independent experiments (n=2) 24h after transfection. Mean intensities are presented as mean values and the dashed line separates the pVAX-GFP from the remaining PP and MC construction values scale.

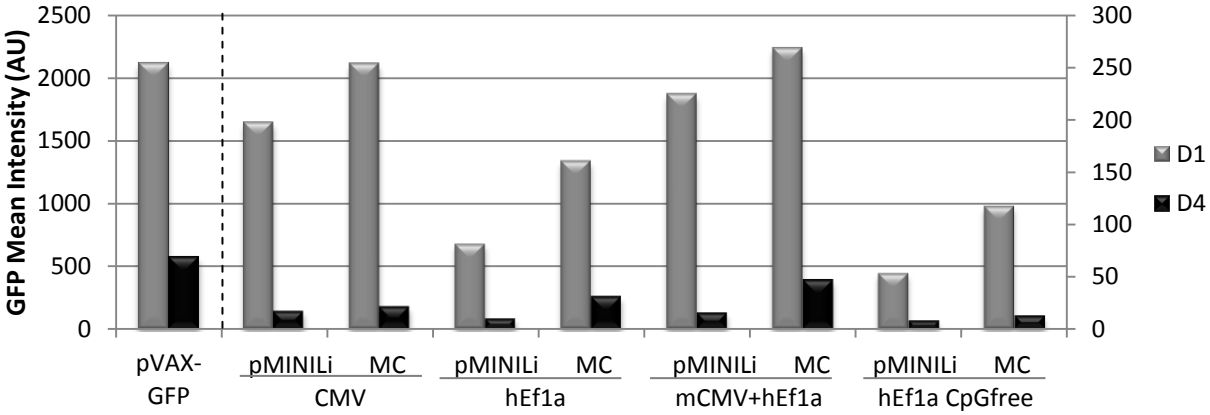

Figure 54 - GFP expression mean intensity of CHO cells after transfection with pVAX-GFP, VEGF-GFP encoding pMINILi vectors and their respective MC. Cell Data obtained one single experiments (n=1) 24h and 4 days of culture after transfection. The dashed line separates the pVAX-GFP from the remaining PP and MC construction values scale.

Concerning day 4 after transfection (Figure 54), all GFP mean intensities dropped significantly with values of 73% to 93% of decrease rates. Since these results are from one single experiment no conclusions can be afforded about transgene silencing rate because there was not observed the superior transgene silencing in vectors with more bacterial motifs. pVAX-GFP had the smallest decrease as well as GFP mean intensity of pMINILi CMV and hEf1α CpG free dropped less than their respective MC values. Only MC hEf1α and mCMV+hEf1α CpG free revealed the expected behavior in relation to their PP, which is a lower decrease in GFP mean intensity over time. Nevertheless, all MC GFP mean intensities on day 4 remained higher to the respective ones in PP.

8.6.1.6 CHO cell GFP Expression Mean Intensity related results

For a more accurate discussion of GFP and implied VEGF expression profiles by CHO cells, two additional product values, which have an increased importance compared to the rest of parameters, were calculated taking into account GFP expression mean intensity, yield of transfection and GFP^+ cells percentage values.

Analyzing both product values (Figure 55 and Annex 18), the different promoter constructions can be ordered in the same way according to their transfection performance. By this way, mCMV+hEf1α CpG free promoter led to the best CHO transfection results 24h after transfection, followed by CMV, hEf1α and hEf1α CpG free, respectively. Moreover, CHO cell transfections with MC-based vector also proved to achieve enhanced GFP expression in comparison with their respective PP.

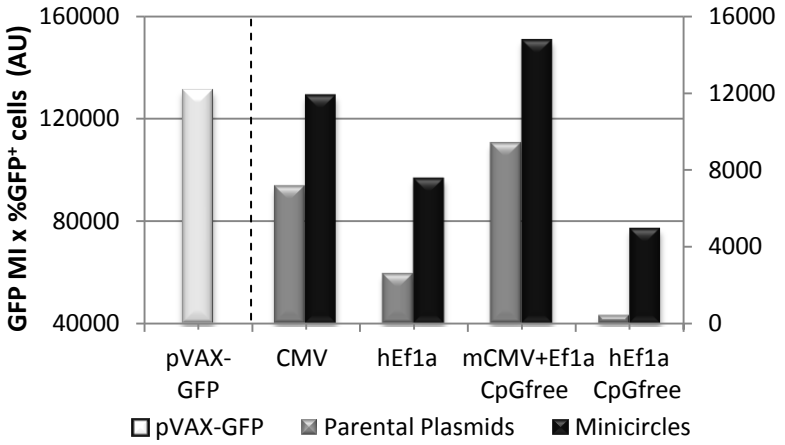

Figure 55 – GFP expression mean intensity and GFP^+ cells percentage product values of CHO cells transfection experiments with pVAX-GFP, VEGF-GFP encoding pMINILi vectors and their respective MC. Cell Data obtained from two independent experiments (n=2) 24h after transfection. Mean intensities are presented as mean values and the dashed line separates the pVAX-GFP from the remaining PP and MC construction values scale.

As observed for GFP mean intensity and GFP^+ cell percentage, there was a deep fall in GFP expression mean intensity and GFP^+ cells percentage product values after 4 days of cell culture (Figure 56) and, with exception of pVAX-GFP, mCMV+hEf1α CpG free transfections, both MC and PP, obtained the best results, followed by CMV transfections. Although better results were expected, the possible substitution of CMV promote to a combined version of mouse CMV enhancer with human hEF1α core promoter, which does not contain CpG motifs, is an attractive idea for the specific therapeutic application of the present study.

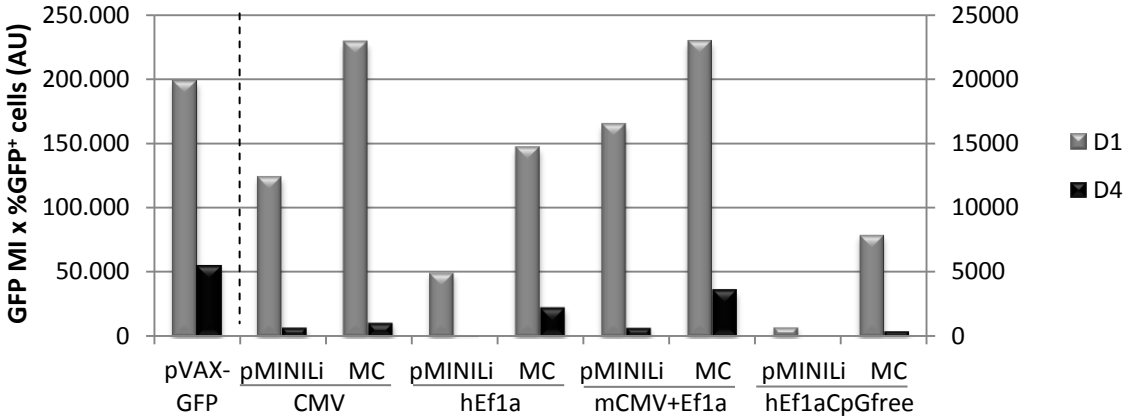

Figure 56 – GFP MI and GFP^+ cells percentage product values of CHO cells transfection experiments with pVAX-GFP, VEGF-GFP encoding pMINILi vectors and their respective MC. Cell Data obtained one single experiments (n=1) 24h and 4 days of culture after transfection. The dashed line separates the pVAX-GFP from the remaining PP and MC construction values scale.

8.6.2 MSC Transfections by Microporation

As previously optimized [100], $1.5x10^5$ MSC/10µL were microporated using a DNA mass equivalent to 1 µg of pVAX-GFP (Table 15). After transfection, MSC were plated in two wells from a 6-well plate and since a different and lower number of cells effectively attached to the well surface due to the difficulty of the cell collection

after centrifugation and before transfection and the microporation process itself, the cell density was variable. Three different BM MSC donors were tested (males with 35, 58 and 60 years old).

In parallel with CHO cells screening, the same variables were tested: cell viability and recovery, yield of transfection, percentage of GFP^+ cells and GFP mean intensity and derived results attained by each vector. In addition to what was analyzed in CHO cells transfection, supernatant and cell samples were collected, whenever possible, for plasmid copy number per cell determination and VEGF secretion by RT-PCR and ELISA analysis, respectively.

8.6.2.1 MSC Cell Recovery

According to Equation 4 and Figure 57, the highest cell recovery obtained was for MC CMV which is not the smallest MC but its entrance to the cell led to a lower cell death. Also pVAX-GFP transfected cells demonstrated a higher cell recovery in relation to the other MC vectors which was not expected, since it is larger in size. However in literature, an even higher cell recovery in the same microporation conditions was reported (≈80%) [100]. One possible explanation for this event might be related to the vector topology at the moment of microporation. Supercoiled molecules cause less cell perturbation during its entry to the cell in comparison to open circular and linear isoforms of the same vector [107]. Therefore, the presence of a higher percentage of SC molecules in the MC CMV and pVAX-GFP samples could lead to the observed high cell recovery. As predicted, pVAX-VEGF-GFP presented the lowest cell recovery due to its larger size and no significant differences were detected within cell recoveries from MC hEF1α, mCMV+hEF1α CpG free and hEF1α CpG free experiments.

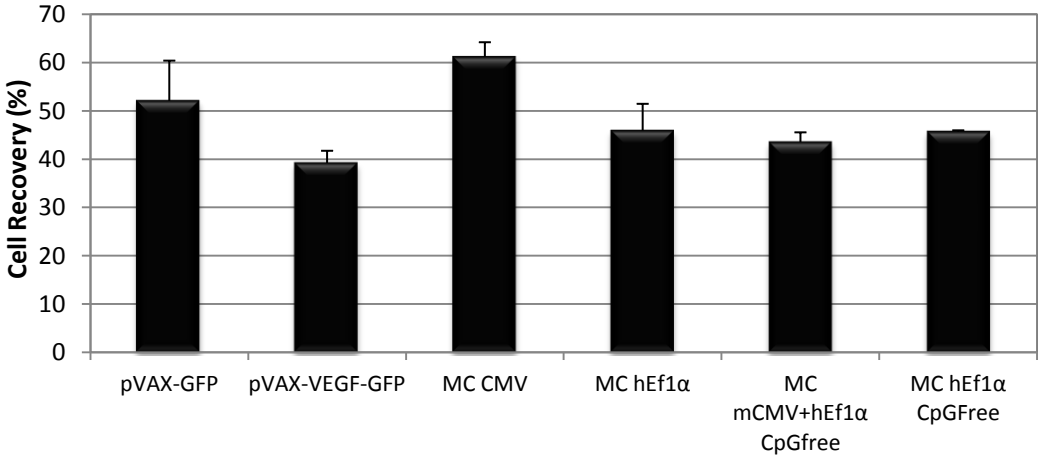

Figure 57 - Cell recovery of MSC after transfection with pVAX-GFP, pVAX-VEGF-GFP and VEGF-GFP encoding MC. Cell Data obtained from three independent experiments (n=3) 24h after transfection. Cell recoveries are presented as mean values ± SEM.

8.6.2.2 MSC Cell Viability

The cell viability is given by the ratio of surviving cells and the total number of cells of the same sample (Equation 3) and as shown in Figure 58, high cell viabilities were obtained in all conditions. However, cell recovery, being the ratio of alive cells of a given sample by the control reflects more accurately the level of cell

death caused by transfection procedure in each condition [100]. As previously mentioned for CHO cells transfections, the presence of vectors inside cells showed do not cause significant damages over time unless during their entrance to the cell where it was observed significant decrease of alive cells after transfection. Regarding cell viabilities values, there were no significant differences between each vector neither with control cells and the values were all above 90% during 7days of experiment. pVAX-GFP cell viability was in agreement with the literature [100].

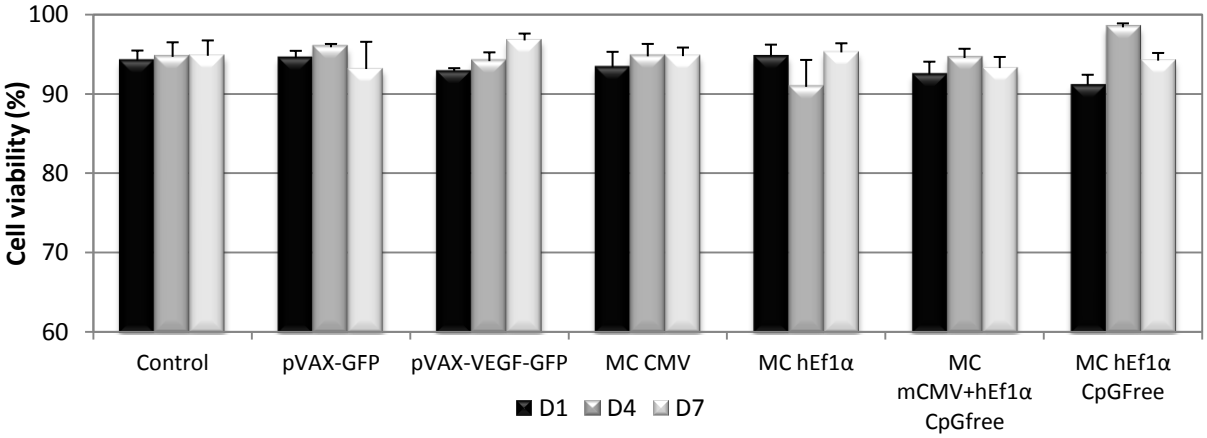

Figure 58 - Cell viability of MSC cells after transfection with pVAX-GFP, pVAX-VEGF-GFP and VEGF-GFP encoding MC. Cell data obtained from three independent experiments (n=3) 1, 4 and 7 days of cell culture after transfection. Cell viabilities are presented as mean values ± SEM.

8.6.2.3 GFP$^+$ MSC percentage

In the first instance, lower percentages of GFP$^+$ cells regarding MC were obtained in MSC transfections (Figure 59) in comparison with CHO cells transfections (Figure 50). Since the microporation conditions used for each type of cells are described by the manufacturer as the ideal ones and the vectors are the same, the most probable reason for this difference is based on the transfection ability of these two types of cells, being human MSC less able to be genetically modified. In fact, many efforts have been made to improve gene delivery methods to MSC in order to enhance their therapeutic properties and still exist the need to ameliorate them.

In Figure 59, pVAX-GFP transfected MSC presented similar GFP$^+$ cells percentage in relation to previous reported value on day 1 after transfection [100]. In the present study, pVAX-GFP led to the highest percentage of GFP$^+$ cells over time, with an increase of approximately 10% on day 4 and a decrease of roughly of 20% on day 7. The verified higher number of GFP$^+$ cells on day 4 might be again attributed to the accumulation of GFP in transfected cells leading to elevated detection level [77] once the number of cells from day 1 to 4 did not increase substantially. About the observed decrease in GFP$^+$ cells percentage, it is an expected result since all vectors with or without a bacterial origin of replication do not replicate in mammalian cells and the cell division over time leads to their diminution. Particularly in pVAX-VEGF-GFP, the cell number doubled from day 4 to 7.

Considering the correspondent pVAX-VEGF-GFP, which only differ from pVAX-GFP by the presence of VEGF gene and as a result it is larger in size, it was possible to verify that this difference resulted in reduction in about half the value of the GFP^+ cells percentage after 24h of transfection. This result was also observed in the fluorescence images, wherein more pVAX-GFP MSC were counted in the same field in comparison with pVAX-VEGF-GFP MSC (Figure 60). The size of the plasmids is certainly responsible for the different number of surviving cells that could express GFP or VEGF-GFP proteins but also as discussed before the number of mRNA transcripts of VEGF-GFP is certainly lower than GFP mRNA molecules.

Analyzing the differences on day 1 between pVAX-VEGF-GFP and MC that contain the same expression cassette, it is possible to observe that MC CMV and MC mCMV+hEF1α achieved similar or slightly higher values of GFP^+ cells, but on day 4 the decrease of GFP^+ cells was more pronounced in these MC transfections (≈54% and ≈60% respectively for MC CMV and mCMV+hEF1α CpG free, against ≈30% for pVAX-VEGF-GFP). Once more, since the increase of number of cells from day 1 to 4 was larger for the MC transfections, it was expected this difference in GFP^+ cells percentage. After 7 days of cell culture, both vectors obtained very low GFP^+ cells with even higher decrease rates.

From the beginning, GFP^+ cells percentages of MC hEF1α and hEF1α CpG free were immediately extremely low and over time attained null values. Since cell recovery values from these MC were similar to the other vectors (Figure 57), it is possible to notify that these low values were not associated to the experimental procedure variability but to the vectors themselves.

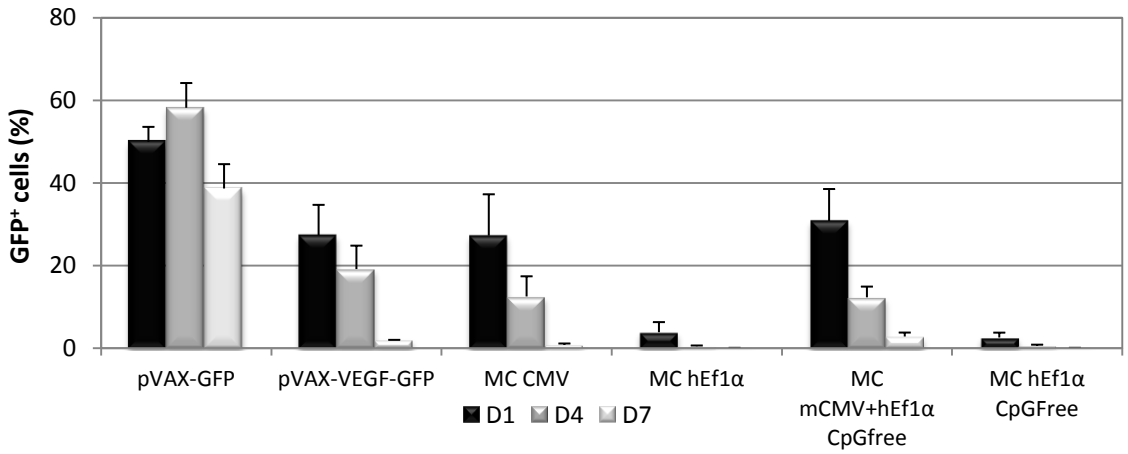

Figure 59 - GFP^+ cells percentage of MSC after transfection with pVAX-GFP, pVAX-VEGF-GFP and VEGF-GFP encoding MC. Cell data obtained from three independent experiments (n=3) 1, 4 and 7days of culture after transfection. Values are presented as mean values ± SEM.

The fluorescence intensity decrease over time for all vectors was also observed by fluorescence and bright field images (Figure 60).

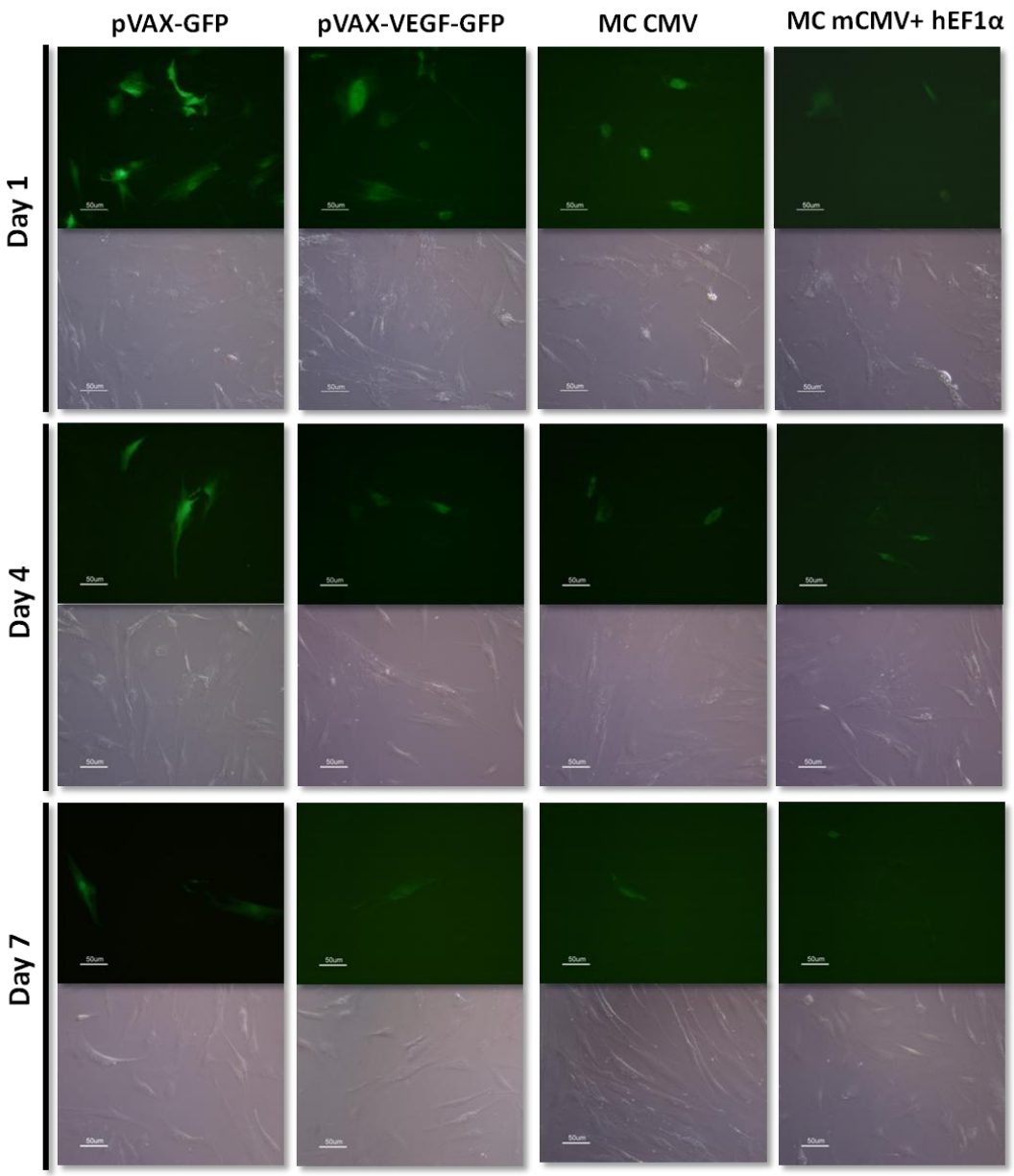

Figure 60 – Fluorescence and bright field microscopic images (200X) of transfected MSC with pVAX-GFP, pVAX-VEGF-GFP, MC CMV and MC mCMV+hEF1α CpG free 1, 4 and 7 days after microporation experiment.

8.6.2.4 MSC Yield of Transfection

Correspondingly to CHO cells transfections, pVAX-GFP demonstrated the highest transfection yield (≈25%, Figure 61) due to the high GFP^+ cells percentage (Figure 59). This value is supported by the literature [100].

After 24h of transfection, there were recovered more MC CMV transfected MSC than MSC microporated with MC mCMV+hEF1α CpG free. Even MC mCMV+hEF1α CpG free attained a slightly higher GFP^+ cells percentage than MC CMV, its transfection yield was lower. Regarding pVAX-VEGF-GFP, since its transfection experiment showed simultaneously a lower number of recovered cells and GFP^+ cells, the yield of transfection was somewhat smaller comparatively to the significant MC values. Although in MC hEF1α and MC hEF1α CpG free

transfections more cells were collected after transfection, due to their reduced GFP^+ cells percentage, an insignificant yield of transfection lower than 5% was obtained.

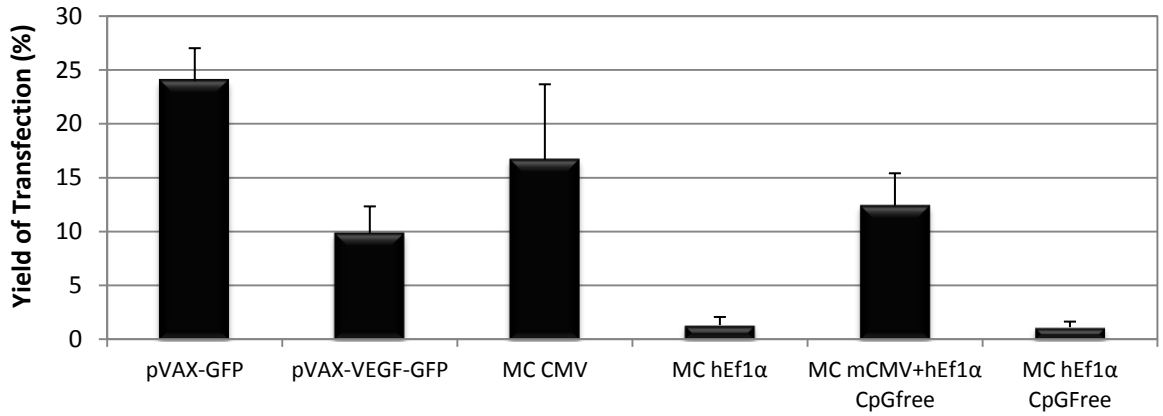

Figure 61 - Yield of transfection of MSC cells after transfection with pVAX-GFP, pVAX-VEGF-GFP and VEGF-GFP encoding MC. Cell data obtained from three independent experiments (n=3) 24h after transfection. Values are presented as mean values ± SEM.

8.6.2.5 MSC GFP Expression Mean Intensity

In parallel to what was previously discussed for CHO cells transfection, pVAX-GFP presented a much higher GFP mean intensity on day 1 after transfection (Figure 62), at least 3 times more GFP protein expression, in comparison with the other vectors. Once again the higher transcription rate for GFP gene and consequently the higher number of GFP mRNA transcripts and protein should be the cause for this discrepancy. However after the first day, the decrease of mean intensity is clearly significant in pVAX-GFP MSC transfected cells. There was an approximately 2.5-fold decrease in GFP expression from day 1 to 4 and 4.5-fold decrease from day 4 to 7, wherein the values were similar with the other vector constructions GFP mean intensities. Due to the scale differences, this result is not perceptible. Moreover, the GFP MI for MSC transfections were about twice smaller in comparison with the CHO cells microporation (Figure 54).

Accordingly to pVAX-GFP, also pVAX-VEGF-GFP demonstrated higher values of GFP mean intensity relatively to the different MC on day 1, but rather than sustain the intensity, it dropped almost 2-fold from day 1 to 4 and day 4 to 7. This reduction effect was less observable in MC CMV and mCMV+hEF1α CpG free that showed at maximum a 1.5-fold decrease in GFP mean intensities. These results once more emphasize the lower consequence of transgene silencing in MC in comparison with plasmid vectors with a high CpG motifs content.

Concerning MC hEF1α and hEF1α CpG free transfections, GFP mean intensity of day 7 from MC hEF1α presented a higher SEM value that reduced the statistical significance of that high value and MC hEF1α CpG free mean intensities seemed to end up in very low values. Additionally, the variation of their GFP mean intensities over time did not present a plausible relation, therefore no conclusions could be mentioned about them.

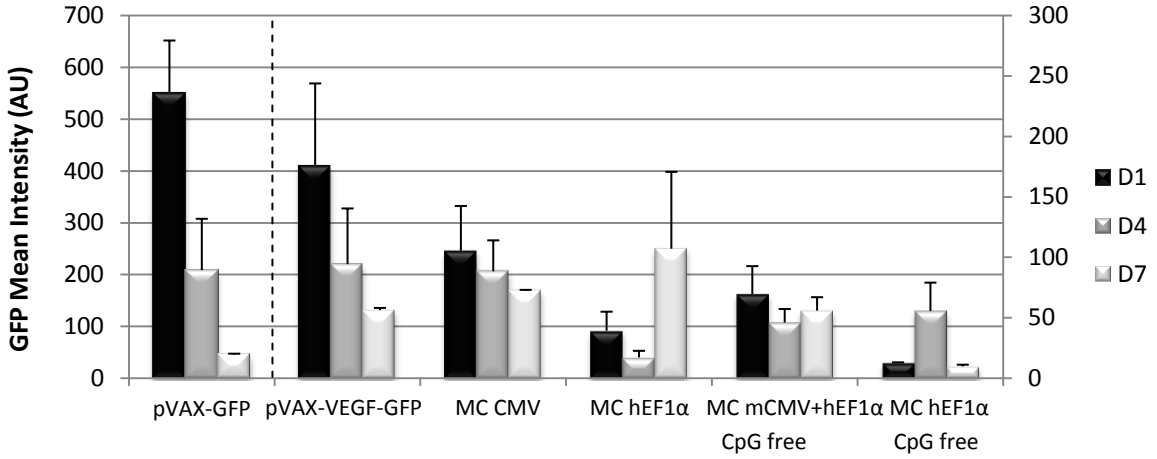

Figure 62 – GFP Expression Mean Intensity of MSC cells after transfection with pVAX-GFP, pVAX-VEGF-GFP and VEGF-GFP encoding MC. Cell data obtained from three independent experiments (n=3) 1, 4 and 7 days of culture after transfection. Values are presented as mean values ± SEM the dashed line separates the pVAX-GFP from the remaining vector values scale.

8.6.2.6 GFP Expression Mean Intensity related results

Reanalyzing the previous results about pVAX-GFP, the highest values for both products using GFP mean intensity, yield of transfection and percentage of GFP^+ cells were expected (Figure 63 and Figure 64). On the other hand, MC hEf1α and hEf1α CpG free proved to be inadequate vectors for the goal of this genetic and cellular therapy due to their significant low values of transfection parameters and also GFP expression.

In Figure 63, MC CMV product value which includes GFP mean intensity and yield of transfection was the highest, excluding pVAX-GFP from this analysis, followed by pVAX-VEGF-GFP. Both vector results regarding this product value have a relevant SEM value that shows the need to carry out further experiments in order to conclude if the GFP expression differences of these vectors are significant or not. Contrary, MC mCMV+hEF1α product result was lower than pVAX-VEGF-GFP and MC CMV but presented a higher level of confidence since SEM value was lower.

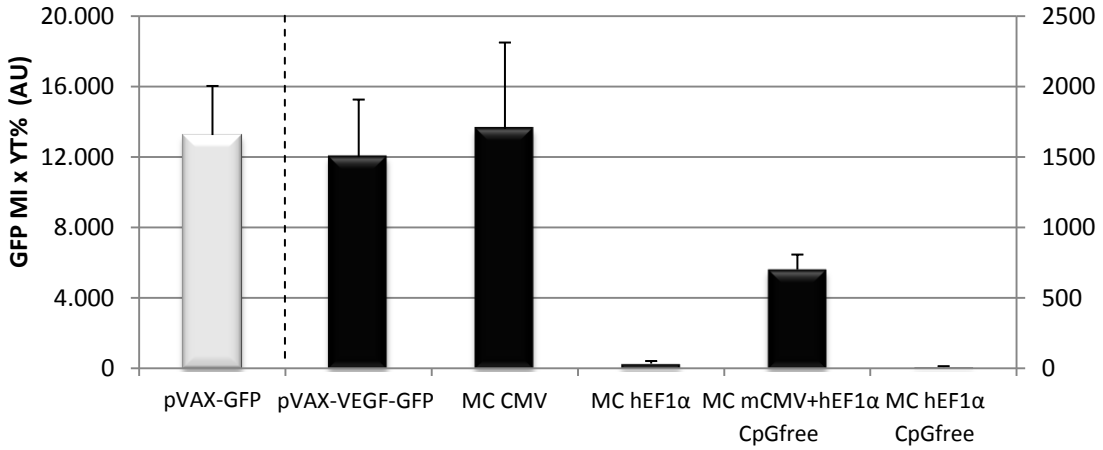

Figure 63 - GFP MI and yield of transfection product values of MSC transfection experiments with pVAX-GFP, pVAX-VEGF-GFP and VEGF-GFP encoding MC. Cell data obtained from three independent experiments (n=3)

24h after transfection. Values are presented as mean ± SEM and the dashed line separates the pVAX-GFP from the remaining vector values scale.

In Figure 64, pVAX-VEGF-GFP showed an initial better product result but on day 4 it approached to the one from MC CMV, which supports the larger drop of pVAX-VEGF-GFP GFP expression in comparison with MC CMV. The previously SEM values significance for pVAX-VEGF and MC CMV was verified in this graph, whereas MC mCMV+hEF1α CpG free showed a more constant decrease rate in GFP expression with lower relative SEM values. On day 7, independently of the vector, all product results reached insignificant values in terms of GFP expression relatively to the initial ones.

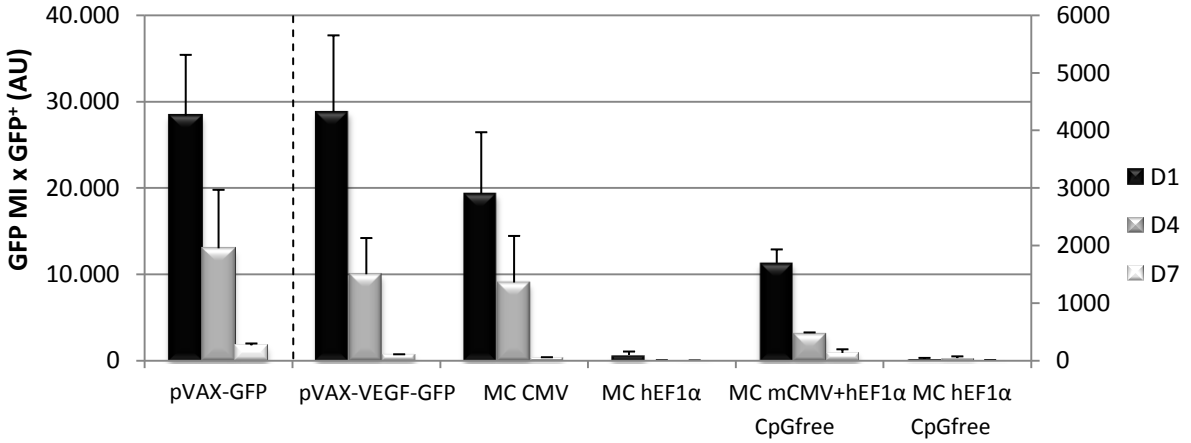

Figure 64 - GFP MI and GFP^+ percentage product values of MSC transfection experiments with pVAX-GFP, pVAX-VEGF-GFP and VEGF-GFP encoding MC. Cell data obtained from three independent experiments (n=3) 1, 4 and 7 days of cell culture after transfection. Values are presented as mean ± SEM and the dashed line separates the pVAX-GFP from the remaining vector values scale.

8.6.2.7 Plasmid Copy Number by RT-PCR

When gene delivery methods are applied to transfect or transduce cells, gene expression results are the biological end point of interest. If the results of experiments, such as quantification of a fluorescent reporter protein, either by microscopy or flow cytometry, or even ELISA quantification of specific products, reveal desirable effects there is no problem with this straightforward strategy. However, most of the times unexpected results emerge and more detailed techniques are crucial to detect possible explanations. Particularly, in non-viral gene delivery methods, the determination of the number of DNA molecules that enter into the cells is important to understand the results from other techniques and to optimize the delivery process itself [124]. For this quantification, Real Time PCR method can be used.

In a RT-PCR assay, the C_T (cycle threshold) is defined as the number of amplification cycles required for the fluorescent signal to cross the background threshold. C_T values are inversely proportional to the amount of target nucleic acid in the sample that is being amplified. Since it is an amplification method, there is not a direct way to determine the number of initial molecules from C_T values. To achieve those results, a calibration curve to provide the relationship between the C_T and the plasmid mass and consequently the number of plasmid copies should be constructed. By adding serial dilutions of plasmid DNA standards to a suspension of

nontransfected whole MSC, a range of C_T values are obtained and used to construct the calibration curve. These calibration curves are present in Annex 19.

Since no successful results were obtained for MC hEF1α and MC hEF1α CpG free in flow cytometry, there were not performed more experiments with them.

In the same 48-well plate, besides the determination of C_T for each standard concentration of a specific vector and control cells, C_T values for 10 000 MSC transfected with the same vector for each time point were determined by this technique. Control MSC revealed the highest C_T values in the different time points which were a condition to verify the functionality of the process. Final results of the PCN/cell for each vector over time are present in Table 16 and intermediate calculations are present in Annex 20.

Table 16 – Plasmid copy number per cell of pVAX-GFP, pVAX-VEGF-GFP, MC CMV and MC mCMV+hEF1α CpG free transfection experiments. Values are presented as mean ± SEM of two independent MSC transfection experiments.

Vector		PCN/cell
pVAX-GFP	D1	722 ± 467
	D4	4408 ± 1537
	D7	486 ± 314
pVAX-VEGF	D1	4315 ± 975
	D4	605 ± 165
	D7	118 ± 78
MC CMV	D1	6 ± 3
	D4	247 ± 172
	D7	5 ± 3
MC mCMV+ hEf1α CpG free	D1	7 ± 5
	D4	143 ± 95
	D7	43 ± 2

Analyzing RT-PCR results, different values and relations from the ones obtained were expected. Firstly, it is important to note that since the cells continue to divide after the transfection procedure, reduction in PCN/cell from day 1 to 7 should be observed and attributed to vector distribution between daughter cells, since it do not replicate, and also to degradation [58]. In this study, with exception of the pVAX-VEGF results that demonstrated the decrease in PCN/cell over time, the other vector results showed a significantly higher value of PCN on day 4. As a matter of fact, cell counting on day 1 is much more prone to errors that on day 4 wherein the cell number is larger. Therefore, samples from day 1 could have less than 10 000 MSC. Moreover, 10 000 MSC pellet after centrifugation is almost invisible, thus the supernatant aspiration could drag out a considerable number of cells.

Besides this unanticipated result, more discordance was observed. In the literature, the entrance of a higher number of MC molecules into the cells comparatively with pDNA was several times reported [118-121] and associated to the greater efficiency of MC in gene expression. Our results showed a completely discordant relation between PCN/cell values of pDNA and MC trasnfected MSC in relation to what was described in the literature. pDNA transfected MSC gave higher PCN/cell numbers than MC MSC.

Additionally, when RT-PCR results were compared with the percentage of transfected cells assessed by flow cytometry analysis, no proportionality was obtained. Flow cytometry-based results are not always proportional to plasmid cellular uptake determined by RT-PCR [124]. MC CMV and mCMV+hEF1α CpG free flow cytometric results were comparable and sometimes even better than the pVAX-VEGF-GFP and the PCN/cell values did not demonstrate that correspondence. Another matter of discussion is the overall low number of PCN/cell for both

type of vectors, but mainly for MC, once the theoretical value of PCN/cell before transfection is $1.67x10^6$ vectors per cell ($2.51x10^{11}$ molecules were added to each $1.5x10^5$ MSC).

Moreover, there is an important observation to point out about the RT-PCR results, namely the high values of SEM, which reveals that the differences between the two independent transfection experiments tested are significant. Only one sample of 10 000 MSC for each time point was collected and in this particular case it would have been much better if there were duplicate samples in order to confirm the C_T values in the same experiment and time point.

Still the observed PCN/cell decrease from day 4 to 7 may represent an advantage for therapeutic approach since these modified MSC will present a transient transgene expression [119].

8.6.2.8 VEGF expression and secretion by ELISA analysis

VEGF is the protein of interest in this study since it is the key molecule to enhance angiogenesis for our therapeutic purpose. Therefore, a final quantification of VEGF secretion to the media by MSC was performed in order to establish if MC vectors increased the VEGF production and consequently its secretion. Furthermore, this analysis was accomplished to further clarify the flow cytometry and RT-PCR results. MSC have been demonstrated to express VEGF as mentioned in introductory chapter, thus non-transfected MSC were used as control and in parallel, VEGF production by engineered MSC was assessed (pVAX-VEGF-GFP, MC CMV and MC mCMV+hEF1α CpG free transfected MSC). Such as in RT-PCR technique, also in ELISA method a calibration curve was created according to manufacturer instructions and known VEGF standard concentrations (Annex 21).

During 7 days, the non-tranfected and transfected MSC media was not changed, thus an increased VEGF concentration in the supernatants over time was expected. This increasing trend was verified and it was supported by results present in Figure 65, Figure 66 and Annex 22. Both pVAX-VEGF-GFP and MC modified MSC produced more VEGF comparatively to non-transfected MSC. On day 1, VEGF concentration of MC CMV transfected cells presented an approximately 8-fold increase in relation to control cells, whereas MC mCMV+hEF1α CpG free and pVAX-VEGF-GFP presented just about 3 and 2-fold increase, respectively (Figure 66). On day 4 and comparatively to day 1, control cells produced 5.3 times more VEGF and pVAX-VEGF-GFP, MC CMV and MC mCMV+hEF1α CpG free expressed 11.3, 4.2 and 11.9 times more VEGF respectively. Relatively to control cells, MC CMV transfected MSC attained the highest concentration with 6.1-fold increase, immediately followed by the 5.9-fold increase from MC mCMV+hEF1α CpG free. On day 7, the VEGF concentrations in all transfected MSC were 3.4 (pVAX-VEGF-GFP), 4.9 (MC CMV) and 4.6 (MC mCMV+hEF1α CpG free) times superior than the concentration from control cells and from day 4, their increase was not more than twice. At the end, MC CMV presented the highest VEGF concentration (23 812 pg/mL), followed by MC mCMV+hEF1α CpG free (22 514 pg/mL) and then pVAX-VEGF-GFP (16 641 pg/mL). VEGF production in MSC transfected with MC was 1.3-fold higher than pVAX-VEGF-GFP modified MSC.

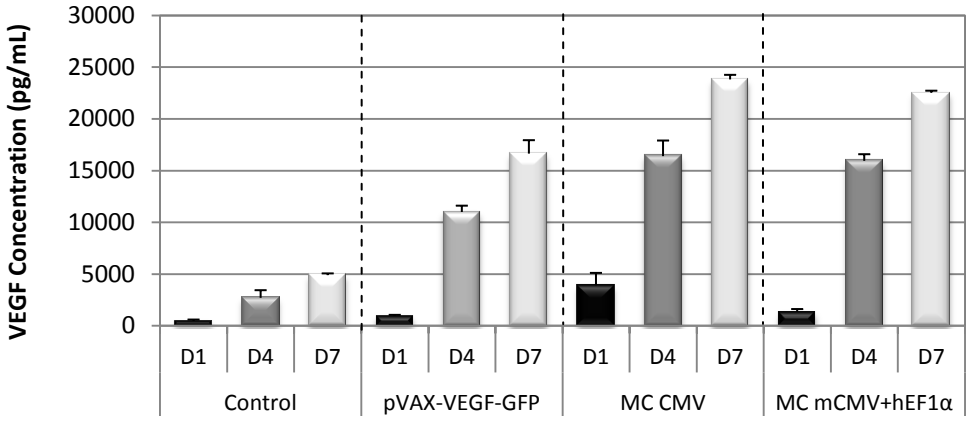

Figure 65 – Concentration of human VEGF on days 1, 4 and 7 after MSC transfection with pVAX-VEGF-GFP, MC CMV and MC mCMV+hEF1α CpG free. Non-transfected MSC were analyzed as control cells and values are presented as mean of the duplicates from one single experiment ± SEM.

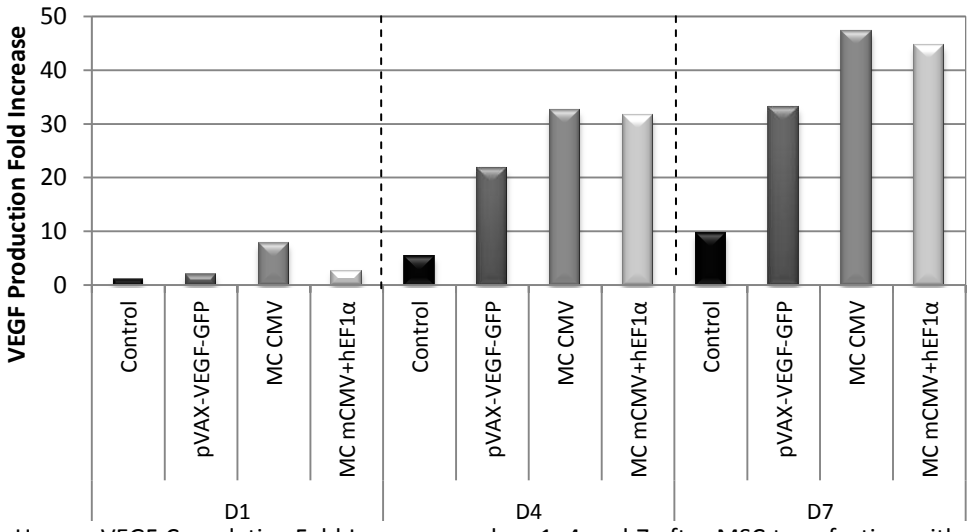

Figure 66 - Human VEGF Cumulative Fold Increase on days 1, 4 and 7 after MSC transfection with pVAX-VEGF-GFP, MC CMV and MC mCMV+hEF1α CpG free. Non-transfected MSC were analyzed as control cells and values are presented as mean of the duplicates from one single experiment ± SEM.

These concentration values were superior to the one obtained using MC-CMV-VEGF in BM MSC [118] and similar to what was obtained with a MC-CMV-VEGF transfection in C2C12 skeletal muscle cell line [69]. However it is desirable, because supernatant samples were not centrifuged before freezing at -80^{o}C, these concentrations can be overestimated. In fact, cell lysis promoted by the freezing and thawing processes from -80^{o}C could release the intracellular VEGF-GFP protein content to the media. On the other hand, since alive MSC were attached to the well surface, only death cells were collected in supernatants and their VEGF-GFP content can be considered negligible.

9. Conclusions and Future Perspectives

The VEGF-encoding MC production by the process developed in our laboratory and BM MSC microporation with these MC in order to overexpress VEGF in a sustained and transient manner were the main goals of this master thesis. To achieve these aims, some successful optimizations and alternative procedures were tested and introduced, particularly in the MC production technology.

E.coli BW2P growth behavior regarding the best recombination conditions such as time and optical density of induction as well L-arabinose concentration was clarified. More than 90% of recombination efficiency was achieved when the L-arabinose induction was performed in the period between mid-late exponential phase and before the stationary phase. From now on, since medium composition and other factors can influence the growth, before any recombination induction experiment, a growth curve of this strain transformed with a different PP should be performed to identify the best induction parameters. On the other hand, since MC mass produced using batch system with LB medium is considerably low for the proposed therapeutic approach, an optimization process is a crucial requirement. However, the same line of reasoning described previously can be translated to the new optimized conditions.

A recent study reported a 2.21-fold increase in MC production by optimization of key parameters such as growth temperature, inducer concentration and recovery time.[79]. As previously described in our system, 0.01%L-arabinose is enough to promote high recombination efficiencies, but different medium composition and growth temperature must be tested. According to other studies, pDNA production can be improved by growing *E.coli* at higher temperatures (42ºC), because it has been previously described that plasmid vectors that withhold the pUC origin of replication pDNA presents a higher production level in this temperature profile [125]. The improved MC strategy previously described confirmed this hypothesis and added some explanations: higher biomass and lower template plasmid yields are obtained at 37ºC [67] than at 42ºC [79] because in presence of a plasmid and under stressful conditions bacterial biosynthetic/energy metabolism genes are downregulated and the metabolic burden can be focused in pDNA amplification [126] . Since this particular characteristic is also imprinted in our PP and MC results from PP intra-recombination, a larger MC production is expected in this new temperature condition. Moreover, LB medium should be change to SB (Super Broth) or TB media which are commonly applied to achieve high yield protein and pDNA production in *E.coli*. TB medium has one advantage relatively to SB medium since it is a phosphate buffered rich medium that allows pH control during fermentation. Another improvement reported in that study was the substitution of 0.01% L-arabinose addition alone by the introduction of a MC induction mix (250 ml of LB medium, 10 ml of 1 M NaOH and 0.01% L-arabinose) that remarkably improved the overall recombination yield [79].

Concerning chromatographic methods used for MC purification, MC recoveries from both methods must be improved once significant quantities of MC were lost during these purification procedures. HIC strategy showed to be superior for our purpose in terms of quality of final MC, although it was not better regarding MC recovery values. Since CIM-DEAE monolithic chromatography is described in the literature as a better method than resin based purifications, besides the MC recovery increase need, its further optimization is required in order to

eliminate high molecular weight smear and also to eliminate bacterial contaminations in MSC transfection experiments, if it happen again. Furthermore, considering both methods, additional testing should be performed taking into account their MC separation performance in relation to the non-MC species DNA load added to the column. This topic of discussion is suggested because MC separation from non-MC species was possible in both methods and if their separation performance would not be affected, recombination induction during growth could be performed a little later, which would lead to a little lower recombination efficiency but more PP would be accumulated and higher MC mass could be obtained at the end. Even in presence of more MP and PP species, after enzymatic digestion of purified pDNA samples, their elimination could be possible by these chromatographic methods.

After production of pure MC samples comprising different promoter constructions, their biological activity was tested. In CHO cells transfections, by fluorescence microscopy, obvious green fluorescence from GFP expression in all vectors was observed (data not showed). However, in MSC cell transfections the same fluorescence was not clearly identified until flow cytometry was realized to obtain values of this expression. Besides the conclusion that produced MC are biological active molecules, differences amongst CHO cells and MSC transfections results can be explained by a sum of factors including the type of cells, small differences in plasmid batches (DNA purity, percentage of different pDNA isoforms, among others), microporation process and cell confluence after transfection [58].

Compiling all the results and analyzes from cell counting and viability, flow cytometry, RT-PCR and ELISA, no clear conclusions can be accomplished about the enhanced VEGF-GFP expression of MSC transfected with MC molecules. Nevertheless, there was more than one evidence that VEGF-GFP encoding MC with CMV and mCMV+hEF1α CpG free promoters could provide at least a similar VEGF expression when compared to pVAX-VEGF-GFP. In flow cytometric results, the differences between MSC transfected with pVAX-VEGF-GFP and these two particular MC were often non discrepant and since MC transfections led to a higher number of cells throughout the established time points, more VEGF-GFP expressing MSC could be observed in these experiments. This argument can be supported by the at least 1.3-fold higher VEGF concentrations observed in MC CMV and mCMV+hEF1α CpG free supernatants in comparison with pVAX-VEGF-GFP. However, just one independent MSC experiment supernatants were tested by ELISA and more should be tested.

Contrary, RT-PCR results did not support the aforementioned results. A higher number of DNA molecules inside cells that would result in higher levels of VEGF expression should be observed in MC-modified MSC relatively to pVAX-VEGF-GFP. Moreover, the large difference in values of PCN/cell from pDNA and MC was not observed in flow cytometric results. Consequently, RT-PCR must be repeated and if the same relation is obtained, other techniques should be used to confirm the results, such as stained DNA /membrane interaction studies as described by Chabot *et al*.[120].

On the other hand, the decrease of the VEGF concentration fold increase over time might be associated to the decrease in the number of DNA vectors inside cells due to cell division or degradation, supported by RT-PCR results, or by silencing of the transgene expression [121]. This decrease tendency was also observed in flow citometry results that analyzed GFP expression. Regarding flow cytometric results, there is an important issue

that should be highlighted, namely the VEGF-GFP secretion to the media. Since flow cytometry targeted GFP expression inside cells, the portion that was secreted to the media was not accounted. Thus, assuming that VEGF secretion rate was similar to non-transfected and transfected MSC, flow cytometric results could be underestimated but the discussed relations between vector constructions should be correct. This is one more explanation for the fact that pVAX-GFP transfected MSC attained much better results than the correspondent pVAX-VEGF-GFP, because GFP is not secreted to the media. About MC constructions with hEF1α and hEF1α CpG free promoters, they are not clearly adequate for the goal of this project.

Regarding MSC culture settings, since VEGF expression is up-regulated in hypoxic conditions [48] and MSC expansion is more effective under hypoxia[127], hypoxia environment might be test for transfected MSC expansion. Furthermore, DMEM medium supplemented with FBS might be changed to xeno-free conditions, which leads to higher cell densities and less safety concerns[128].

From the point of view of the application of this genetic and cellular MSC therapy to patients that suffered a cardiovascular accident, the angiogenesis stimulation by VEGF action in order to ameliorate the functionality of the damaged tissue seems to be a good strategy. However a major concern has been raised, which is migration of these cells to cancers [129], where angiogenesis potential cause a more pronounced proliferation of tumor cells and increase the probability of migration of these tumor cells, leading to metastases. Therefore, before any subscription of this MSC therapy, tumor tests among others should be performed to the patient. Alternatively to VEGF, other target genes can be study to treat CVD. For example, activation of growth hormone releasing hormone (GHRH) receptor of cardiac myocytes and cardiac stem cells by GHRH stimulates cardiac reverse remodeling, enhancing functional recovery of the heart after a myocardial infarction episode [130-132]. In a rodent model, the infarct size was substantially reduced, whereas myocyte and nonmyocyte mitosis was markedly increased by the delivery of an agonist of GHRH (GHRH-A)[130].

With the knowledge obtained from previous works developed in our laboratory involving MC, MSC and VEGF [71, 118], this present master thesis contributed with positive evidences that MC are a good alternative to conventional plasmids for VEGF expression and that CMV promoter can be used or alternatively substituted by mCMV+hEF1α CpG free promoter. Finally, human β-actin promoter might not be forgotten because when compared with CMV in a MC-based angiogenic gene therapy, the VEGF expression results were better [69].

Out the aim of this master thesis, as a result of the heterogeneity of the MSC populations, it is important to standardize the MSC generation protocols, including cell culture conditions, source, passage and cell density, as they may impact MSC phenotype as well as their therapeutic functions in experiments. In addition, the successful combination of genetically modified MSC with biomaterial scaffolds that mimic the *in vivo* niche of these cells and the economically-feasible MSC large scale production by the optimization of serum-free culture conditions are also required for a successful clinical application [25]. Moreover, further randomized, controlled, multicenter clinical trials are a requirement for determining the optimal conditions for MSC therapy [30].

10. References

1. Global status report on noncommunicable diseases 2010. Edited by Alwan A. Genebra: World Health Organization; 2011.
2. Yang F. *et al*. *Proc Natl Acad Sci U S A* 2010, **107**(8):3317-22.
3. Hwang N.S. *et al*. *Tissue Eng* 2006, **12**(9):2695-706.
4. Phillips M.I. Genetically Modified Stem Cells for Transplantation. In: *Emerging Trends in Cell and Gene Therapy.* Edited by Danquah M.K., Mahato R.I. New York: Springer; 2013: 119-20.
5. Zwaka T.P. Use of genetically modified stem cells in experimental gene therapies. In: *Regenerative Medicine.* Edited by Winslow T: U.S. Department of Health and Human Services; 2006: 45-51.
6. Wirth T. *et al*. *Gene* 2013, **525**(2):162-9.
7. Melton D. "Stemness": Definition, Criteria, and Standards. In: *Essentials of Stem Cell Biology.* Edited by Lanza R, Atala A, 3rd Edition edn. U.S.: Elsevier; 2014: 7-17.
8. Alvarez C.V. *et al*. *J Mol Endocrinol* 2012, **49**(2):R89-111.
9. Polak J. *et al*. *Gene Ther* 2005, **12**(24):1725-33.
10. Berdasco M. *et al*. *Stem Cell Res Ther* 2011, **2**(5):42.
11. Pappa K.I. *et al*. *Regen Med* 2009, **4**(3):423-33.
12. Trounson A. Why Stem Cell Research? Advances in the field. In: *Essentials of Stem Cell Biology.* Edited by Atala A., Lanza R., 3rd Edition. U.S.: Elsevier; 2014: 3-7.
13. Kumar S. *et al*. *Gene Ther* 2008, **15**(10):711-5.
14. Lin R. *et al*. Vascular Stem Cell Therapy. In: *Stem Cells and Gene Therapy.* Edited by Al-Rubeai M, Naciri M, vol. 8. Dordrecht: Springer; 2014: 49-70.
15. Yu J. *et al*. Embryonic Stem Cells. In: *Regenerative Medicine.* Edited by Winslow T. U.S.: U.S. Department of Health and Human Services; 2006: 1-12.
16. Diogo M.M. *et al*. Separation Technologies for Stem Cell Bioprocessing. In: *Stem Cells and Gene Therapy.* Edited by Al-Rubeai M, Naciri M, vol. 8. Dordrecht: Springer; 2014: 157-81.
17. Laustriat D. *et al*. *Biochem Soc Trans* 2010, **38**(4):1051-7.
18. Owen M. *et al*. *Ciba Found Symp* 1988, **136**:42-60.
19. Dominici M. *et al*. *Cytotherapy* 2006, **8**(4):315-7.
20. Browne C.M. *et al*. The Biology of Mesenchymal Stem Cells in Health and Disease and Its Relevance to MSC-Based Cell Delivery Therapies. In: *Mesenchymal Stem Cell Therapy.* Edited by Chase LG, Vemuri MC. New York: Springer; 2013: 63-86.
21. Uccelli A. *et al*. *Nat Rev Immunol* 2008, **8**(9):726-36.
22. Abdallah B.M. *et al*. *Gene Ther* 2008, **15**(2):109-16.
23. Murphy M.B. *et al*. *Exp Mol Med* 2013, **45**:e54.
24. Hass R. *et al*. *Cell Commun Signal* 2011, **9**:12.
25. Griffin M. *et al*. *Discov Med* 2010, **9**(46):219-23.
26. Sharma R.R. *et al*. *Transfusion* 2014, **54**(5):1418-37.
27. Fraser J.K. *et al*. *Trends Biotechnol* 2006, **24**(4):150-4.
28. Zarrabi M. *et al*. *Cell J* 2014, **15**(4):274-81.
29. Krause U. *et al*. *Methods Mol Biol* 2011, **698**:215-30.
30. Farini A. *et al*. *Stem Cells Int* 2014, **2014**:306573.
31. Solchaga L.A. *et al*. *Methods Mol Biol* 2011, **698**:253-78.
32. Scott M.A. *et al*. *Stem Cells Dev* 2011, **20**(10):1793-804.
33. Kim N. *et al*. *Korean J Intern Med* 2013, **28**(4):387-402.
34. Sensebe L. *et al*. *Hum Gene Ther* 2011, **22**(1):19-26.
35. Marquez-Curtis L.A. *et al*. *Biomed Res Int* 2013, **2013**:561098.
36. Yagi H. *et al*. *Cell Transplant* 2010, **19**(6):667-79.
37. Lazarus H.M. *et al*. *Bone Marrow Transplant* 1995, **16**(4):557-64.
38. https://clinicaltrials.gov/
39. Choi D. *et al*. *J Control Release* 2009, **140**(3):194-202.
40. Murry C.E. *et al*. *J Am Coll Cardiol* 2006, **47**(9):1777-85.
41. Laflamme M.A. *et al*. *Nature* 2011, **473**(7347):326-35.
42. Whelan R.S. *et al*. *Annu Rev Physiol* 2010, **72**:19-44.
43. http://www.euro.who.int/en/home
44. Buttar H.S. *et al*. *Exp Clin Cardiol* 2005, **10**(4):229-49.
45. Malecki M. *et al*. *Gene Ther* 2005, **12 Suppl 1**:S159-69.
46. Nagy J.A. *et al*. *Angiogenesis* 2008, **11**(2):109-19.
47. Olsson A.K. *et al*. *Nat Rev Mol Cell Biol* 2006, **7**(5):359-71.
48. Ferrara N. *et al*. *Nat Med* 2003, **9**(6):669-76.
49. Pons J. *et al*. *J Gene Med* 2009, **11**(9):743-53.
50. Ledley F.D. *et al*. *Gene Ther* 2014, **21**(2):188-94.

51. Gascón A.R. *et al*. Non-Viral Delivery Systems in Gene Therapy In: *Gene Therapy - Tools and Potential Application.* Edited by Molina FM: In Tech; 2013: 3-34.
52. Ginn S.L. *et al*. *J Gene Med* 2013, **15**(2):65-77.
53. Sivalingam J. *et al*. Recent Advances and Improvements in the Biosafety of Gene Therapy In: *Gene Therapy - Developments and Future Perspectives.* Edited by Kang C: In Tech; 2011: 145-88.
54. Santos J.L. *et al*. *Curr Gene Ther* 2011, **11**(1):46-57.
55. Nowakowski A. *et al*. *Acta Neurobiol Exp (Wars)* 2013, **73**(1):1-18.
56. Wolff J.A. *et al*. *Science* 1990, **247**(4949 Pt 1):1465-8.
57. Mayrhofer P. *et al*. *Methods Mol Biol* 2009, **542**:87-104.
58. Azzoni A.R. *et al*. *J Gene Med* 2007, **9**(5):392-402.
59. Chen Z.Y. *et al*. *Mol Ther* 2003, **8**(3):495-500.
60. Tan Y. *et al*. *Hum Gene Ther* 1999, **10**(13):2153-61.
61. Klinman D.M. *Nat Rev Immunol* 2004, **4**(4):249-58.
62. Chen Z.Y. *et al*. *Gene Ther* 2004, **11**(10):856-64.
63. Qin L. *et al*. *Hum Gene Ther* 1997, **8**(17):2019-29.
64. Suzuki M. *et al*. *J Virol* 2006, **80**(7):3293-300.
65. Riu E. *et al*. *Mol Ther* 2007, **15**(7):1348-55.
66. Lu J. *et al*. *Mol Ther* 2012, **20**(11):2111-9.
67. Chen Z.Y. *et al*. *Hum Gene Ther* 2005, **16**(1):126-31.
68. Argyros O. *et al*. *J Mol Med (Berl)* 2011, **89**(5):515-29.
69. Chang C.W. *et al*. *J Control Release* 2008, **125**(2):155-63.
70. Grund M. *et al*. Minicircle Patents: A Short IP Overview of Optimizing Nonviral DNA Vectors. In: *Minicircle and Miniplasmid DNA Vectors: The Future of Non-viral and Viral Gene Transfer.* Edited by Schleef M, First Edition: Wiley-VCH Verlag GmbH & Co. KGaA; 2013: 1-6.
71. Simcikova M. Development of a process for the production and purification of minicircles for biopharmaceutical applications. Lisboa: Universidade de Lisboa; 2013.
72. Darquet A.M. *et al*. *Gene Ther* 1997, **4**(12):1341-9.
73. Jechlinger W. *et al*. *J Mol Microbiol Biotechnol* 2004, **8**(4):222-31.
74. Dong Y. *et al*. *J Biotechnol* 2013, **166**(3):84-7.
75. Jakobsen J. *et al*. *Biotechniques* 2010, **48**(4):313-6.
76. Kay M.A. *et al*. *Nat Biotechnol* 2010, **28**(12):1287-9.
77. Kobelt D. *et al*. *Mol Biotechnol* 2013, **53**(1):80-9.
78. Mayrhofer P. *et al*. *J Gene Med* 2008, **10**(11):1253-69.
79. Gaspar V.M. *et al*. *Hum Gene Ther Methods* 2014, **25**(2):93-105.
80. Simcikova M. *et al*. *Sociedade Portuguesa de Biotecnologia* 2013, **2**(4):28-30.
81. Stenler S. *et al*. *Mol Ther Nucleic Acids* 2014, **2**:e140.
82. Asahara T. *et al*. *Gene Ther* 2000, **7**(6):451-7.
83. Stender S. *et al*. *Eur Cell Mater* 2007, **13**:93-9.
84. Madeira C. *et al*. *J Biomed Biotechnol* 2010, **2010**:735349.
85. Boura J.S. *et al*. *Hum Gene Ther Methods* 2013, **24**(1):38-48.
86. Torchilin V.P. *Adv Drug Deliv Rev* 2008, **60**(4-5):548-58.
87. Hoare M. *et al*. *J Gene Med* 2010, **12**(2):207-18.
88. Noiseux N. *et al*. *Mol Ther* 2006, **14**(6):840-50.
89. Tang J. *et al*. *Eur J Cardiothorac Surg* 2006, **30**(2):353-61.
90. Myers T.J. *et al*. *Expert Opin Biol Ther* 2010, **10**(12):1663-79.
91. Moon H.H. *et al*. *Biomaterials* 2014, **35**(5):1744-54.
92. Fierro F.A. *et al*. *Stem Cells* 2011, **29**(11):1727-37.
93. Tang J. *et al*. *Mol Cell Biochem* 2010, **339**(1-2):107-18.
94. Thomson J.G. *et al*. *Transgenic Res* 2009, **18**(2):237-48.
95. Guzman L.M. *et al*. *J Bacteriol* 1995, **177**(14):4121-30.
96. Simcikova M. *et al*. *Vaccine* 2014, **32**(24):2843-6.
97. Khlebnikov A. *et al*. *Microbiology* 2001, **147**(Pt 12):3241-7.
98. Carapuca E. *et al*. *Mol Biotechnol* 2007, **37**(2):120-6.
99. Alves C. Development of a method for the purification of minicircles. Lisboa: Universidade de Lisboa; 2014.
100. Madeira C. *et al*. *J Biotechnol* 2011, **151**(1):130-6.
101. Lim J.Y. *et al*. *BMC Biotechnol* 2010, **10**:38.
102. Neon™ Transfection System User Manual (Invitrogen™)
103. Listner K. *et al*. *Methods Mol Med* 2006, **127**:295-309.
104. NucleoBond® Xtra Midiprep kit (Macherey-Nagel) Protocol.
105. Urthaler J. *et al*. *J Chromatogr A* 2005, **1065**(1):93-106.
106. Prazeres D.M.F. *et al*. *Chemical Engineering and Processing: Process Intensification* 2004, **43**(5):609-24.
107. Remaut K. *et al*. *J Control Release* 2006, **115**(3):335-43.
108. CIM® Disk Monolithic Column Instruction Manual (BIA Separations)

109. Freitas S.S. *et al*. *Separation and Purification Technology* 2009, **65**(1):95-104.
110. Pereira L.R. *et al*. *J Sep Sci* 2010, **33**(9):1175-84.
111. Phenyl Sepharose 6 Fast Flow Instruction Manual (GE Healthcare)
112. Kunz W. *et al*. *Current Opinion in Colloid & Interface Science* 2004, **9** (1-2):19-37.
113. Peterka M. *et al*. Convective Interaction Media Monoliths for Separation and Purification of pDNA and Viruses. In: *Monolithic Chromatography and Its Modern Applications.* Edited by Wang PJ. UK: ILM Publications; 2010: 439-508.
114. Norrman K. *et al*. *PLoS One* 2010, **5**(8):e12413.
115. Gruh I. *et al*. *J Gene Med* 2008, **10**(1):21-32.
116. http://www.bitgene.com/cgi/gene_analysis.cgi
117. http://www.basic.northwestern.edu/biotools/oligocalc.html
118. Pereira T. Non-viral engineered human mesenchymal stem/stromal cells to promote angiogenesis. Lisboa: Universidade de Lisboa; 2013.
119. Ribeiro S. *et al*. *Cell Reprogram* 2012, **14**(2):130-7.
120. Chabot S. *et al*. *Gene Ther* 2013, **20**(1):62-8.
121. Madeira C. *et al*. *Biomacromolecules* 2013, **14**(5):1379-87.
122. Hyde S.C. *et al*. *Nat Biotechnol* 2008, **26**(5):549-51.
123. Guzman-Hernandez M.L. *et al*. *Mol Biol Cell* 2014, **25**(7):1061-72.
124. Ribeiro S.C. *et al*. *Biotechnol Prog* 2010, **26**(5):1501-4.
125. Carnes A.E. *et al*. *Biotechnol Appl Biochem* 2006, **45**(Pt 3):155-66.
126. Ow D.S.W. *et al*. *Enzyme and Microbial Technology* 2006, **39**:391-98.
127. Dos Santos F. *et al*. *J Cell Physiol* 2010, **223**(1):27-35.
128. Santos F. *et al*. *Tissue Eng Part C Methods* 2011, **17**(12):1201-10.
129. Studeny M. *et al*. *J Natl Cancer Inst* 2004, **96**(21):1593-603.
130. Kanashiro-Takeuchi R.M. *et al*. *Proc Natl Acad Sci U S A* 2012, **109**(2):559-63.
131. Kanashiro-Takeuchi R.M. *et al*. *Proc Natl Acad Sci U S A* 2010, **107**(6):2604-9.
132. Gomes S.A. *et al*. *Proc Natl Acad Sci U S A* 2013, **110**(8):2834-9.

11. Annexes

Annex 1 - Distribution of MSC clinical trials throughout the world (29th October 2014)[38].

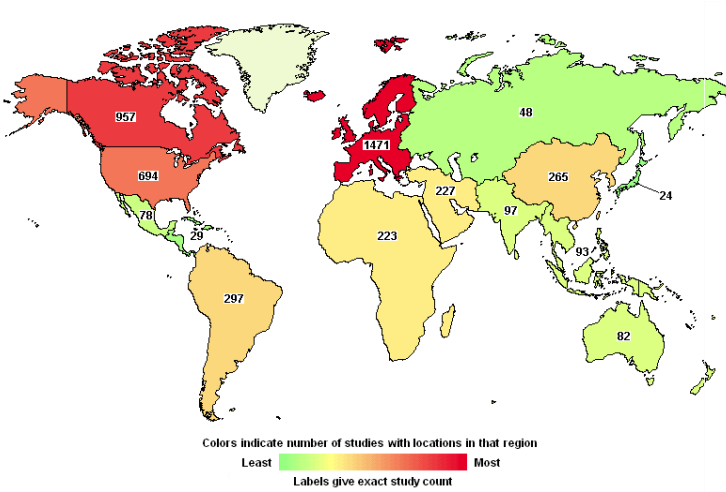

Global distribution of
MSC Clinical Trials Studies

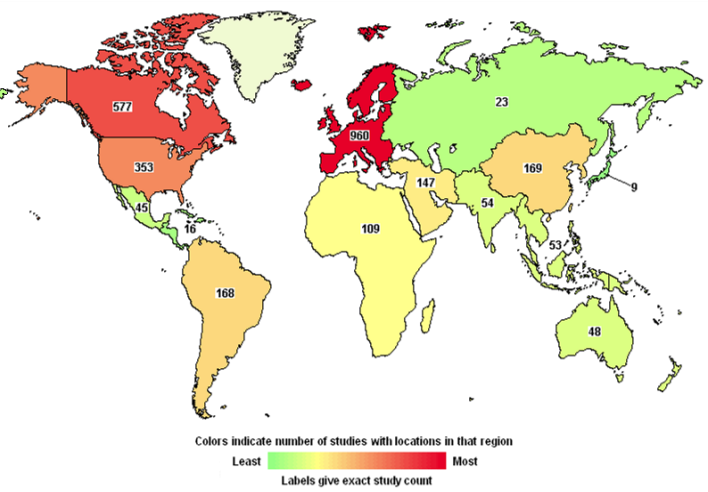

Global distribution of
Currently Open MSC Clinical Trials Studies

Annex 2 - siRNA action in gene silencing [15].

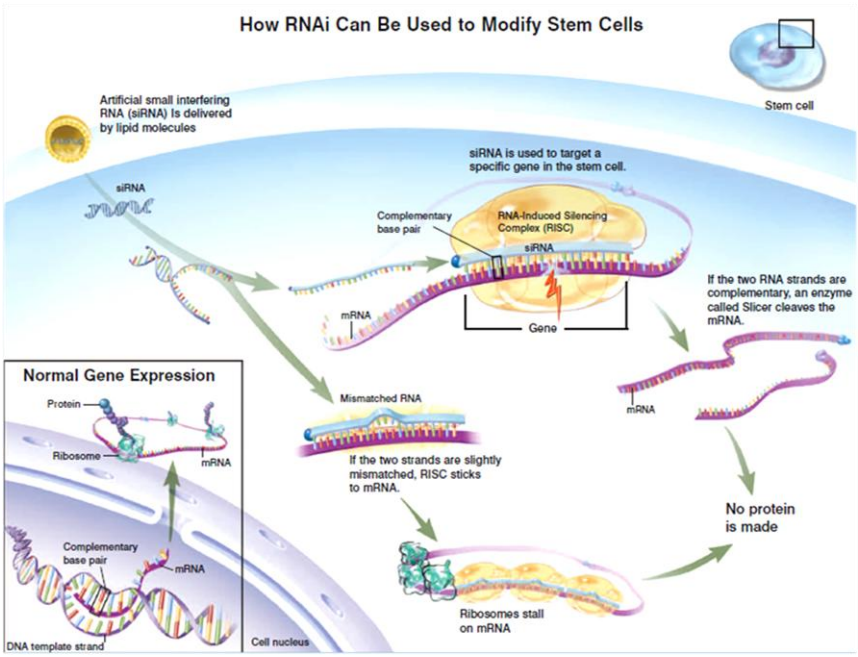

Annex 3- Primers used for plasmid constructions and RT-PCR.

Name	Size	Sequence (5' to 3')	Restriction sites
Mut1_AgeI_Fwd	37bp	CAGCAGCAAAAATAA**ACCGGT**CAGTCGACAGCAAGCG	AgeI
Mut1_AgeI_Rev	37bp	CGCTTGCTGTCGACTG**ACCGGT**TTATTTTTGCTGCTG	AgeI
Mut2_AgeI_Fwd	40bp	CAATGCTTGCATAATGT**ACCGGT**CAAATGGACGAAGCAGG	AgeI
Mut2_AgeI_Rev	40bp	CCTGCTTCGTCCATTTG**ACCGGT**ACATTATGCAAGCATTG	AgeI
hEF1a_Fwd	20bp	GAT**ACTAGT**AAGGATCTGCG	SpeI
hEF1a_rev	20bp	CGGCCG**CGGTACC**GATTTAA	KpnI
hEF1a_PvuII_Fwd	30bp	GCCGCCAGAACACACGTGAAGCTTCGAGGG	-
hEF1a_PvuII_Rev	30bp	CCCTCGAAGCTTCACGTGTGTTCTGGCGGC	-
GFP_Fwd	21bp	TCGAGCTGGACGGCCACGTAA	-
GFP_Rev	20bp	TGCCGGTGGTGCAGATGAAC	-
BGH_Fwd	20bp	GTTGCCAGCCATCTGTTGTT	-
T7_Fwd	20bp	TAATACGACTCACTATAGGG	-
Promoter_Fwd	23bp	GCTCACATGTTCTTGCTGCTTCG	-
GFP_pVX_Fwd	22bp	TCGAGCTGGACGGCGACGTAAA	RT-PCR
GFP_pVX_Rev	20bp	TGCCGGTGGTGCAGATGAAC	RT-PCR

Annex 4 – Individual average Logarithmic growth curves of different *E.coli* BW2P/pMINILi strains in 250mL LB medium.

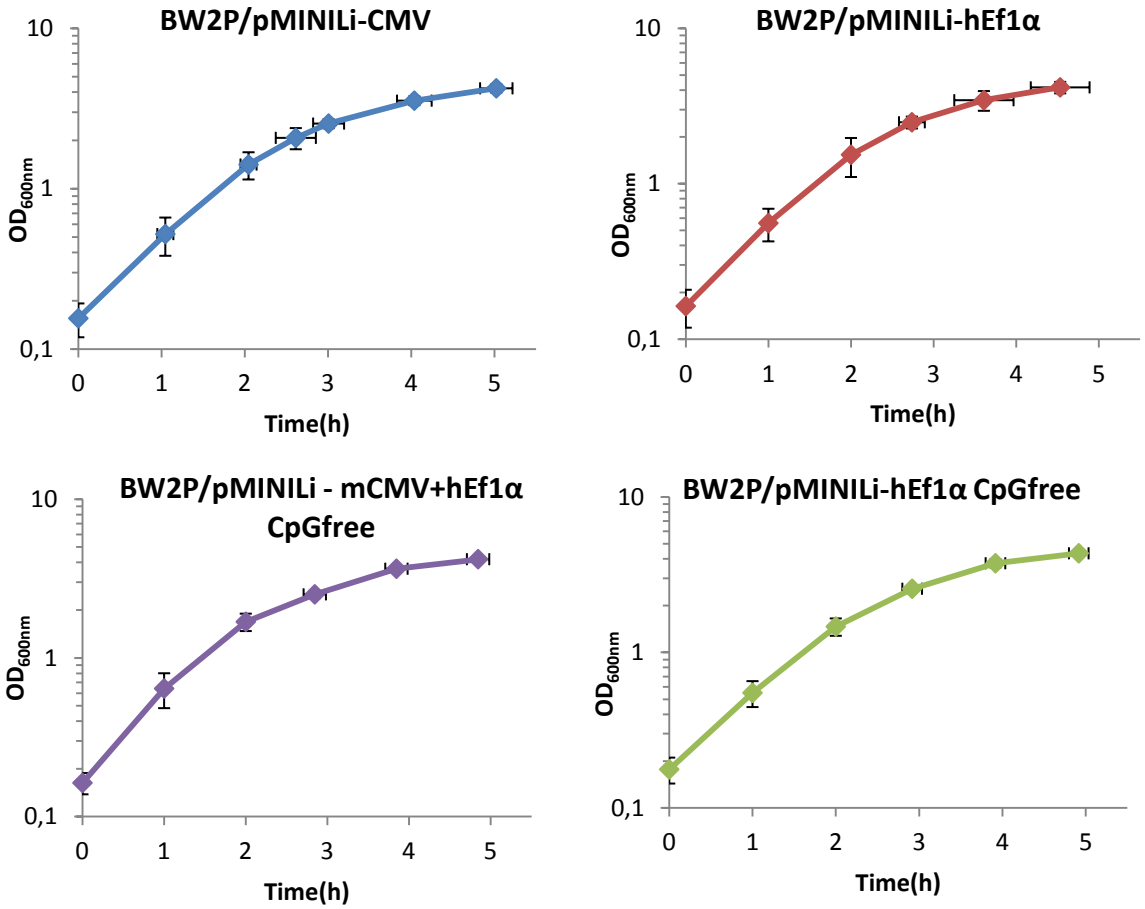

Annex 5– Average Logarithmic growth curves of different *E.coli* BW2P/pMINILi strains in 500mL LB medium.

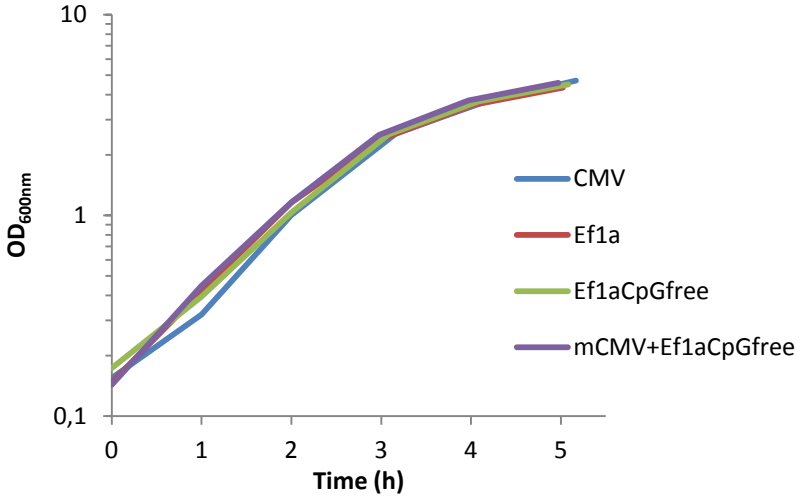

Annex 6 – Individual average Logarithmic growth curves of different *E.coli* BW2P/pMINILi strains in 500mL LB medium.

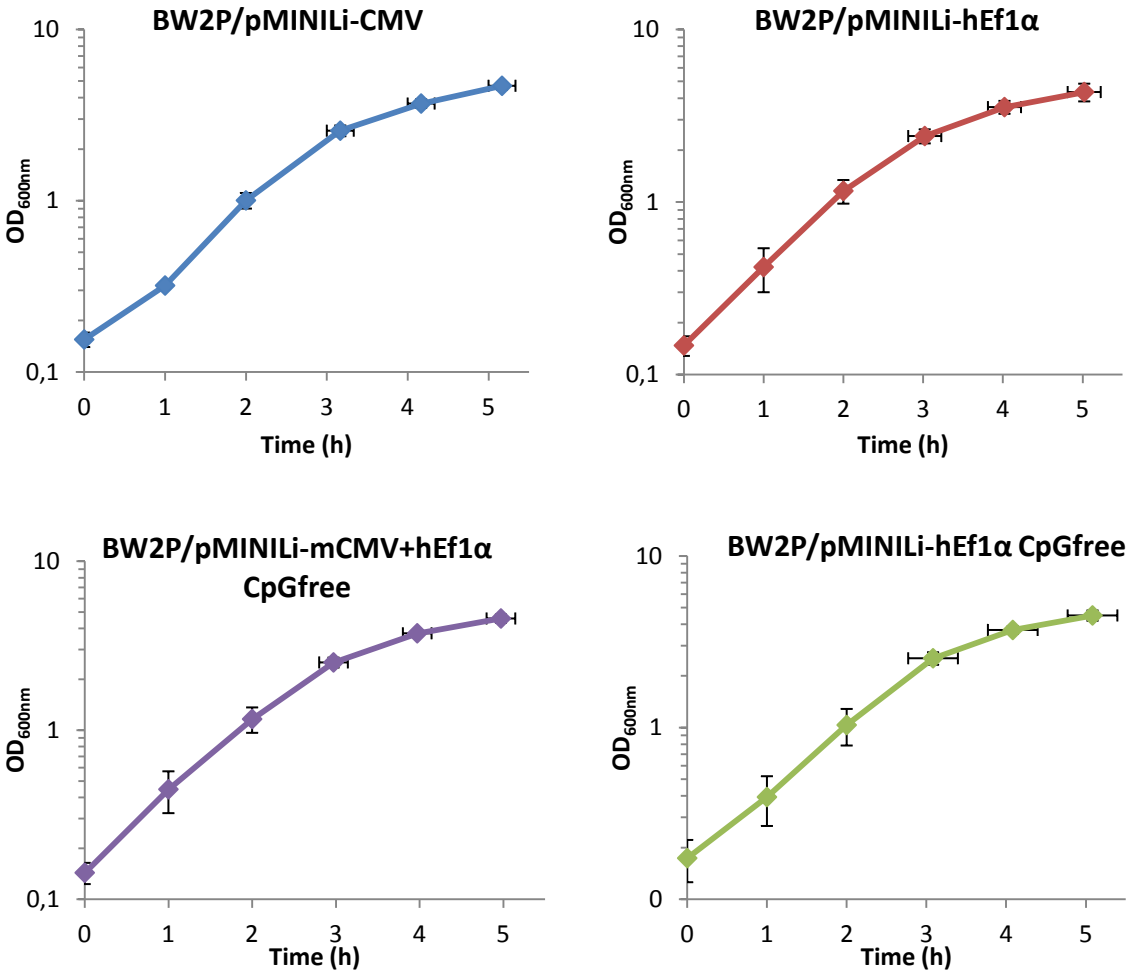

Annex 7 – Growth and recombination variables of different *E.coli* BW2P/pMINILi strains in 250 and 500mL LB medium.

Strain/pDNA	μ_{max} (h^{-1})		OD_{600nm} of Induction		Recombination Efficiency(%)	
	250mL	500mL	250mL	500mL	250mL	500mL
BW2P/pMINILi-CMV	0.95 ± 0.07	0.96*	2.56 ± 0.17	2.75*	96.44 ± 2.78	99.17*
BW2P/ pMINILi-hEf1a	1.03 ± 0.09	0.94 ± 0.08	2.49 ± 0.22	2.49 ± 0.14	98.65 ± 1.68	98.15 ± 1.07
BW2P/ pMINILi-mCMV+hEf1a (CpG free)	1.02 ± 0.09	1.00 ± 0.09	2.51 ± 0.13	2.46 ± 0.09	98.70 ± 1.32	98.46 ± 0.32
BW2P/ pMINILi-hEf1aCpG free	0.94 ± 0.06	0.91 ± 0.11	2.56 ± 0.15	2.53 ± 0.21	92.68 ± 4.27	96.37 ±1.59

*Only one growth experiment was performed

Annex 8 – Recommended culture volumes and respective final OD_{600nm} for high-cppy plasmids for each purification column in Endotoxin-free Plasmid DNA Purification NucleoBond® XtraMidi kit (Macherey-Nagel)[104].

Table 2: Recommended culture volumes for high-copy plasmids

NucleoBond® Xtra	Pellet wet weight	Rec. ODV	OD_{600} = 2	OD_{600} = 4	OD_{600} = 6	OD_{600} = 8	OD_{600} = 10
Midi	0.75 g	400	200 mL	100 mL	66 mL	50 mL	40 mL
Maxi	2.25 g	1200	600 mL	300 mL	200 mL	150 mL	120 mL

Annex 9 - PvuII digestions of pMINILi-hEf1α, pMINILi-mCMV+hEf1α CpG free and pMINILi hEf1α CpG free.

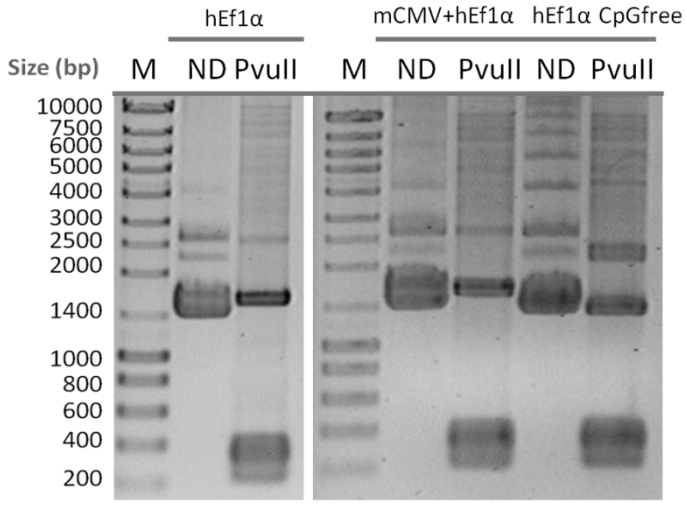

ND- PvuII Non-digested sample; PvuII- PvuII digested samples of recombined and pure plasmid constructions.

Annex 10 - CIM®-DEAE Disk basic characteristics according to the manufacture [108].

Basic characteristics	CIM®-DEAE Disk
Channel size	600-750nm
Working Flow Rates	2-4mL/min max=6mL/min(18CV/min)
Dimensions	Diameter: 12.0mm Thickness: 3.0mm Bed volume:0.34mL
Working system pressure	Up to 50bar (5MPa)
Temperature Stability	4°C to 40°C
Recommended pH	Working range: 3-9 Cleaning in Place: 2-14
Dynamic Binding Capacity	>21mg BSA/mL wet support (Conditions: BSA 1.0mg/mL, 20mM Tris-HCl buffer, pH 7.4, flow rate 3mL/min

Annex 11 – Illustrative representation of the salt concentration determination (first asterisk) of the additional step included in the optimized method of CIM®-DEAE step gradient.

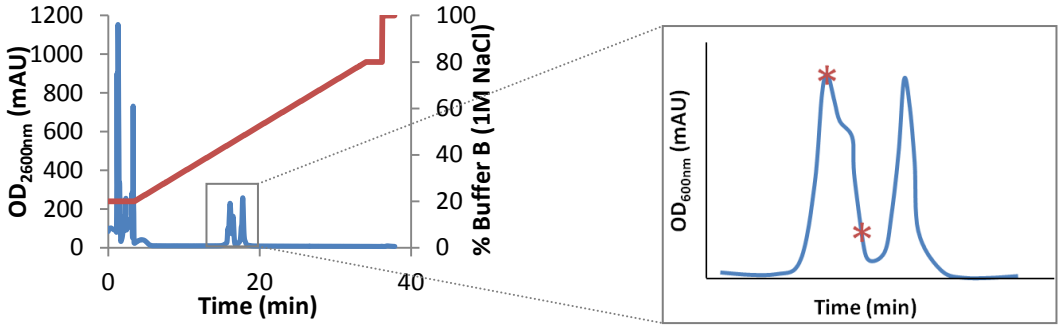

Annex 12 - Chromatographic separation of recombined and digested pMINILi-Ef1α-VEGF on a CIM®-DEAE disk using a step gradient (25.0%B; 41.8%B; 43.4%B; 60.0%B; 100.0%B) **(A)** and corresponding peak fractions are visualized on electrophoretic gel **(B).**

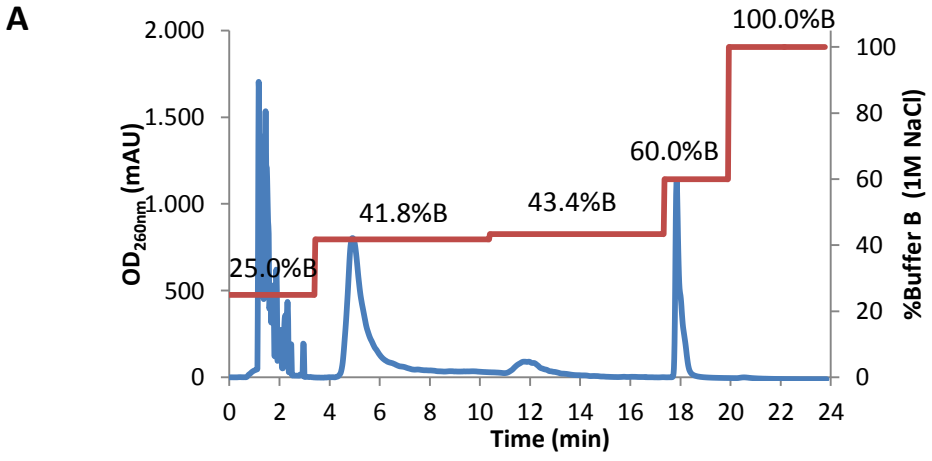

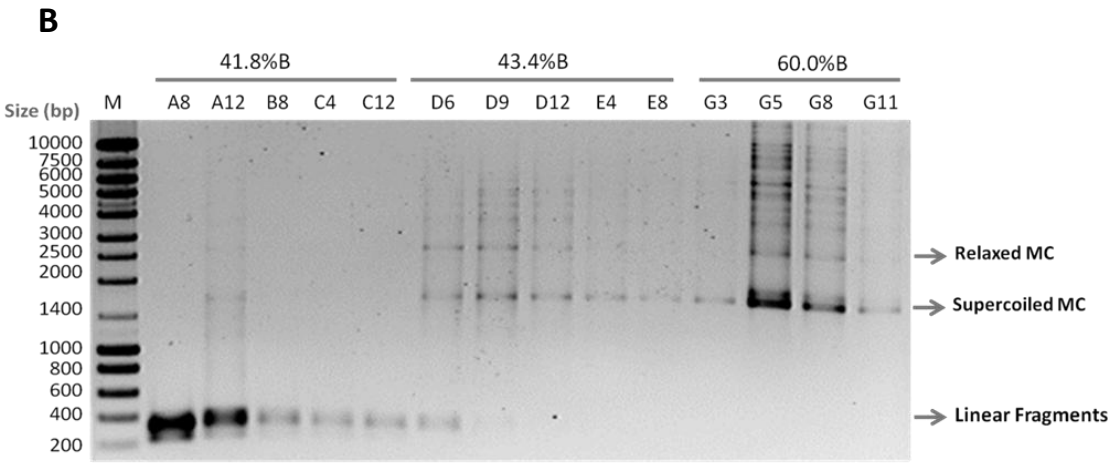

Annex 13 – Chromatographic separation of recombined and digested pMINILi-CMV-VEGF on a CIM®-DEAE disk using a step gradient (25.0%B; 43.5%B; 45.2%B; 60.0%B; 100.0%B) **(A)** and corresponding peak fractions are visualized on electrophoretic gel **(B).**

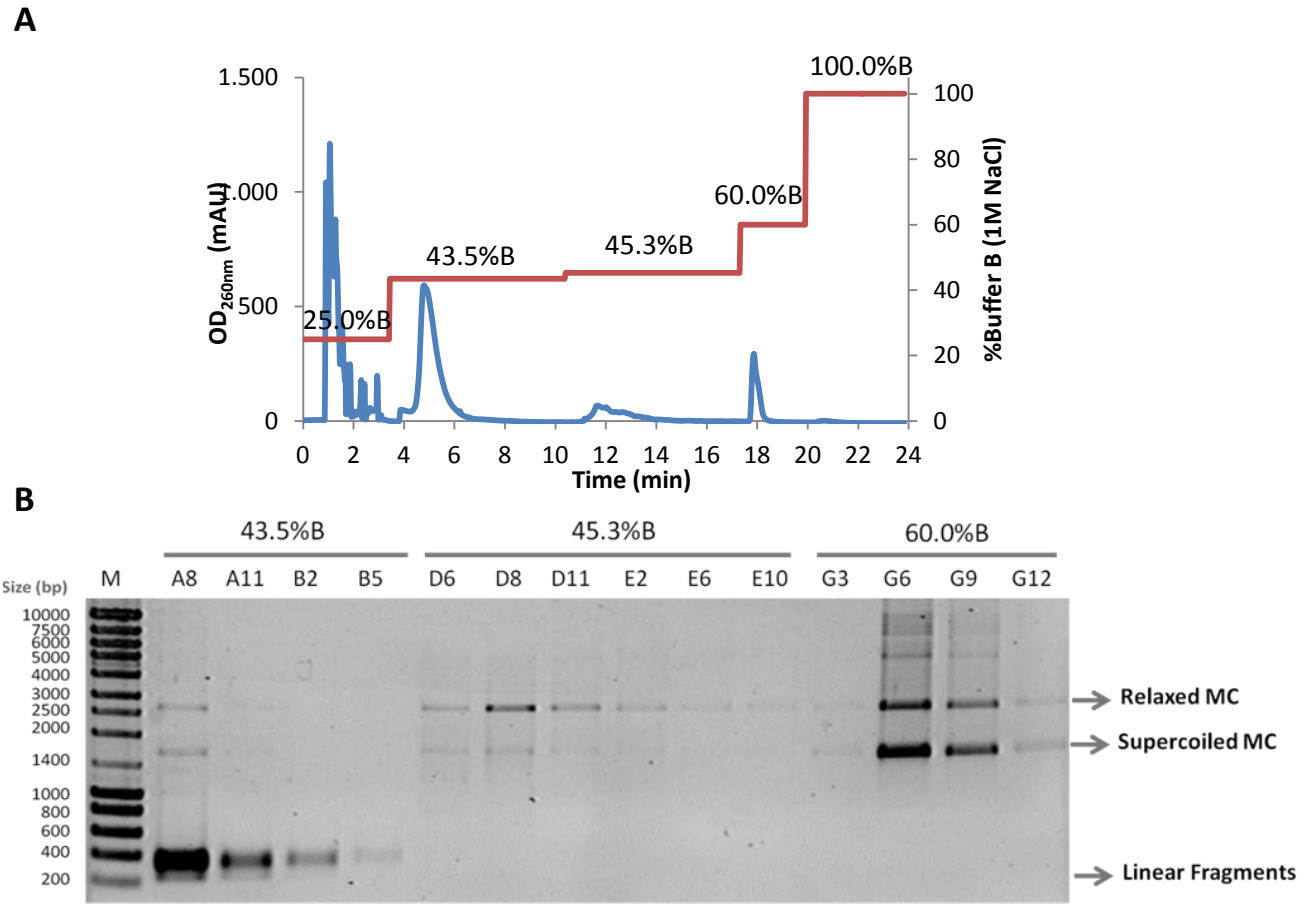

Annex 14 - PheFF-HS resin basic characteristics according to the manufacturer [111].

Basic characteristics	PheFF-HS
Degree of substitution	Approx. 40µmol phenyl per mL medium
Mean particle size	90µm
Bead size range	45-165µm
Bead structure	Highly cross-linked agarose, 6% spherical
Linear flow rate at 25°C	200 to 400 cm/h at 100kPa (1bar, 14.5psi)

Recommended pH	Working range: 3-13 Cleaning in Place: 2-14
Chemical stability 40°C for 7days in	- 1M NaOH - 3M ammonium sulphate - 70% ethanol - 30% isopropanol - 0.5% SDS - 6M guanidine hydrochloride - 8M urea - 10%ethylene glycol
Autoclavable	at 121°C for 20min in H_2O
Storage	4°C to 30°C in 20%ethanol; do not freeze

Annex 15 – Individual HIC chromatographs.

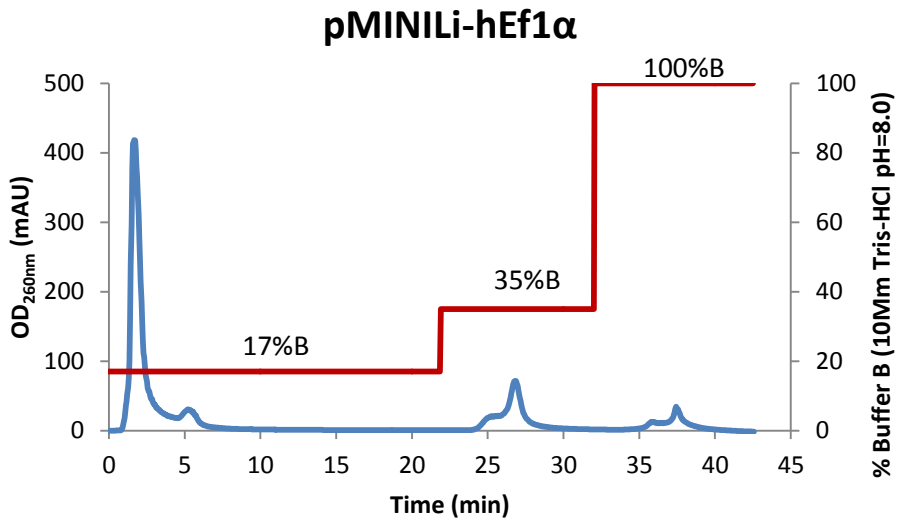

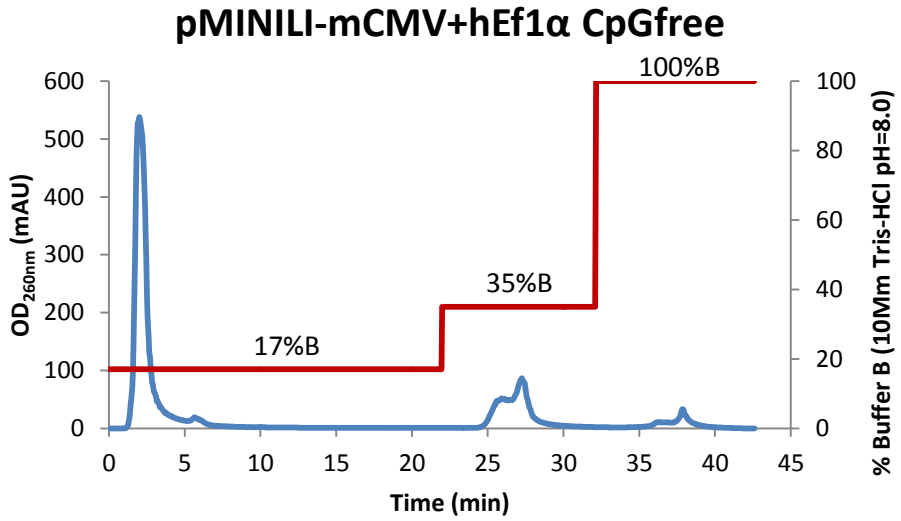

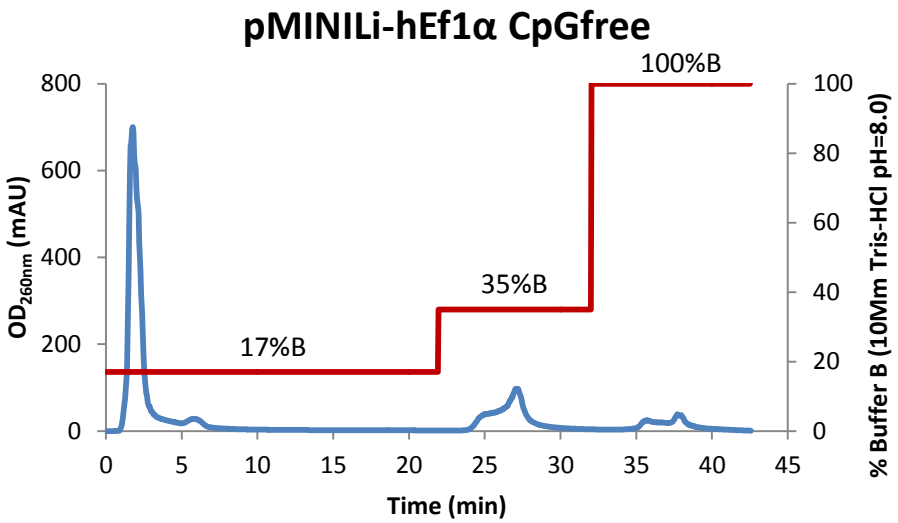

Annex 16 – DNA sequencing results from purified MC.

- Alignment of DNA sequencing results from sequence of VEGF gene and fusion with GFP gene with MC CMV reference sequence (highlighted sequence). All the other promoter constructions had the same result.

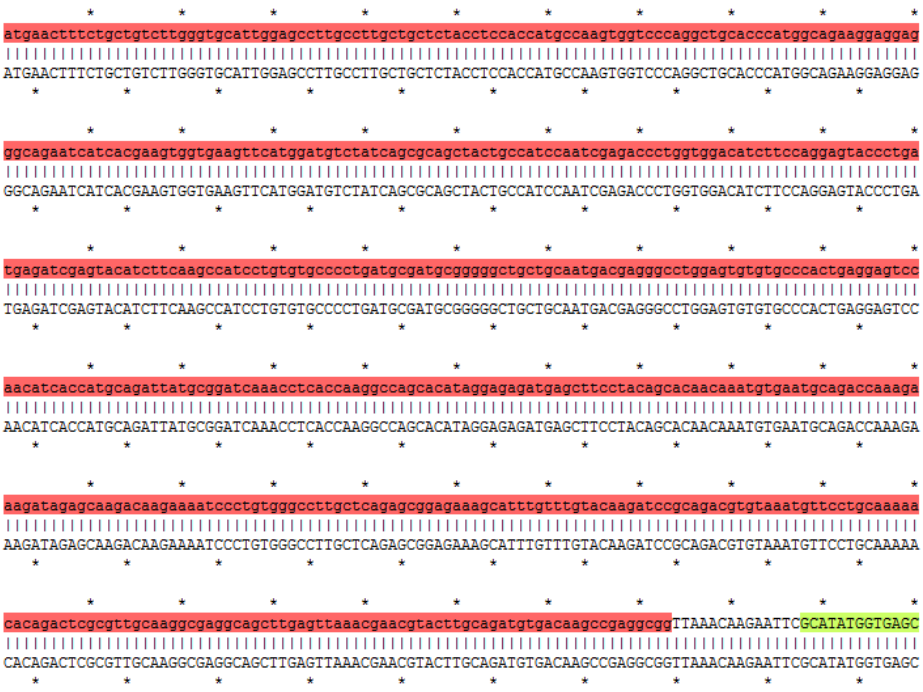

- Alignment of DNA sequencing results from sequence of GFP gene, fusion with VEGF gene and BGH polyadenilation signal with MC CMV reference (highlighted sequence). All the other promoter constructions had the same result and revealed the presence of the same mutation, confirmed by the chromatogram.

```
gagttaaacgaacgtacttgcagatgtgacaagccgaggcggTTAAACAAGAATTCGCATATGGTGAGCAAGGGCGAGGAGCTGTTCACCGGGGTGGTGC
||||||||||||||||||||||||||||||||||||||||||||||||||||||||||||||||||||||||||||||||||||||||||||||||||||||
GAGTTAAACGAACGTACTTGCAGATGTGACAAGCCGAGGCGGTTAAACAAGAATTCGCATATGGTGAGCAAGGGCGAGGAGCTGTTCACCGGGGTGGTGC

CCATCCTGGTCGAGCTGGACGGCGACGTAAACGGCCACAAGTTCAGCGTGTCCGGCGAGGGCGAGGGCGATGCCACCTACGGCAAGCTGACCCTGAAGTT
||||||||||||||||||||||||||||||||||||||||||||||||||||||||||||||||||||||||||||||||||||||||||||||||||||||
CCATCCTGGTCGAGCTGGACGGCGACGTAAACGGCCACAAGTTCAGCGTGTCCGGCGAGGGCGAGGGCGATGCCACCTACGGCAAGCTGACCCTGAAGTT

CATCTGCACCACCGGCAAGCTGCCCGTGCCCTGGCCCACCCTCGTGACCACCCTGACCTACGGCGTGCAGTGCTTCAGCCGCTACCCCGACCACATGAAG
||||||||||||||||||||||||||||||||||||||||||||||||||||||||||||||||||||||||||||||||||||||||||||||||||||||
CATCTGCACCACCGGCAAGCTGCCCGTGCCCTGGCCCACCCTCGTGACCACCCTGACCTACGGCGTGCAGTGCTTCAGCCGCTACCCCGACCACATGAAG

CAGCACGACTTCTTCAAGTCCGCCATGCCCGAAGGCTACGTCCAGGAGCGCACCATCTTCTTCAAGGACGACGGCAACTACAAGACCCGCGCCGAGGTGA
||||||||||||||||||||||||||||||||||||||||||||||||||||||||||||||||||||||||||||||||||||||||||||||||||||||
CAGCACGACTTCTTCAAGTCCGCCATGCCCGAAGGCTACGTCCAGGAGCGCACCATCTTCTTCAAGGACGACGGCAACTACAAGACCCGCGCCGAGGTGA

AGTTCGAGGGCGACACCCTGGTGAACCGCATCGAGCTGAAGGGCATCGACTTCAAGGAGGACGGCAACATCCTGGGGCACAAGCTGGAGTACAACTACAA
||||||||||||||||||||||||||||||||||||||||||||||||||||||||||||||||||||||||||||||||||||||||||||||||||||||
AGTTCGAGGGCGACACCCTGGTGAACCGCATCGAGCTGAAGGGCATCGACTTCAAGGAGGACGGCAACATCCTGGGGCACAAGCTGGAGTACAACTACAA

CAGCCACAACGTCTATATCATGGCCGACAAGCAGAAGAACGGCATCAAGGTGAACTTCAAGATCCGCCACAACATCGAGGACGGCAGCGTGCAGCTCGCC
||||||||||||||||||||||||||||||||||||||||||||||||||||||||||||||||||||||||||||||||||||||||||||||||||||||
CAGCCACAACGTCTATATCATGGCCGACAAGCAGAAGAACGGCATCAAGGTGAACTTCAAGATCCACCACAACATCGAGGACGGCAGCGTGCAGCTCGCC

GACCACTACCAGCAGAACACCCCCATCGGCGACGGCCCCGTGCTGCTGCCCGACAACCACTACCTGAGCACCCAGTCCGCCCTGAGCAAAGACCCCAACG
||||||||||||||||||||||||||||||||||||||||||||||||||||||||||||||||||||||||||||||||||||||||||||||||||||||
GACCACTACCAGCAGAACACCCCCATCGGCGACGGCCCCGTGCTGCTGCCCGACAACCACTACCTGAGCACCCAGTCCGCCCTGAGCAAAGACCCCAACG

AGAAGCGCGATCACATGGTCCTGCTGGAGTTCGTGACCGCCGCCGGGATCACTCTCGGCATGGACGAGCTGTACAAGTAATGGATCCTCTAGAGGGCCCG
||||||||||||||||||||||||||||||||||||||||||||||||||||||||||||||||||||||||||||||||||||||||||||||||||||||
AGAAGCGCGATCACATGGTCCTGCTGGAGTTCGTGACCGCCGCCGGGATCACTCTCGGCATGGACGAGCTGTACAAGTAATGGATCCTCTAGAGGGCCCG

TTTAAACCCGCTGATCAGCCTCGACTGTGCCTTCTAGTTGCCAGCCATCTGTTGTTTGCCCCTCCCCCGTGCCTTCCTTGACCCTGGAAGGTGCCACTCC
||||||||||||||||||||||||||||||||||||||||||||||||||||||||||||||||||||||||||||||||||||||||||||||||||||||
TTTAAACCCGCTGATCAGCCTCGACTGTGCCTTCTAGTTGCCAGCCATCTGTTGTTTGCCCCTCCCCCGTGCCTTCCTTGACCCTGGAAGGTGCCACTCC
```

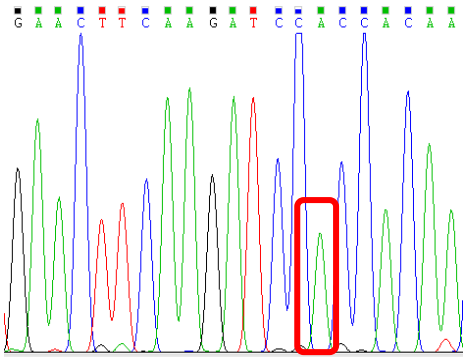

Mutation:
CGC → CAC
Arg → His
Aminoacid 168 of 239
Structural Position: β-strand

- Alignment of DNA sequencing results from sequence of CMV promoter and fusion with VEGF gene with MC CMV reference (highlighted sequence).

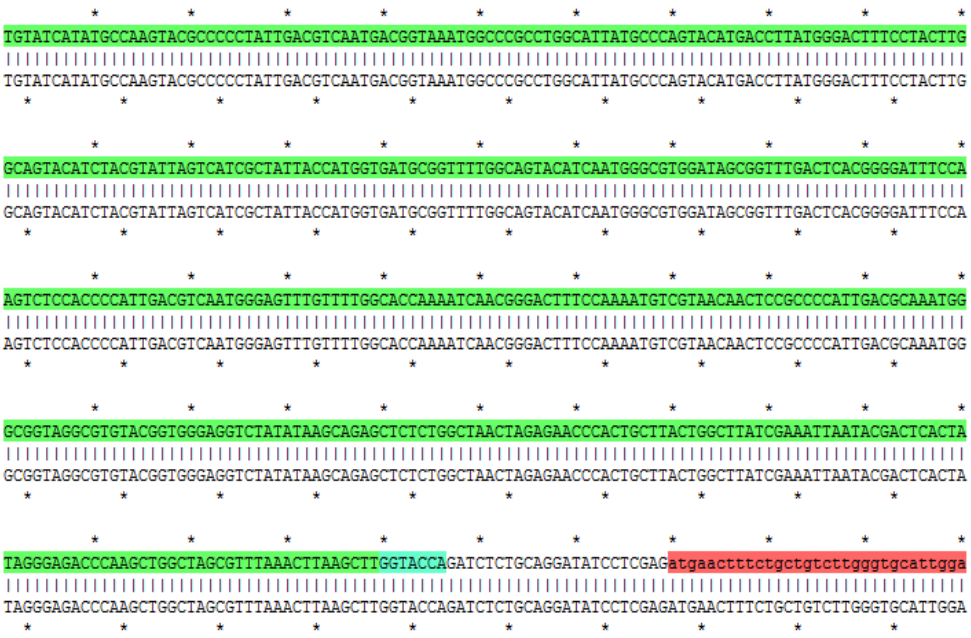

- Alignment of DNA sequencing results from sequence of hEF1α promoter and fusion with VEGF gene with MC EF1α reference (highlighted sequence).

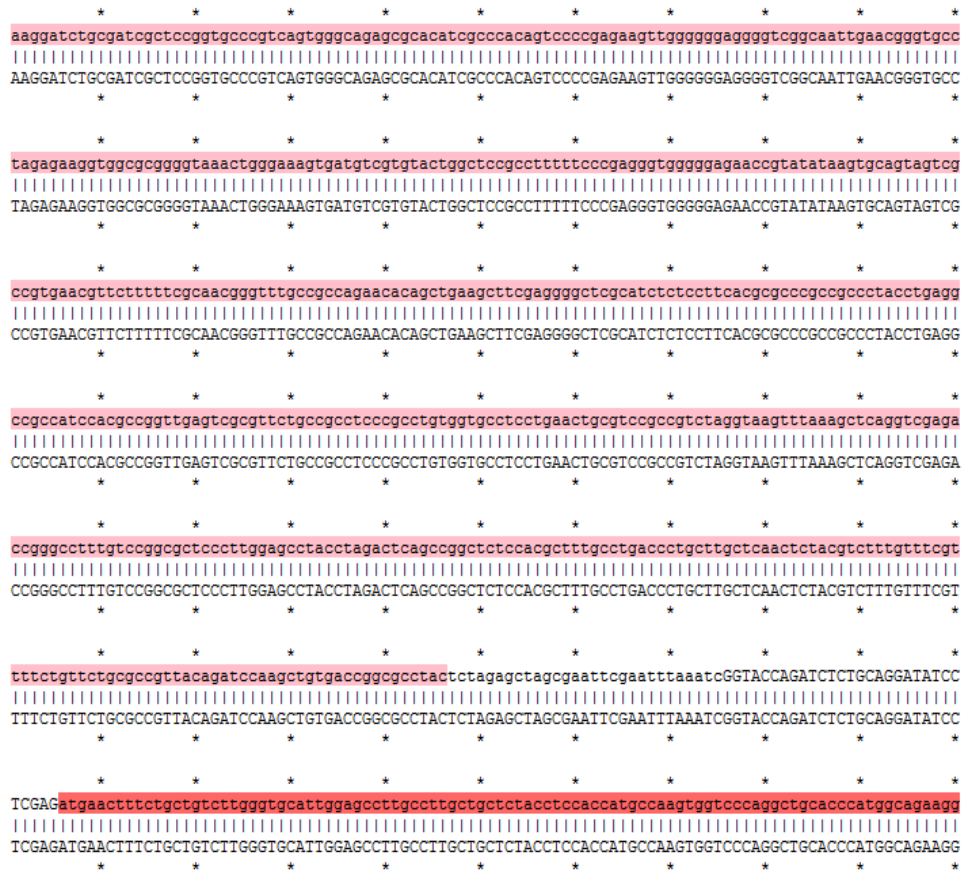

- Alignment of DNA sequencing results from sequence of hEF1α CpG free promoter and fusion with VEGF gene with MC hEF1α CpG free reference (highlighted sequence).

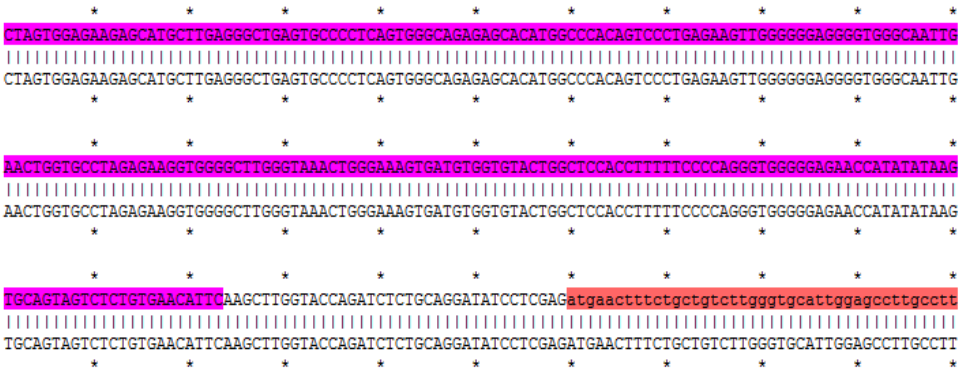

- Alignment of DNA sequencing results from sequence of mCMV+hEF1α CpG free promoter and fusion with VEGF gene with MC mCMV+hEF1α CpG free reference (highlighted sequence).

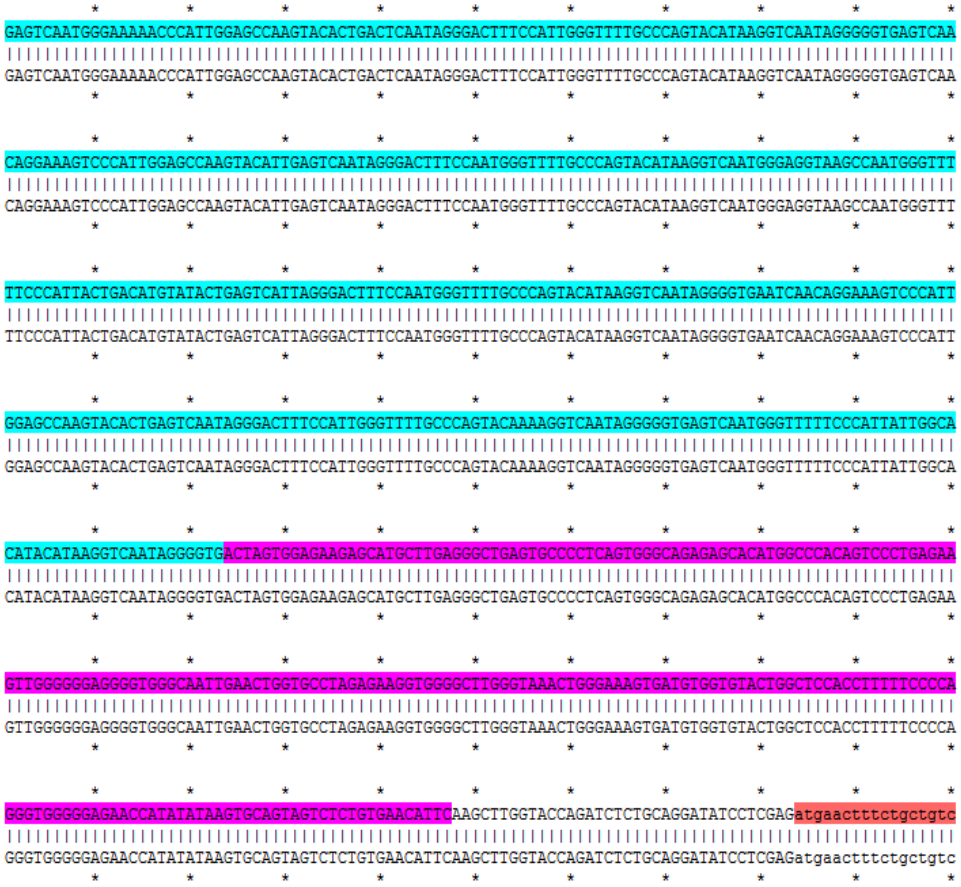

Annex 17 - Schematic diagram of pVAX-GFP (3697bp) and pVAX-VEGF-GFP (4273bp) plasmids.

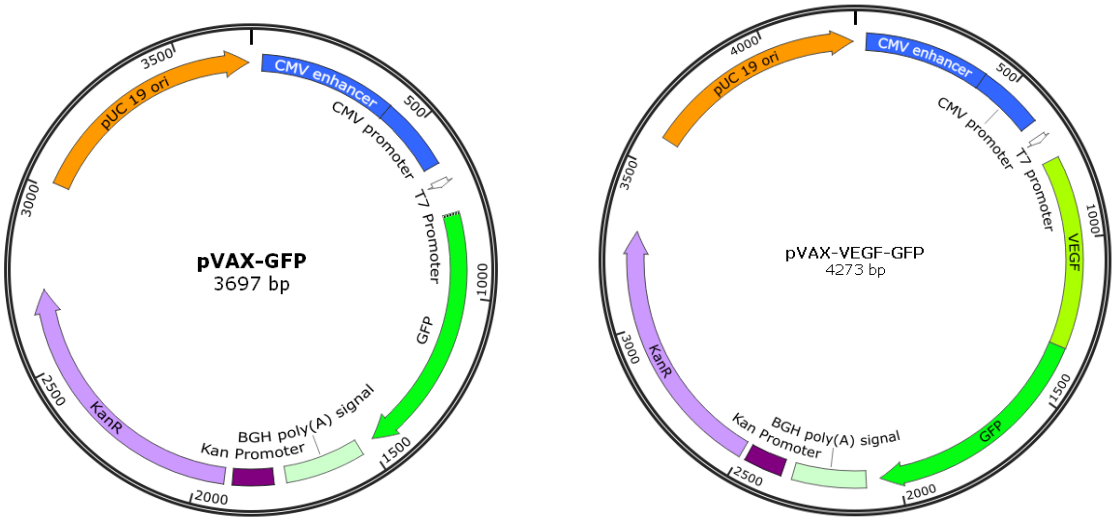

Annex 18- GFP expression mean intensity and yield of transfection product values of CHO cells transfection experiments with pVAX-GFP, VEGF-GFP encoding pMINILi vectors and their respective MC. Cell Data obtained from two independent experiments (n=2) 24h after transfection. Mean intensities are presented as mean values and the dashed line separates the pVAX-GFP from the remaining PP and MC construction values scale.

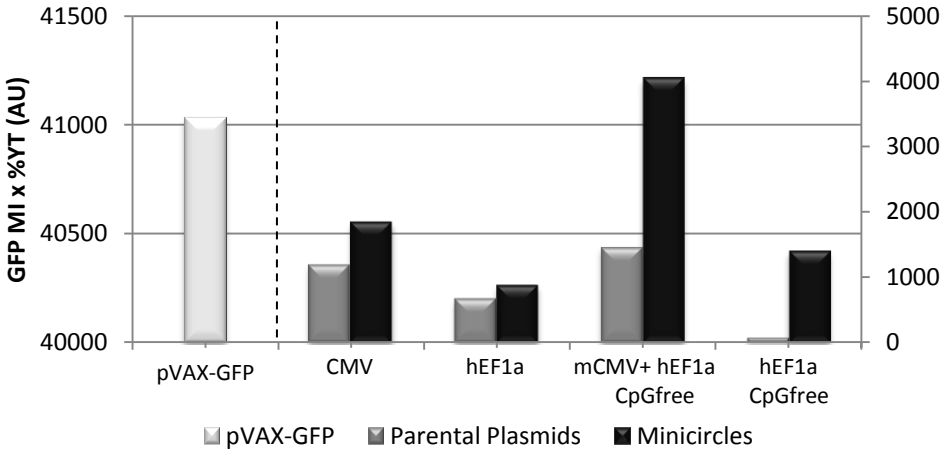

Annex 19 - Calibration curves of pVAX-GFP, pVAX-VEGF, MC CMV and MC mCMV+hEf1α CpG free for PCN/cell calculations. Each standard concentration C_T value are presented as mean of duplicate samples.

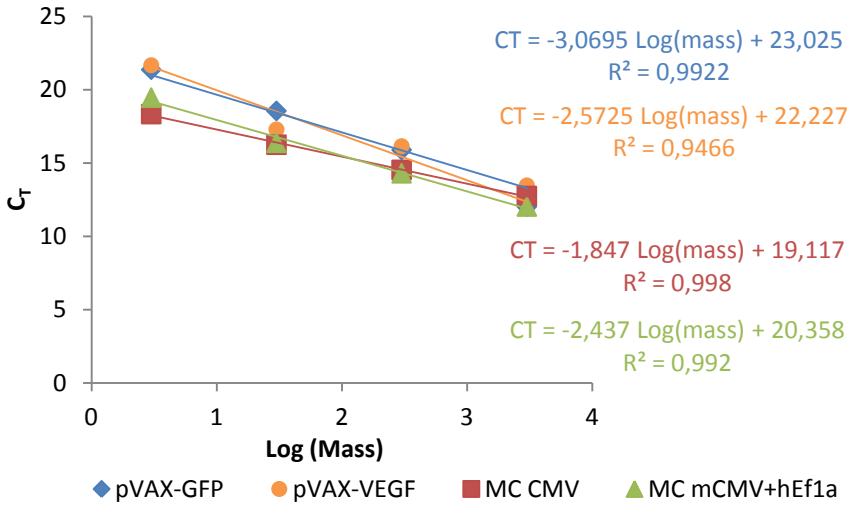

Annex 20 – Intermediate calculations for PCN/cell results.

Vector		C_T	Log(Mass) $C_T = a \times Log(Mass) + b$	Mass $10^{Log(Mass)}$	Mol $\frac{Mass}{MW}$	PCN $\frac{mol}{6.022 \times 10^{23}}$	PCN/cell $\frac{PCN}{10000\ cells}$
pVAX-GFP	D1	21.83	0.39	2.45	$1.02x10^{-18}$	$6.15x10^{5}$	722 ± 467
	D1	17.68	1.74	55.12	$2.30x10^{-17}$	$1.38x10^{7}$	
	D4	15.60	2.42	262.40	$1.09x10^{-16}$	$6.58x10^{7}$	4408 ± 1537
	D4	17.04	1.95	89.09	$3.71x10^{-17}$	$2.23x10^{7}$	
	D7	18.21	1.57	37.04	$1.54x10^{-17}$	$9.29x10^{6}$	486 ± 314
	D7	22.33	0.23	1.68	$7.01x10^{-19}$	$4.22x10^{5}$	
pVAX-VEGF	D1	16.80	2.11	128.71	$4.87x10^{-17}$	$2.94x10^{7}$	4315 ± 975
	D1	16.06	2.40	249.62	$9.45x10^{-17}$	$5.69x10^{7}$	
	D4	18.20	1.57	36.76	$1.39x10^{-17}$	$8.38x10^{6}$	605 ± 165
	D4	19.11	1.21	16.28	$6.17x10^{-18}$	$3.71x10^{6}$	
	D7	19.65	1.00	10.04	$3.80x10^{-18}$	$2.29x10^{6}$	118 ±78
	D7	23.47	-0.48	0.33	$1.24x10^{-19}$	$7.50x10^{4}$	
MC CMV	D1	21.44	-1.26	0.06	$3.64x10^{-20}$	$2.19x10^{4}$	6 ± 3
	D1	20.26	-0.62	0.24	$1.58x10^{-19}$	$9.54x10^{4}$	
	D4	17.10	1.09	12.36	$8.14x10^{-18}$	$4.90x10^{6}$	247 ± 172
	D4	21.21	-1.13	0.07	$4.85x10^{-20}$	$2.92x10^{4}$	
	D7	20.30	-0.64	0.23	$1.51x10^{-19}$	$9.08x10^{4}$	5 ± 3
	D7	22.07	-1.60	0.03	$1.66x10^{-20}$	$9.99x10^{3}$	
MC mCMV+ hEf1α CpG free	D1	21.44	-0.44	0.36	$2.37x10^{-19}$	$1.43x10^{5}$	7 ± 5
	D1	28.19	-3.21	0.001	$4.03x10^{-22}$	$2.43x10^{2}$	
	D4	18.30	0.84	6.99	$4.61x10^{-18}$	$2.78x10^{6}$	143 ± 95
	D4	22.02	-0.68	0.21	$1.37x10^{-19}$	$8.26x10^{4}$	
	D7	20.22	0.06	1.14	$7.51x10^{-19}$	$4.52x10^{5}$	43 ± 2
	D7	20.34	0.01	1.02	$6.71x10^{-19}$	$4.04x10^{5}$	
Control	D1	30.76					
	D1	32.66					
	D4	27.33					
	D4	31.60					
	D7	31.95					
	D7	30.26					

Annex 21 - Calibration curve of VEGF concentrations. OD_{450nm} values represent the mean absorbance for each duplicate standard, after subtracting the average zero standard optical density.

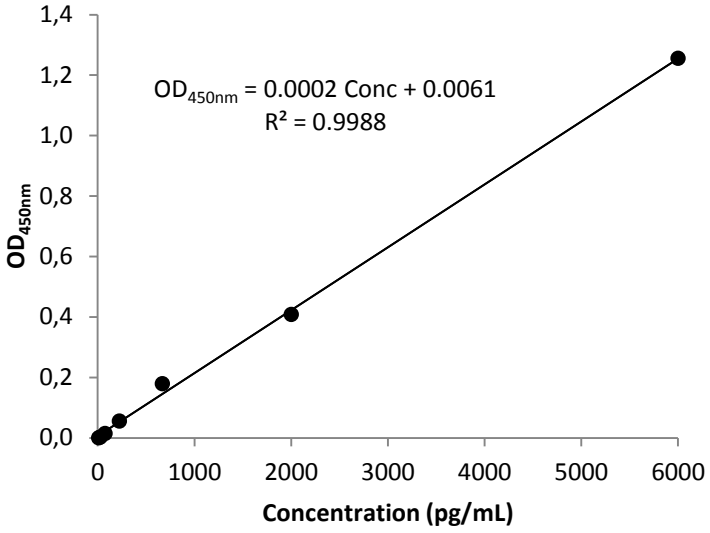

Annex 22 - Intermediate calculations for determination of VEGF concentrations.

Vector		OD_{450nm}	VEGF Concentration (pg/mL) $OD_{450NM} = a \times Conc + b$	Mean VEGF Concentration ± SEM (pg/mL)
Control	D1	0.285	10	505 ± 98
	D1	0.265	407	
	D4	0.421	1964	2703 ± 739
	D4	0.568	3442	
	D7	0.730	5063	4894 ± 169
	D7	0.697	4725	
pVAX-VEGF	D1	0.313	889	972 ± 83
	D1	0.330	10385	
	D4	1.263	10385	10998 ± 614
	D4	1.385	11612	
	D7	2.018	15342	16641 ± 1299
	D7	1.758	17941	
MC CMV	D1	0.496	2721	3917 ± 1196
	D1	0.735	5114	
	D4	1.713	14891	16399 ± 1508
	D4	2.015	17907	
	D7	2.645	24257	23812 ± 445
	D7	2.561	23368	
MC mCMV+ hEf1α CpG free	D1	0.331	1065	1342 ± 278
	D1	0.386	1620	
	D4	1.754	15298	15942 ±644
	D4	1.883	16586	
	D7	2.497	22725	22514 ± 210
	D7	2.455	22304	